

POLITECNICO DI MILANO
Dipartimento di Ingegneria Idraulica, Ambientale,
Infrastrutture viarie, e Rilevamento



**WAVE ENERGY IN ITALIAN SEAS:
PRELIMINAR DESIGN OF A POINT
ABSORBER**

Relatore: Prof. Giuseppe Passoni

Correlatore: Dott. Silvia Bozzi

Tesi di laurea di:

Adrià Moreno Miquel Matr. 764442

Anno accademico 2011/2012

Acknowledgements

It is hard to think of myself doing that work by my own, it would be a titanic task, almost impossible. This is why the following lines are dedicated to those who, to a greater or lesser extent, helped making that Master Thesis come true.

Firstly, my gratitude goes to Professors Giuseppe Passoni and Silvia Bozzi that undoubtedly have been the main pillars of this work. Renata Archetti and Alessandro Antonini from the University of Bologna, who played also an important role in the development of this project, thanks for their collaboration and knowledge sharing, which have been very useful to reach the goal with such success.

To my family, which has always accepted and respected all my decisions, overall the academic ones and that with their effort have allowed me to carry most of them out, especially to my Mum.

To my girlfriend Maria for the cheering and patience and finally, to all of my friends, from the ones I was practically born with until the most recent ones that have integrated me and have made me feel “almost” like Italian.

Adrià Moreno Miquel.

Abstract

It was in the mid 1970s when the research in the Wave Energy Converters began as a consolidated field, but it wasn't until between the late 1990s and the beginnings of the 21st century that the sector boomed. Unlike many other renewable energy forms, the wave energy can be considered as a teenager, almost ready to show the world its enormous potential. Many prototypes are being tested throughout the oceans and even a commercial wave energy plant has been set already. Its growth is being unbalanced though.

There are no current and prospective research studies with this scope for the Mediterranean Sea, it seems logical so the Mediterranean Sea is one of the least energetic seas in the world but this doesn't exclude the fact that also in the Mediterranean Sea there is wave energy to be exploited and the purpose of this work is to initiate that path.

The point absorber is the type of Wave Energy Converter chosen, it consists of a floating body that exploiting the motion produced by an incident wave generates electricity via an electric linear generator. Several simulations have been done with different kinds of buoys in two different locations in the Mediterranean Sea, Alghero and Mazara. The simulation's goal is to compute the output power of the devices. Although the values state that the average extracted energy is of minor entity than the ones tested in big oceans such as the Atlantic Ocean or the Pacific Ocean, where the wave energetic regime is much higher, the results are hopeful, confirming its feasibility and opening a new door to renewable energies in the Mediterranean regions.

The conclusions drawn in this work are always under the bases that there is still a lot of work to do and a full sea of possibilities.

List of contents

**WAVE ENERGY IN ITALIAN SEAS: PRELIMINAR DESIGN OF A POINT
ABSORBER I**

ACKNOWLEDGEMENTS..... I

ABSTRACT III

LIST OF CONTENTS..... V

LIST OF FIGURES..... VII

LIST OF TABLES..... XI

CHAPTER 1: INTRODUCTION 1

CHAPTER 2: LITERATURE.....5

CHAPTER 3: THEORY.....25

 3.1 WAVE MECHANICS25

 3.1.1 WAVE GENERATION25

 3.1.2 WAVE ANALYSIS AND STATISTICS30

 3.1.3 LINEAR WAVE THEORY.....37

 3.2 ELECTROMAGNETICS OF LINEAR GENERATOR.....50

 3.3 FLOATING BODY DYNAMICS56

CHAPTER 4: MATHEMATICAL MODELING61

 4.1 MODEL OF THE FLOATING BODY63

 4.2 MODEL OF THE LINEAR GENERATOR.....70

 4.2.1 ELECTROMAGNETIC MODEL.....70

 4.2.2 MECHANICAL MODEL.....76

 4.3 MODEL OF THE WAVE ENERGY CONVERTER78

CHAPTER 5: SIMULATIONS81

 5.1 DESCRIPTION81

 5.2 RESULTS87

CHAPTER 6: CONCLUSIONS.....	101
REFERENCES.....	105
APPENDIX A: MATLAB CODES.....	111
A.1. MAIN SCRIPTS.....	111
A.1.1 <i>Sim_WEC.m</i>	111
A.1.2 <i>Energy_Production.m</i>	115
A.1.3 <i>optimization.m</i>	116
A.2. FUNCTIONS:	119
A.2.1 <i>Archimede.m</i>	119
A.2.2 <i>CiambC.m</i>	120
A.2.3 <i>CiambS.m</i>	120
A.2.4 <i>interpolazione1.m</i>	121
A.2.5 <i>interpolazione_cilindro.m</i>	122
A.2.6 <i>LIN_GEN.m</i>	123
A.2.7 <i>fou.m</i>	124
A.2.8 <i>linear generator.m</i>	124
A.2.9 <i>positiveFFT.m</i>	126
A.2.10 <i>positiviFFT.m</i>	126
A.2.11 <i>PTO.m</i>	127
A.2.12 <i>efficiencies.m</i>	128

List of figures

- 1.1 General Sketch of a point absorber wave energy converter. Main parts of the generator and the floating body are pointed down.....p 2
- 1.2 Map of the central area of the Mediterranean Sea. Alghero and Mazara are specified because the available data for this work is located in these geographical areas.....p 2
- 1.3 Illustration of the six degrees of freedom of a floating body. Each degree of freedom is based on a reference coordinate system and their names are the most commonly used in the naval sector.....p 3
- 2.1 Picture of Yoshio Masuda. The man who made the first serious investigations about Wave Energy Converters.....p 6
- 2.2 Illustration of the Salter Duck Device. A WEC designed in the mid 70's and with the highest efficiency ever built.....p 7
- 2.3 Map of the world with the wave energetic regimes illustrated in its corresponding areas. The units of the mean power contained in the waves is expressed in [kW/m]...p 9
- 2.4 Map of the Mediterranean and Black Seas area with the wave energetic regimes illustrated in its corresponding areas. The units of the mean power contained in the waves is expressed in [kW/m].....p 10
- 2.5 Raw description of the Wave Energy Converters type depending on its orientation corresponding with the incident wave direction.....p 11
- 2.6 General division of WEC technologies. Classified depending on the working principle, then structure type or position and finally, depending on the motion type.....p 12
- 2.7 Sketch and picture of the OWC's Pico plant located in the Portuguese coast.....p 13
- 2.8 Aerial picture of the breakwater integrated OWC plant in Mutriku, Basque Country, Spain.....p 14
- 2.9 Schematic representation of the Backward Bent Duck Buoy. A floating structure OWC oriented backwards to improve energy absorption.....p 14
- 2.10 Computer rendering of the Mighty Whale. A floating Structure OWC designed in Japan.....p 15
- 2.11 Four different pictures of the tests conducted in Uppsala University. Each picture shows a different buoy of the same kind of WEC, floating body point absorbers.....p 16
- 2.12 Schematic illustration of the working principle of the AWS WEC and picture of the prototype.....p 18
- 2.13 Schematic top and side views of the Pelamis device.....p 19

2.14	Different Pictures of the Pelamis device. The first picture shows the prototype in a front view while it was being tested in the English coasts. The Second shows how it was introduced into the water. The third pictures shows the wave energy plant that was installed in the Portuguese coast, composed by three devices.....	p 20
2.15	Schematic illustration of the SeaRev device. Including its mechanical, hydraulic and electric elements.....	p 21
2.16	Computer rendering of a wave energy plant made of Oyster devices, developed in the U.K.....	p 22
2.17	Illustration of the working principle and picture of the Tapchan power Plant in Norway.....	p 23
2.18	Top and front view of the Wave Dragon device and illustration of the working principle.....	p 24
2.19	Picture of the Wave Dragon prototype.....	p 24
3.1	Graphical representation of the wave Generator. The graphic shows how the significant height and period evolve when are within the Fetch extension and outside for duration restricted generation and Fetch restricted generation.....	p 28
3.2	Variation of the Wave Spectrum depending on which point of the Fetch the measurement is done.....	p 29
3.3	Illustration of a wave record representing the sea surface elevation over the time....	p 30
3.4	Graphic of the probability distribution of the different wave heights registered in a wave record.....	p 31
3.5	Logarithmical adapted version of the Rayleigh distribution made by the U.S. Naval Forces.....	p 32
3.6	Non-dimimensionalized graphic which shows the curves of equal-probability of wave heights over the wave periods.....	p 33
3.7	Difference from the wave spectrum obtained via the JONSWAP method or through the Pierson-Moskowitz method.....	p 36
3.8	Spatial and frequency description of a linear wave with all its parameters.....	p 38
3.9	Water particle velocities in a wave.....	p 41
3.10	Water particle orbits in deep water.....	p 42
3.11	Water particle orbits in shallow water.....	p 42
3.12	Pressure distribution along the depth in the wave crest and the wave trough.....	p 43
3.13	Geometric configuration to compute the Potential Energy.....	p 44
3.14	Geometric configuration to compute the Kinetic Energy.....	p 45
3.15	Evolution of the shoaling coefficient over the ration sea depth by wave length in deep waters.....	p 47
3.16	Geometric representation of the Snell's law applied in sea waves in the near-shore area.....	p 47
3.17	Representation of the wave behavior when waves are refracting.....	p 48
3.18	Wave diffraction behavior depending on the obstacle.....	p 49
3.19	Conceptual Scheme of the magnetic induction.....	p 50

3.20	Magnetization curve for a ferromagnetic material.....	p 52
3.21	Physical description of the translator and stator parts of the linear Generator and its conceptual function.....	p 53
3.22	Equivalent Electric Circuit. With voltages, currents, resistance and reactance.....	p 54
3.23	Conceptual representation of the load angle.....	p 55
3.24	Floating body full coordinate system.....	p 56
3.25	Illustration of the six degrees of freedom of a floating body. Each degree of freedom is based on a reference coordinate system and their names are the most commonly used in the naval sector.....	p 56
3.26	Excitation Force restricted in heave mode depending on the wave frequency and the radius of the sphere floating body.....	p 58
3.27	Stages of the model creation process and factors that have some kind of influence in that process.....	p 61
3.28	Description of the geometrical figures used as floating bodies. All the needed parameters to model them are described in the figure. Namely, the radius, draft and vertical distance where the floating body is partly submerged.....	p 65
4.3	Distribution of the unitary radiation damping, ϵ , and the unitary added-mass coefficient, μ , in surge mode, $j=1$, and heave mode, $j=3$, of a spherical floating body of radius a over the product of the angular repetency, $k= \omega^2/g$, by the sphere's radius a	p 66
4.4	Distribution of the unitary radiation damping, ϵ , and the unitary added-mass coefficient, μ , in surge mode, $j=1$, and heave mode, $j=3$, of a cylindrical floating body of radius a over the product of the angular repetency, $k= \omega^2/g$, by the sphere's radius a	p 67
4.5	Vertical Position and vertical Speed of a spherical floating body induced by incident monochromatic waves with constant height and period over the time.....	p 68
4.6	Vertical Position and vertical Speed of a cylindrical floating body induced by incident monochromatic waves with constant height and period over the time.....	p 68
4.7	General Sketch of a point absorber wave energy converter. Main parts of the generator and the floating body are pointed down.....	p 70
4.8	General sketch of the electric linear generator, with its main parts such as the translator and stator are illustrated in detail.....	p 71
4.9	Electrical field induced by the wave motion in the stator of the generator. Phases a , b and c are represented. The voltage between two phases is also plotted and the root mean squared voltage is also marked due to its importance.....	p 74
4.10	Electrical current induced by the wave motion in the stator of the generator. Phases a , b and c are represented. The root mean squared current is also marked due to its importance.....	p 74
4.11	Electrical power generated by the wave motion. There are also plotted the time averaged power for the whole time and for a mobile window. The root mean squared current is also marked due to its importance.....	p 75

4.12	Magnetic Force generated by the wave motion in the translator of the generator. The time averaged force is also plotted.....	p 75
4.13	Illustration of the mechanical equivalent of the electric linear generator, a mass-spring-damper system with its parameters m , k and c as the mass, the spring coefficient and the damping coefficient respectively.....	p 76
4.14	Illustration of the mechanical equivalent of the point absorber WEC, a mass-spring-damper system.....	p 78
4.15	Simplification of a mass-spring system and its condition to reach resonance.....	p 79
5.1	Schematic representation of the capture width concept. This figure shows how the capture width can be larger than the devices width maximizing the energy absorption.....	p 86
5.2	Vertical Position and vertical Speed of the spherical floating body WEC induced by incident monochromatic waves with constant height and period over the time.....	p87
5.3	Vertical Position and vertical Speed of the cylindrical floating body WEC induced by incident monochromatic waves with constant height and period over the time.....	p 88
5.4	Fourier Spectrum. The upper plot shows the amplitude of the signal over a range of frequencies, and the lower plot shows the phase of the signal over a range of frequencies.....	p 89
5.7	Optimized spring coefficient for the spherical floating body over different sea states.....	p 90
5.8	Optimized spring coefficient for the cylindrical floating body over different sea states.....	p 91
5.9	Evolution of the Capacity Factor over the spring coefficient of the Spherical WEC.....	p 94
5.10	Evolution of the Capacity Factor over the spring coefficient of the Cylindrical WEC.....	p 94
5.11	Power Matrix for the optimized Spherical device.....	p 96
5.12	Power Matrix for the optimized Cylindrical device.....	p 96
5.13	Efficiency Matrix for the optimized spherical device.....	p 97
5.14	Efficiency Matrix for the optimized cylindrical device.....	p 97
5.15	Capture Width Matrix for the optimized spherical device.....	p 98
5.16	Capture Width Matrix for the optimized cylindrical device.....	p 98
5.17	Histograms of the Energy and Power Outputs for both devices in Alghero.....	p 99
5.18	Histograms of the Energy and Power Outputs for both devices in Mazara.....	p 99
5.19	Histograms of the Full load hours and the Capacity Factor for both devices in Alghero.....	p 100
5.20	Histograms of the Full load hours and the Capacity Factor for both devices in Mazara.....	p 100
6.1	Deeply submerged body attached to the floating body to increase the resonance frequency.....	p 109

List of tables

3.1 Birth-to-death process of sea waves. States the process since are generated in an irregular form by the wind pressure until they finish breaking against the shore losing the energy gathered in the travel, going through the swell and shoaling states.....	p 26
3.2 Description of the six degrees of freedom of a floating body given a reference coordinate system.....	p 57
4.1 Description of the electromagnetic parameters of the linear generator; with name, parameter, value and unit.....	p 73
5.1 Description of the physical parameters of the spherical floating body of the WEC; with name, parameter, value and unit.....	p 81
5.2 Description of the physical parameters of the cylindrical floating body of the WEC; with name, parameter, value and unit.....	p 82
5.3 Description of both, the electromagnetic and physical parameters of the linear generator; with name, parameter, value and unit.....	p 82
5.4 Initial states of the spherical buoy and cylindrical buoy when running the simulations. Describes, vertical position, vertical velocity and units.....	p 84
5.5 Spring coefficient determination for each device and location.....	p 95
5.6 Wave energy converters Maximum Power output.....	p 101
5.7 Wave energy converters Maximum Efficiency.....	p 101
5.8 Wave energy converters Maximum Capture Width.....	p 101
5.9 Mean Annual Features for each Wave energy converter.....	p 102

CHAPTER 1:

INTRODUCTION

When thinking of renewable energies, several different names such as wind, solar, hydraulic or biomass energy come quickly to mind. Lately, due to the threads of the climate change impacts in the foreseeable future and to the ever increasing oil price, a whole new variety of new kinds of renewable energy sources and technologies are being explored. Within this frame, wave energy plays a very significant role, if not the pole position, in terms of potentiality of power absorption and conversion into its electrical form.

Wave energy, with exception of tidal waves which are generated by the earth's rotation within the gravity fields of the moon and the sun, is a concentrated type of solar energy. Strictly speaking, the sun's energy, in form of electromagnetic waves, reaches the earth's atmosphere and surface with a well known span of intensities according to its latitude. Namely, the further up north from the equator for the northern hemisphere and vice versa for the southern hemisphere the lower it is the amount of energy received by our planet. The reason for that phenomenon to happen is the almost spherical earth's shape and the variation of the angle of incidence that implies. As a result of this unbalanced input of energy, the temperature on the earth varies depending on the latitude and in turn, so does the atmospheric pressure, creating the winds moving from high pressure areas to lower ones. If that wind is located in an oceanic area part of this wind energy is transferred to the water surface and thus causing waves, that initially are ripples and then depending on the wind speed, direction, duration and the distance over which it blows ("the fetch") can evolve into a big and powerful swell. Such waves can travel vast distances, thousands of miles, with an extremely low loss of energy. The wave power density is much higher than wind or solar power, more specifically, five times higher than the former and twenty to thirty times higher than the latter just below the ocean's surface.

To help understand the big potential of this kind of energy let's put it into numbers; on regular day the coasts of the British Islands receive an amount of wave energy of about 1 TWh. Applying a feasible efficiency of extraction of 10-25% means that the daily energy

demand in the U.K. could be fed only by the waves that reach its coasts. To sum up, it is believed that wave energy could supply over the 10% of the world's current electricity consumption, taking a significant part of the energetic mix.

The aim of this Master Thesis is to understand and realize if it is possible and, to which extent, to extract wave energy from the Mediterranean Sea and which is the best way to achieve it. The research is done through a point absorber wave energy converter (See Fig 1.1) which basically consists of a heaving buoy and linear electric generator placed on the seabed. This specific device is fully described further in the second and fourth chapters. The areas selected to conduct this study are l'Alghero and Mazara, the former is located in the west coast of Sardinia, the biggest island in Italy and the latter is located in also in the western point of the Sicilian coast. These two spots, according to the available data gathered by more than 20 buoys, are the most energetic places in Italy (See Fig 1.2.).

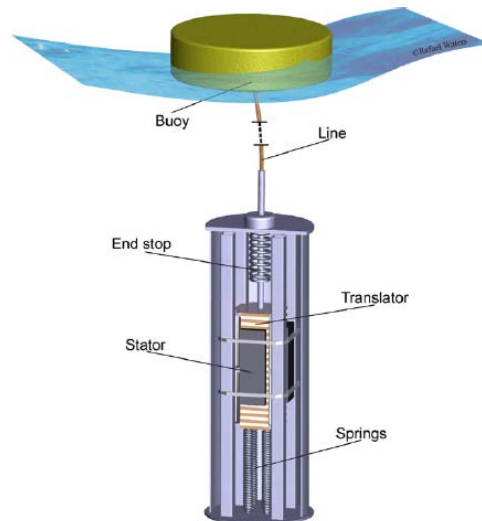


Figure 1.1: General Sketch of a point absorber wave energy converter.

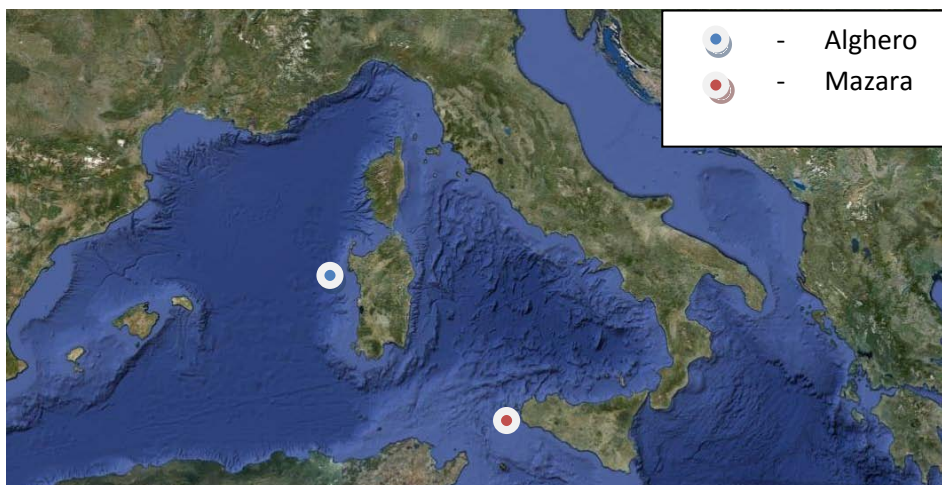


Figure 1.2: Map of the central area of the Mediterranean Sea.

The essay of this master thesis is divided into six different chapters. After the introduction comes the chapter two which gives an overall vision of the short history of the wave energy extraction and a detailed description of all the different types of WEC that are being studied and, in some particular cases, even used commercially.

Nowadays, approximately two thousand different methods are being seriously considered to study wave power extraction. Each of these different devices works in a very different way. There are floats, ramps, funnels, cylinders, air-bags and liquid pistons. These devices can be located at the sea surface, on the sea bed or anywhere else in between. They can be put facing backwards, forwards, sideways or obliquely and they can move in many different modes such as in heave, surge, pitch, sway and roll or any kind of combination among them (See Fig. 1.3). Their power take-off system performance can be based in different principles, working fluids and materials like, oil, air, water, steam, gearing or electro-magnets. They can be placed onshore, on the coast line or offshore reaching a range of different demands as of the mooring system, seabed connections for transportation of the generated power to the mainland grid or the end-stop system to survive extreme storm conditions.

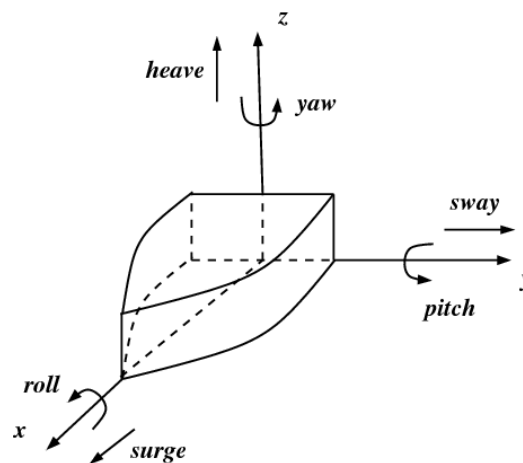


Figure 1.3: Illustration of the six degrees of freedom of a floating body.

In chapter three all the theories related to the WEC's environment are exposed. That is to say, the wave mechanics, which are divided into three main parts. Firstly, the wave generation, explaining in full detail the spectrum subsequently used in this work and its related parameters. Afterwards, the wave analysis and statistic theories used to obtain reliable and trustworthy data. Finally, the famous linear theory which simplifies the complicated physical laws that describe the ocean waves and provides an overall understanding of the wave's movement, actions, reactions and their role in the world of WEC. Further reading in the chapter three, the reader finds the electromagnetic laws that govern the power take-off

system of the studied WEC. And last but not least, the floating body dynamics are described. This is the majority of the base knowledge required to design successfully a WEC.

Chapter four talks about all the mathematical modeling used in this work. It is anything but all the theoretical knowledge gathered in the previous chapter put into practice through the software MATLAB. All the work of this master thesis is resumed in three different mathematical models merged together to form a new bigger mathematical model. The three main subparts of this general model of the WEC are: the model of the floating body and two different conceptual models of the linear generator, its mechanical equivalent and its electromagnetic equivalent.

Subsequently, in chapter five is given a fully detailed description of the diverse numerical simulations done during the work to achieve the optimal working conditions for the WEC and the maximum power outtake. The obtained results are critically commented and discussed.

The last chapter is assigned to draw the required conclusions.

CHAPTER 2:

LITERATURE

Wave energy potential has been recognized throughout the history and mostly, for its destructive nature. It hasn't been until relatively recent times that humankind hasn't started to think of it as a source of energy for its own benefit. The first documented case dated back to 1799 it was a heaving artificial raft invented by Girard père et fils, which is known as the first patent which aim is to capture wave energy and convert it into mechanical energy. During the nineteenth century several wave motors were patented. In the early twentieth century the first motors to supply energy to floating devices, such as buoys with whistles, bells and lighthouses, were built.

A good example of that is the case of Bouchaux-Paceique who built an entire system that fed his house, in Royan (France), with electricity. The system consisted of a tunnel placed three meters below the lowest tidal level, the tunnel was open to the ocean on one edge and connected to a well on the other edge, this well was closed at its top by a dome. A pressure pipe connected the top of the shaft and a turbine which in turn, was connected to a generator that stored the electricity via a battery system that supplied the house electricity needs during the rest periods. To protect the system from the oceanic storms a sea wall was built outside the system.

After that, several isolated inventions kept appearing in some specific parts of the planet. Alva Reynolds in 1909 lighted a dock in Pacifica (California) and in 1919 an experimental pendulum motor was tested in Japan. During the 1930s a series of experiments were carried on by the Société Méditerranéene d'Energie Marine in collaboration with the Société Marocaine d'Etudes de la Houle et du Vent in Algeria, several converging channels supplied a fore-bay for a low head station.

Since 1926 the Oceanographic Institute of Monaco employed a 400 watt wave energy pump to raise the water level in columns up to 20 to 60 meters in museums and laboratories. The system could provide a 7kW peak power thanks to a Savonius rotor that drove double acting pumps to lift the water.

It wasn't until the 1940s when the first important figure of the world of wave energy conversion showed up, his name was Yoshio Masuda (dead in 2009) (See Fig. 2.1). Masuda may be considered as the father of modern wave energy technology, he developed a navigation buoy powered by wave energy, which was in fact the first device to use the principle of, what later would be called, a floating oscillating water column (OWC). These buoys were commercialized in Japan since 1965 and later were exported to the USA. In 1965, Masuda led the construction of Kaimei, a large floating platform (80m x 12m) installed with several OWCs with different kinds of air turbines. The results of the Kaimei testing program weren't exactly the expected ones, owing to the basic level of theoretical knowledge of the subject acquired by that time, the efficiency and power extraction rates achieved were rather low.



Figure 2.1: Picture of Yoshio Masuda. Wave Energy Converters precursor.

The oil crisis that began the autumn of 1973 helped to change the perspectives of a new scenario where the interest of developing renewable energies was born. Wave energy wasn't an exception and serious studies to produce energy from waves in large scale were initiated. A paper published in 1974 in the renowned *Nature* by Stephen Salter, of the University of Edinburgh, was the real kick off of the discipline. That article not only presented a brilliant solution but also brought wave energy extraction to attention of the international scientific community. The paper presented a device known as the Salter Duck (see Fig 2.2), consisting of a floating body that can reach an efficiency of 90%, an exceptional high value compared to other devices performances and it keeps holding the first places in the efficiency podium devices in the present days.

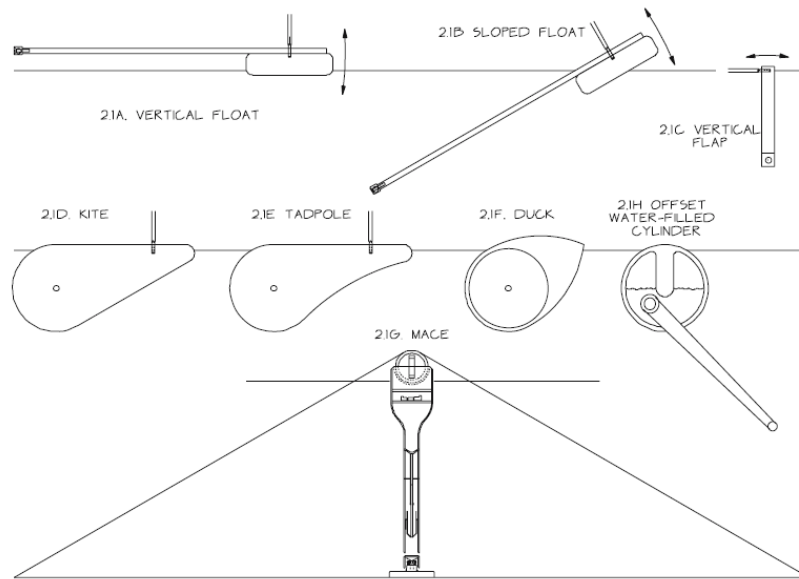


Figure 2.2: Illustration of the Salter Duck Device.

As seen on the previous paragraph the efficiency levels achieved by the Salter Duck were astonishing by that time, but one year later a discovery made by Johannes Falnes and Kjell Budal from the Trondheim University in Norway took a bit of importance to that significant high values of efficiency. Falnes and Budal introduced the concept of “Capture Width” or “Capture Width Ratio” which represents the amount of energy absorbed by unit of length, the big discovery was that this ratio could be bigger than the amount of energy contained in the width of the device, when speaking of point absorbers. So a heaving body can capture more energy than what’s actually within its physical borders, in other words, efficiency can be higher than the theoretical value of 100%. The physical concept behind that parameter is of such difficulty, but in general terms it works that way: due to the properties of waves, which will be explained in the third chapter, the maximum energy which may be absorbed by a heaving axis-symmetric body equals the wave energy transported by the incident wave front of width equal to the wavelength divided by 2π .

That year, the British Government started an important research and development program in wave energy, the same path the Norwegian Government followed some months later. The first conferences dedicated exclusively to wave energy took place in Canterbury and Heathrow (England) in 1976 and 1978 respectively. In 1979 were organized the first two conferences at an international level: *Power from Sea Waves* (Edinburgh) and the *First Symposium on Wave Energy Utilization* (Gothenburg). The *Second international Symposium on Wave Energy Utilization* (Trondheim) celebrated in the 1982 coincided with the cut of funds for research on Sea Wave Energy by the British Government and although the research went on, specially for the UK scientific community was a big step backwards.

Norwegians instead, continued with their own research and development program and in the autumn of 1985 built two full-sized shoreline prototypes in the area nearby the coastal city of Bergen, which were able to achieve 500 kW of power. In the late 1980s the majority of the activity was restrained at the academic level. The only steps forward were a prototype, a 75 kW shoreline OWC, build by the University of Edinburgh in the island of Islay and two more 60 kW OWC integrated into the breakwater at the port of Sakata, in Japan.

The decision of the European Commission, in 1991, of including Wave Energy in the R&D program on renewable energies changed drastically the situation in the sector. The first projects started in 1992 and since then, about thirty projects have been funded by the European Commission involving a large number of active teams in Europe. Few of these projects took the form of coordination activities; one of the most important ones was the *Coordination Action in Ocean Energy*, which involved around forty partners. A big series of *European Wave Energy Conferences* were sponsored and partly funded by the European Commission, the places that hosted those events are the following: Edinburgh (UK, 1993), Lisbon (Portugal, 1995), Patras (Greece, 1998), Aalborg (Denmark,2000), Cork (Ireland, 2003), Glasgow (UK, 2005), Porto (Portugal, 2007), Uppsala (Sweden,2009)and Southampton (UK, 2011), in September 2013 will take place the tenth edition in Aalborg (Denmark).

In 2001, the international Energy Agency established implementing agreement in Ocean Energy Systems in which 17 countries are present and whose endeavor is to coordinate and facilitate ocean energy research, development and demonstration through international cooperation and knowledge sharing. In the last few years, northern American countries, i.e. USA and Canada are making big investments, involving the national and regional administrations, research institutions and private companies favoring meetings and conferences on ocean energy.

As stated in the introduction chapter, wave power is a source of energy with one of the known highest energy density. Although that fact, as commonly happens in the frame of energy extraction, it's not spread throughout the world homogeneously, there are some restricted areas in which the amount of energy delivered by the waves is huge, by contrast, there are some other places which are simply too little energetic and where the wave energy absorption is, frankly speaking, not feasible (See Fig 2.3.).

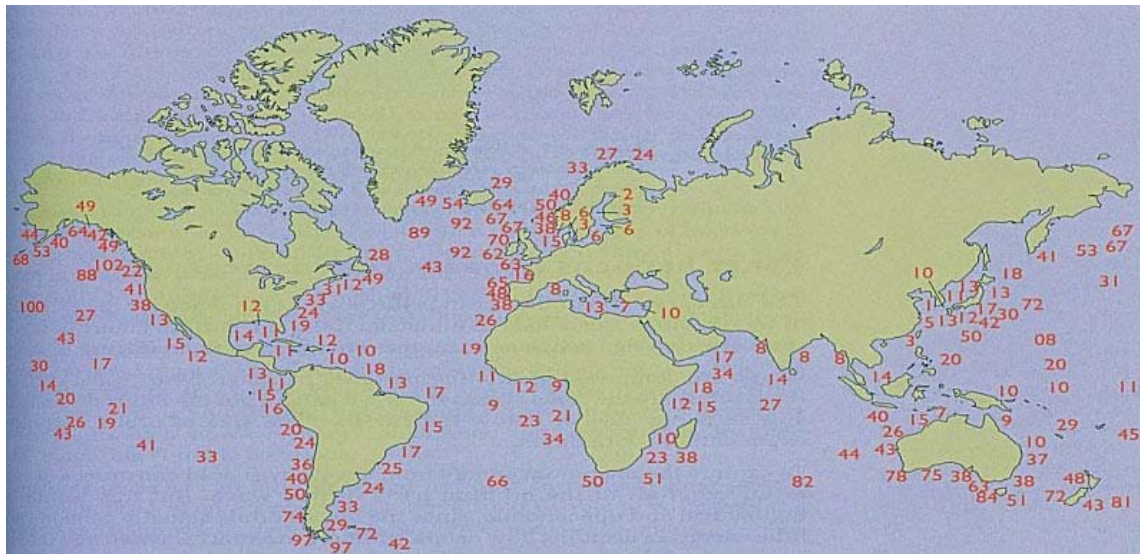


Figure 2.3: Map of the world with the wave energetic regimes illustrated in its corresponding areas. The units of the mean power contained in the waves is expressed in [kW/m].

The figure above shows estimates of the wave power density at various locations around the world. The areas of the world which are subjected to regular wind fluxes are those with the largest wave energy resource. South western winds are common in the Atlantic Ocean, and often travel substantial distances.

There are several regions around the world with high incident wave power levels, particularly well suited to exploiting wave energy. These are located generally in extreme latitudes (between 40° - 60° latitude in the North and South) and in the west coast of continents including the western seabords of South and North America, Northern Europe, Australia, and Asia. In these areas the wave power per unit width of wave crest has a typical annual mean of between 50 - 100 kW/m on the open ocean with values decreasing as the pole or the equator are approached. In tropical regions annual mean power levels of 10 - 20 kW/m are more typical.

Situated at the end of the long fetch of the Atlantic, the wave climate along the western coast of Europe is highly energetic. Higher wave power levels are found only in the southern parts of South America and in the Antipodes. The long-term annual wave power level increases from about 25 kW/m off the southernmost part of Europe's Atlantic coastline (Canary Islands) up to 75 kW/m off Ireland and Scotland. In the North Sea, the resource changes significantly, varying from 21 kW/m in the most exposed (northern) area to about the half of that value in the more sheltered (southern) area. In the Mediterranean basin, the annual power level off the coasts of the European countries varies between 4 and 11 kW/m, the

highest values occurring for the area of the south-western Aegean Sea. The entire annual deep-water resource along the European coasts in the Mediterranean is of the order of 30 GWh (See Fig. 2.4:).

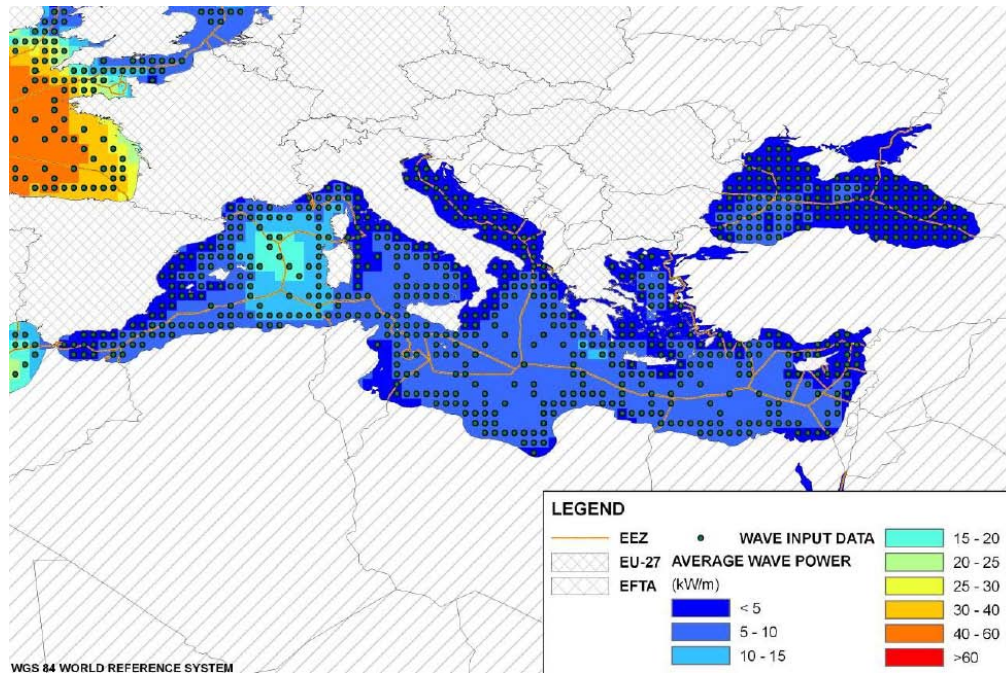


Figure 2.4: Map of the Mediterranean and Black Seas area with the wave energetic regimes illustrated in its corresponding areas. The units of the mean power contained in the waves is expressed in [kW/m].

As opposed to other types of energy sources, such as large wind turbines, in wave energy technologies there are many different methods to perform the energy absorption. Each kind of method uses the physical principle which achieves the highest rates in extracting energy and are based on the water depth and on the location, they can be placed at the shoreline, near-shore or offshore. In the early work, WEC were classified in only three different categories: Point Absorber, Terminator and Attenuator. That classification is still used nowadays, but just to a certain extent because it is quite poor and omits lots of devices used recently, it actually doesn't take into account any device that is not a float body. Consequently, all the devices placed onshore are not considered by this classification.

A point absorber is a device, typically axis-symmetric about a vertical axe with reduced dimensions in comparison to the wavelength of the incident wave. Terminator and Attenuator devices instead, have sizes of the same order of magnitude of the wavelength of the incident waves. The longest side of an attenuator is aligned with the direction of the wave front. The dominant direction of a terminator device is perpendicular to the direction of the incident wave (See Fig. 2.5).

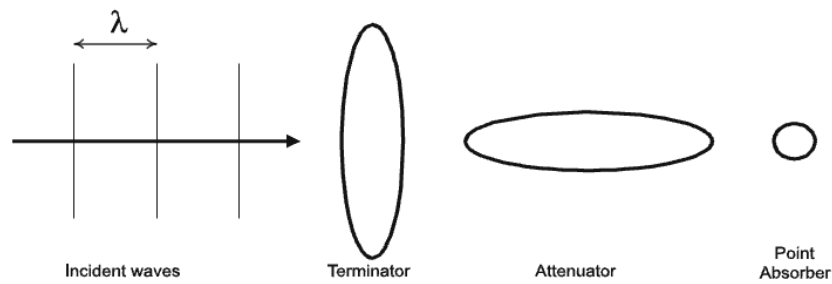


Figure 2.5: Raw description of the Wave Energy Converters type depending on its orientation corresponding with the incident wave direction.

The previous classification, as stated before, leaves apart different device categories, to solve that problem a new classification method came up. It consists in differencing the devices in generations; by now a third generation has been reached. First generation devices are those which are placed onshore or near-shore, typically OWCs. Second generation systems are represented by float pumps and are designed to operate at a wide variety of offshore and near-shore spots where high levels of energy are available in a range of water depth among thirty and a hundred meters. The third and last generation system at the moment it comprises large-scale offshore devices, with vast dimensions and power output. There is not a single form of third generation systems, it can be whether a large single device or a large array of much smaller devices. The former would be either an Attenuator or a Terminator and the latter without confusion it would be a power plant made of several point-absorber devices.

Afterwards, several methods have been proposed to classify wave energy systems depending on location, working principle and size. Figure 2.6 shows a classification of the more advanced technologies in the field, based mainly in the working principle.

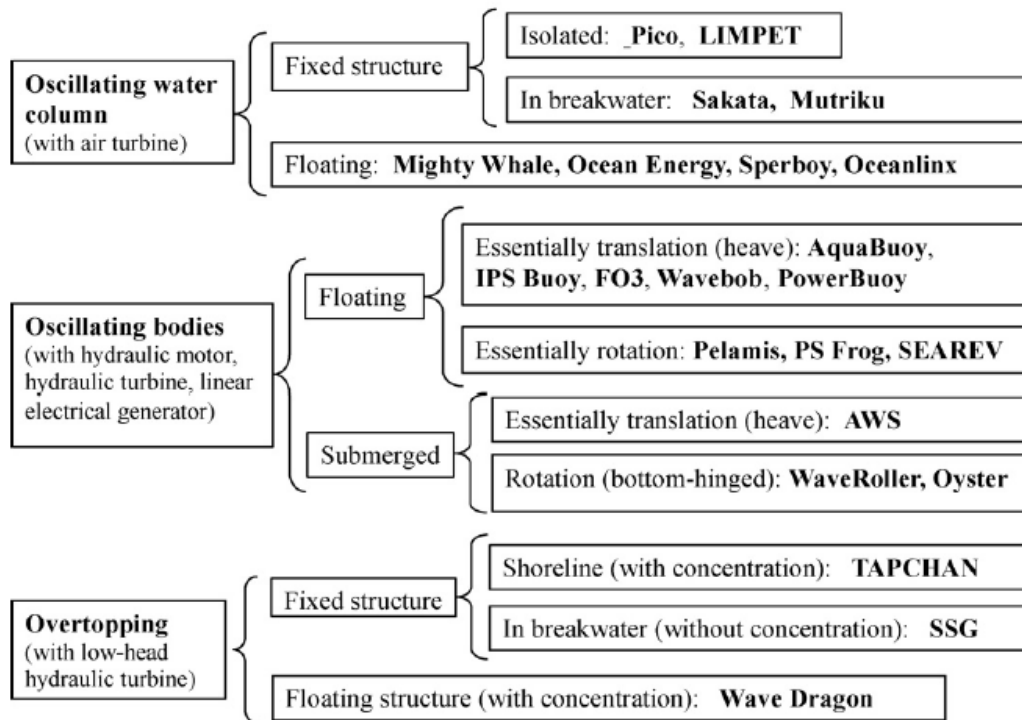


Figure 2.6: General division of WEC technologies

As it can be seen the first subdivision follows a criterion based on the energy conversion principle. Afterwards, comes another subdivision depending on the location of the device, in the case of the OWC and overtopping systems can be onshore or offshore. For oscillating bodies it is always offshore but the differentiation comes to specify if the device is at the water surface or beneath. The third differentiation is more specific, depending on the single kind of technology and can state more specifically the position or working principle.

The following and last part of this chapter will be dedicated to the description of the most successful devices in the current days, which will be also subdivided into several categories following the previous classification.

Fixed-structure OWC are usually placed in open coastal waters, in the majority of the cases are located on the shore line or near-shore; those devices would fit within the first generation system classification. Usually, these devices are fixed to the sea bottom or to a rocky cliff, which also includes port breakwaters. These devices have a major advantage in comparison with other types, which is the easier installation and maintenance, because they do not require deep-water mooring systems and long expensive electrical cables to drive the produced electricity to the main grid. Despite the less energetic wave climate that is given near shore due to wave friction with the seabed and wave breaking, the power outputs of these devices are of the same order of magnitude thanks to the compensation made by the natural refraction and diffraction.

The oscillating water column device is made of a steel or concrete submerged part, open to the open sea below the water surface, inside which air is trapped above the free water surface. The oscillating motion of the internal free water surface, produced by the incident waves, makes the air flow through a pipe in which an air turbine is installed; an electrical generator is connected to the turbine to perform the energy conversion. In the mid 1970s the axial-flow well turbine was invented, this technological advance avoids the need of installing rectifying valves in the turbine well which reduces substantially the cost of the installation and the maintenance tasks, this kind of valves were one of the major technical difficulties of these devices indeed (See Fig 2.7).

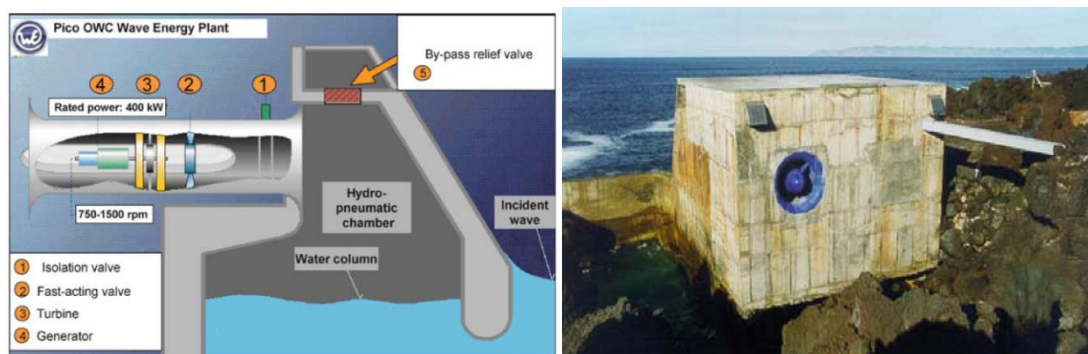


Figure 2.7: Sketch and picture of the OWC's Pico plant located in the Portuguese coast.

Their installed power capacity lies within the range of 60-500 kW with a maximum of 2 MW delivered by OSPREY plant. Unfortunately, the OSPREY plant had a short life, early after its inauguration the plant was hit, destroyed and sunk by the sea; it is believed that the main cause was its steel structure which wasn't strong enough to resist the waves' strokes in fully developed sea states. After that episode no more steel structured OWC are being constructed going back to the heavier and stronger concrete structures.

Since the early 1980s a new technological advance has been introduced in the construction of the fixed OWC power plants. It was discovered that by projecting the walls of the air-water chamber towards the direction of the incident waves, forming a harbor or a collector, the power absorption rates were increased. That meant a major deal in different aspects, not only the energy absorption was higher, it also allowed to reduce the construction costs. The cost of building a fixed-structure OWC plant it is by far way higher than any other entry in the budget for an OWC and that new discovery permitted to integrate the plant structure into a breakwater, which means constructional cost sharing, if a new breakwater is to be built, let's put an OWC plant in it, the cost won't be much higher and there will be a substantial profit based on the energy extraction. That technique makes also much easier operation and maintenance tasks. Good examples of that is the recently constructed breakwater at the port of Mutriku, Basque Country, Spain that includes 16 chambers and 16 Wells Turbines that produce 18,5 kW each. (See Fig. 2.8)



Figure 2.8: Aerial picture of the breakwater integrated OWC plant in Mutriku, Basque Country, Spain.

The OWC devices not only are placed onshore in the coastline or in harbor breakwaters they can also be found offshore in the form of floating-structures. There are basically two clear examples of this kind: the Backward Bent Duct Buoy also known as BBDB and the Mighty Whale. The BBDB bents backwards from the incident wave direction, which was discovered to be a great method to enlarge the size of the water column and through that principle, achieve resonance conditions while keeping the draught of the floating structure within a reasonable size. This device has been used in many countries to empower up to one thousand navigation buoys and since 2006 a 1/4th scale prototype is being tested in Galway Bay (Ireland) with the purpose to prove its feasibility to be grid connected (See Fig. 2.9).

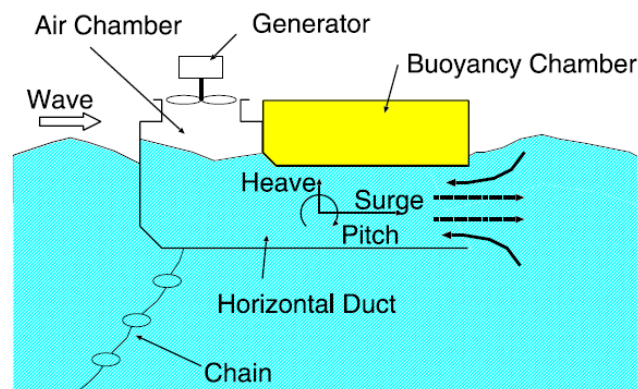


Figure 2.9: Schematic representation of the Backward Bent Duck Buoy. A floating structure OWC oriented backwards to improve energy absorption.

The Mighty Whale is the most famous OWC floating-structure. It has been developed by the Japan Marine Science and Technology Center. Is the only device of his kind in which a full dimension prototype has been built, its floating structure is 50 meters long, 30 meters wide, 12 meters draft and a weight of 4400 t. It has three air chambers located at the front, side by side and several buoyancy tanks. Each air chamber is connected to a Wells Turbine that drives an electrical generator with a total power rate of 110kW (See Fig. 2.10).

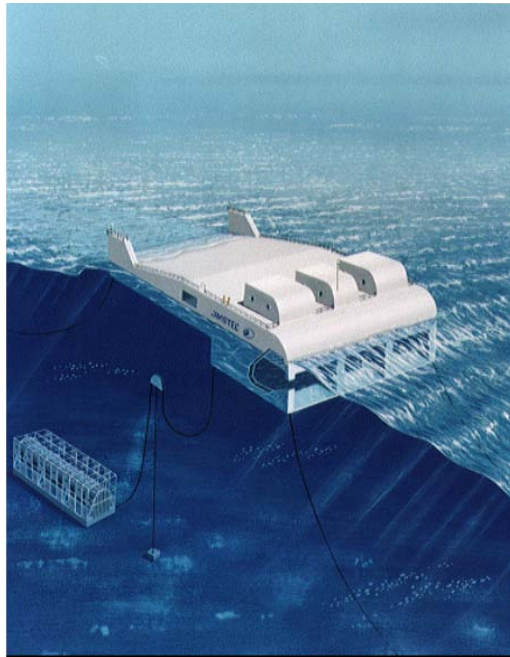


Figure 2.10: Computer rendering of the Mighty Whale. A floating Structure OWC designed in Japan.

The next step in this technology review is to describe the most successful Oscillating body systems. These are offshore devices, often classified as third generation systems and they can be floating in the free water surface or fully submerged below it. The fact that are not onshore or near-shore devices, usually located where the ocean is, at least, more than 40 meters deep makes them the device that exploits the sea in the most possible energetic regimes where there is virtually no loss of energy in wave propagation. Offshore wave energy converters are usually more complicated than first generation devices. Therefore, it is the less developed technology in the field and the one studied in the work of this Master Thesis. The reason for all this complexity is that comprises many different factors, not only the hydrodynamics of the floating body or the electromagnetic of their generators but the mooring systems, the access for maintenance or the need of long underwater electrical cables. The proof of this complexity is that, by now, there is not a single full scale prototype being tested in any of the oceans and seas of the world.

The simplest oscillating body device is the heaving buoy; the buoy reacts against a fixed structure, which can be a hydraulic turbine, an air turbine or a linear electrical generator, attached to the seabed. An early attempt was a device named G-1T, consisting of a wedged-buoy of rectangular plan form and whose vertical movement was guided by a steel structure fixed to a breakwater. The PTO used for the G-1T was a hydraulic ram. In Norway another heaving device was designed. It consisted of a spherical buoy attached to an air turbine, this device could be phase-controlled by latching to achieve the best oscillation regime.

An alternative design is a buoy connected to a structure fixed on the seabed through a cable which is kept tight a spring or an equivalent system. The relative motion between the excited floating body and the fixed structure is used by the PTO to convert the energy. The PTO can be an hydraulic turbine activated by high-pressure piston pump like in the device tested in the coasts of Denmark in the early 1990s or a linear electrical generator like the one developed by the Uppsala University in Sweden. A line from the top of the generator is connected to a buoy located at the ocean free surface, springs attached to the translator of generator store energy during half of a wave cycle act as a restoring force during wave troughs. Tests of a 3 meters cylindrical buoy are being conducted by the Uppsala University (See Fig 2.11).

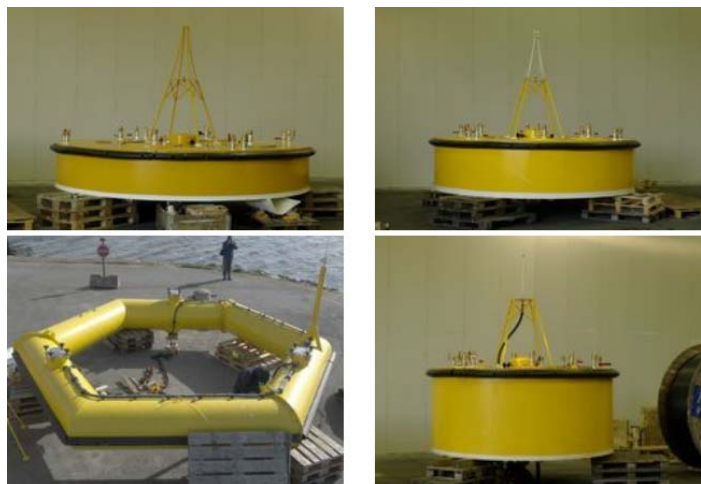


Figure 2.11: Four different pictures of the tests conducted in Uppsala University. Each picture shows a different buoy of the same kind of WEC, floating body point absorbers.

There is though, a major problem when talking about a single floating body reacting against a bottom fixed PTO, which is the distance between the two elements, one way to solve that problem is by thinking of a multiple body system in which the distances are not so big. The energy is converted from the relative motion between two bodies oscillating differently, but also this kind of device raises another kind of problem, control problems. The two-body point absorber concept it could be described as a two point heaving system. It consists of two floaters, the outer one, which has to have very low resonance frequency, works as a structure

that provides a reference for the inner body that acts as a resonating absorber. The mass of the inner body is increased connecting it to a fully submerged body located deep enough to have no effects on diffraction and damping forces.

One of the most interesting two-body systems for wave energy conversion is the IPS buoy, developed in Sweden by the company Interproject Service. This is made of a buoy rigidly connected to a fully submerged tube open at both ends. The tube hosts a piston whose relative motion to the float-tube system drives a power take off mechanism. To solve the end-stop problem the tube bells out to either end from the center part to limit the stroke of the piston. A half scale prototype was built in the mid 1980s and tested in Sweden. A very similar device is the AquaBuoy, developed in the 2000s, uses the IPS concept mixed with a pair of hose pumps to produce a high pressure water flow that drives a Pelton turbine instead of a piston, this device is being tested in the coast of Oregon, USA, since 2007. The Wavebob is one of the latest devices introduced in society; it is still under development in Ireland. It consists of two co-axial axe-symmetric buoys which relative motion is converted into electricity through a high-pressure-oil system. The inner body is connected to another coaxial submerged body whose function is to increase the inertia without affecting other coefficients such as the diffraction or radiation coefficients, a 1/4th scale prototype is being tested in Galway Bay, Ireland.

To finish with the heaving body category there is only one kind left to be explained, the fully submerged heaving systems. The Archimedes Wave Swing also known as AWS is a fully submerged heaving device basically developed in Holland and consists of an air filled chamber fixed to the seabed and open at the top (the silo), closed by another cylinder (the floater). An air lock is created between the two cylinders and so water cannot flood the silo. The floater is pushed down when the crest of the wave passes above it and moves up when the trough passes above it, this movement obeys the instantaneous pressure which varies while the wave passes through, it increases with the wave crest and decreases with the wave trough. The conversion of mechanical energy into electrical energy is made via a linear electrical generation. The AWS was the first device using that PTO principle and is being tested since the second half of 2004 (See Fig. 2.12).

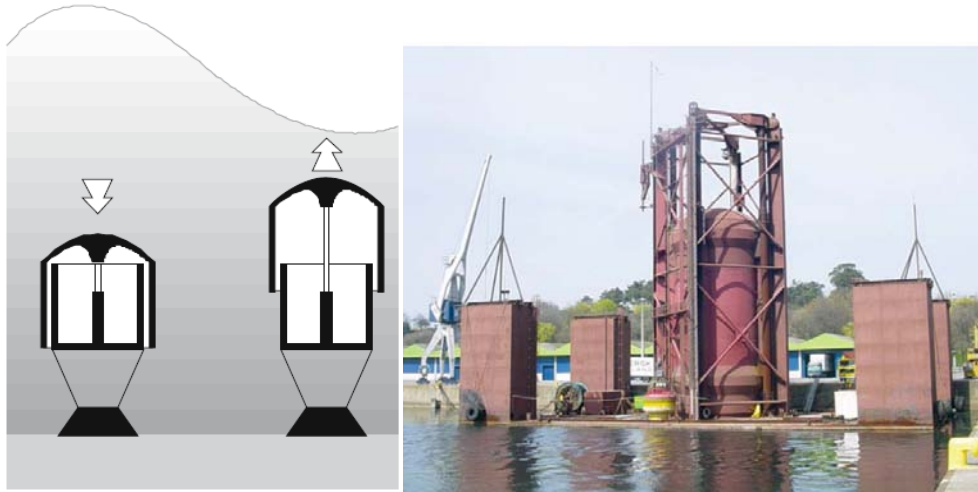


Figure 2.12: Schematic illustration of the working principle of the AWS WEC and picture of the prototype.

The wave energy converter devices briefly described above are heaving systems; that is to say, the energy conversion is performed through a relative translation motion. There are other oscillating-body systems in which the energy conversion is based on relative rotation, mostly pitch, this is the case of the Salter Duck, mentioned in the first part of this chapter. It is basically a cam-like floater oscillating in pitch. The first versions consisted of a string of Ducks mounted on a long spine and located along the wave crest direction, which would be an attenuator WEC, the energy conversion was performed by a hydraulic-electric PTO system. Afterwards, a solo Duck was proposed, in which the frame of reference against which the nodding duck react was provided by gyroscope. Unfortunately, this device never reached the stage of full-scale prototype tested in real seas.

Probably one of the most important wave energy converters is the Pelamis, that device is the only offshore device that has reached the commercialization phase, although it was for a short period of time as it will be seen later on that description. The Pelamis, developed in the UK, is a snake-shaped slack-moored articulated structure made of four cylindrical sections attached by hinged joints. It is another attenuator device and therefore, it is placed on the wave direction.

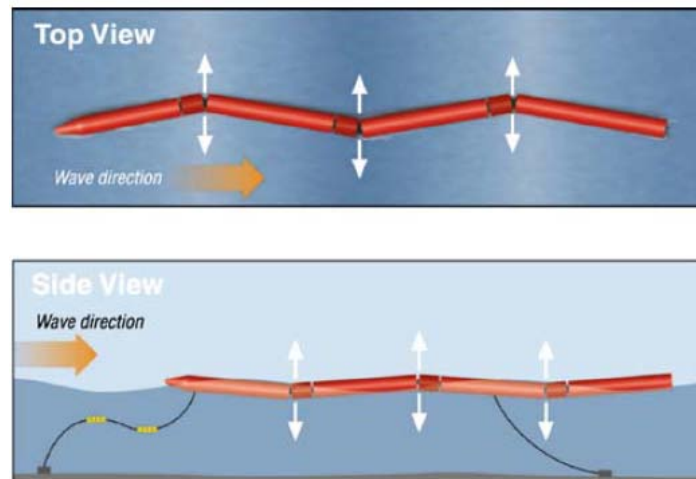


Figure 2.13: Schematic top and side views of the Pelamis device.

The motion induced by the waves in these joints is captured by hydraulic rams that transfer that motion into high pressure oil pumps that drive hydraulic motors coupled to electrical generators. Gas accumulators provide energy storage.

After years of research, beginning with theoretical/numerical modeling and continuing with physical model testing at several scales, sea trials of a full scale prototype took place in Scotland the year 2004. Finally, by the second half of 2008 the northern Portuguese coast hosted the first and, until now, the only grid-connected wave farm, composed of three Pelamis units of 750 kW each. The dimensions of this device are quite astonishing, being one of the largest devices developed, it is 150m long and has a diameter of 3.5m. After some months of operational state of the wave farm, the rams of the devices didn't resist the conditions of a particularly violent storm and the result was catastrophic, resulting in all the devices being useless. Nowadays the wave farm is still inoperative and the company responsible of the devices is working to improve the resistance of the devices in the worst possible conditions. The figures below report some steps of this process to the wave farm.



Figure 2.14: Different Pictures of the Pelamis device. The first picture shows the prototype in a front view while it was being tested in the English coasts. The Second shows how it was introduced into the water. The third pictures shows the wave energy plant that was installed in the Portuguese coast, composed by three devices.

The Searev wave energy converter, developed at Ecole Centrale de Nantes, France, is a floating device containing a heavy horizontal-axis wheel that works as an internal gravity reference. The center of gravity of that wheel is not centered, that makes the mechanic equivalent to a pendulum when it is spinning due to the passing through of the incident wave. The wheel is connected to an electrical generator via two hydraulic rams. Major advantages of these systems are: first, all the moving parts are protected from the sea action because they are placed in the inner part of the device and second, the fact that the mechanism is just a wheel spinning and working as a pendulum avoids the need of end-stop systems due to that it won't be any kind of stroke that could damage the system (See Fig 2.15).

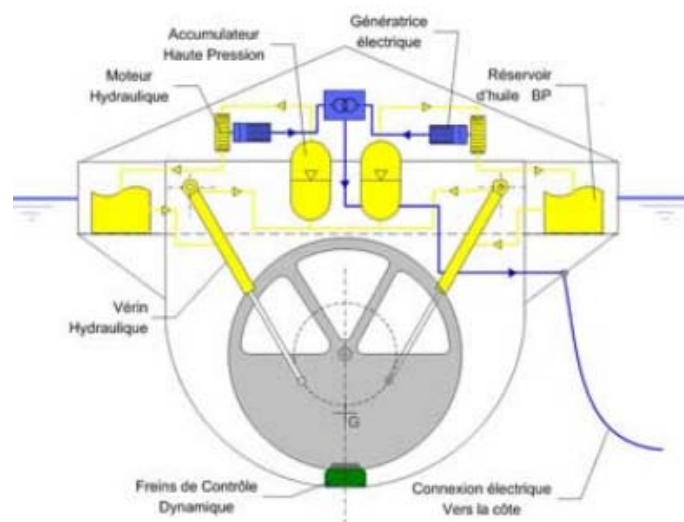


Figure 2.15: Schematic illustration of the SeaRev device. Including its mechanical, hydraulic and electric elements.

The Spanish company Ocean Tec is developing another offshore floating energy converter that extracts the energy basically from the pitching motion. It has the shape of an elongated horizontal cylinder with ellipsoidal ends whose major axis is aligned with the incident wave direction. The energy conversion process is based on the relative inertial motion that the waves cause in a gyroscopic system. A 1/4th scale prototype was deployed in Gipuzkoa, Basque Country in Spain, in September 2008 and was tested for several months.

Single oscillating-body devices operating in pitching mode have been proposed, based on the inverted pendulum concept hinged at the seabed. A buoyant flap hinged at the sea bed, whose pitching oscillations activate a set of double-acting hydraulic rams located on the sea bed that pump high-pressure fluid to the shore via a sub-sea pipeline. The fluid flow is

converted into electric energy by a conventional hydraulic circuit. These devices are intended to be deployed near shore at a maximum depth of 20 meters.

The most famous device of this kind is the Oyster, which is under development in UK. This device has a surface piercing flap that spans the whole water depth and the hydraulic fluid used to generate electricity is sea water that powers a Pelton turbine placed onshore. This device has a significant weak point though; the hydraulic rams and the junctions of the different moving parts can end up blocked by the sand and by deposits carried by the ocean currents.

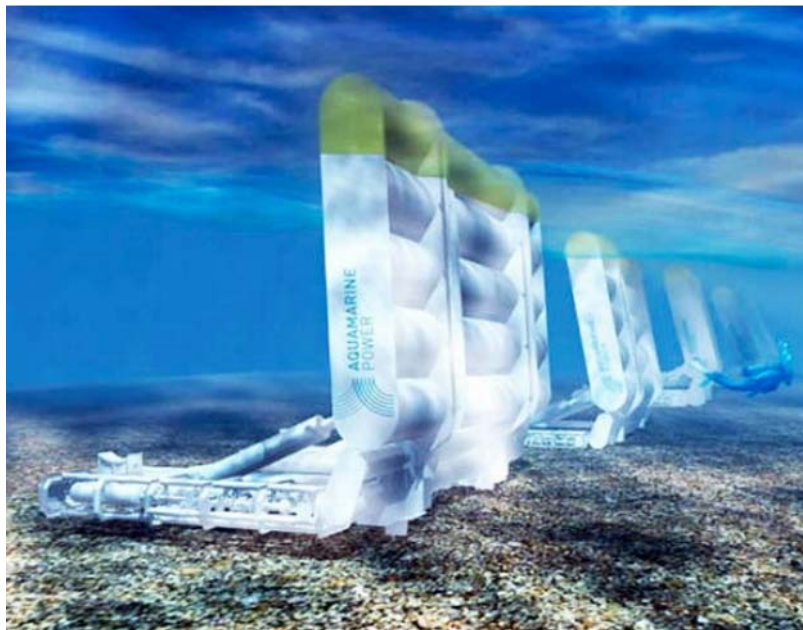


Figure 2.16: Computer rendering of a wave energy plant made of Oyster devices, developed in the U.K.

A very different way of converting wave energy is to capture the water that is close to the wave crest and introduce it by over spilling into a reservoir where it is stored at a level higher than the average free surface level of the surrounding sea. The potential energy contained in the stored water is converted into useful energy through conventional low-head hydraulic turbines. The hydrodynamic behavior of the overtopping devices is strongly non-linear and, unlike the cases of oscillating water column devices and oscillating body devices cannot be approached by the linear water wave theory.

The Tapchan (Tapered Channel Wave Power Device), is a device developed in Norway in the 1980s and deployed in Toftestallen, Norway, in 1985. The Tapchan contains a collector, a converter, a water reservoir and a low-head water turbine. The horn-shaped collector gathers the incoming waves and directs them towards the converter, in the Toftestallen prototype the

collector was directly carved in the rock and is about 60 meter wide at its wider point in the entrance. The converter is a channel which section gradually gets narrower, the walls of that channel has the same height as the reservoir maximum water level. The waves enter the wide section of the channel and as they propagate down to the narrowing end, the wave height is gradually amplified until the water of the crest spills over the walls of the collector and fills the reservoir. As a consequence, the wave energy is gradually converted into potential energy in the reservoir which in turn will be later converted into kinetic energy by the turbine that drives an electrical generator. It is usually used a conventional low-head Kaplan turbine by that purpose. The main function of the reservoir is to supply a constant flow of water, which means that it must be large enough to smooth the fluctuations of the water overtopping the converter walls, about a surface of 8500 m². The Norwegian prototype has a power rate of 350 kW (See Fig. 2.17).

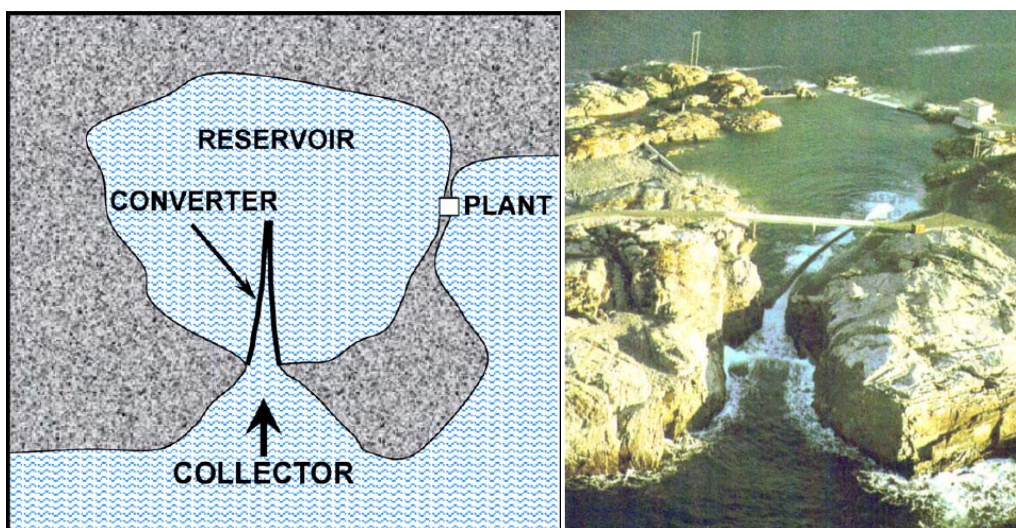


Figure 2.17: Illustration of the working principle and picture of the Tapchan power Plant in Norway.

The Wave Dragon is one of the foremost technologies within the field of wave power. Unlike most other devices this one does not oscillate with the waves; it gathers the wave energy passively by utilizing the overtopping principle. The front face of the device is a curved ramp, incoming waves surge up it, as if it were a beach. Behind the crest of this ramp lies a reservoir which gathers the “overtopping” water which now has higher potential energy than the surrounding water. The effect of Wave Dragon is amplified by long reflector wings. Mounted to the reservoir, they channel the waves towards the ramp. The energy is extracted as the water drains back to the sea through low head hydraulic turbines placed in the reservoir. The Wave Dragon is designed as a floating offshore device to be placed in water depths above 20

m. These areas are where the highest wave energy is, and also where it is easiest to gain the permission to deploy. Over three years, sea testing has been conducted on a prototype in Northern Denmark. This device is by far the largest envisaged wave energy converter today and each unit will have a rated power of 4–11 MW or more depending on how energetic the wave climate is at the deployment site. This will be a device with a displacement of approximately 30,000 tones and dimensions that can reach 57 meters wide. This size brings many advantages, the device will respond minimally to waves, reducing fatigue problems. Also as it is large and stable it will be possible to work on board the device, which will drastically reduce maintenance costs and downtime. As an overtopping device, there are also many advantages from the robustness of the design, in particular there are no end-stop problems as in larger seas the waves will wash over the platform harmlessly (See Fig. 2.18).

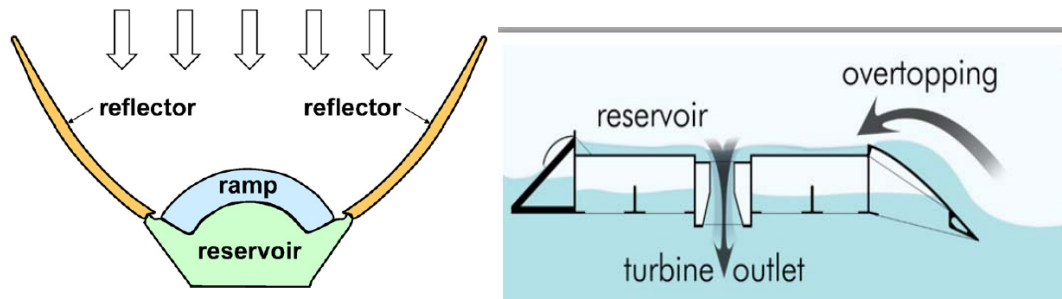


Figure 2.18: Top and front view of the Wave Dragon device and illustration of the working principle.



Figure 2.19: Picture of the Wave Dragon prototype.

CHAPTER 3:

THEORY

3.1 WAVE MECHANICS

3.1.1 WAVE GENERATION

The most common and normally the most important waves in the spectrum of sea waves are those waves generated by the wind. Wind-generated waves are much more complex than the typical mono-chromatic wave widely used in literature. To have a complete outlook of the waves behavior at the sea it is crucial to understand how they are generated. It is important to have a means to quantify wind-generated waves for many varied uses in engineering. It is also important to predict this waves for a given wind condition, essentially those extreme wind-generated wave conditions that will be used as the limit for engineering design. The record of a water surface time history, measured at a point, when storm conditions are given shows a very irregular trace of the free water surface. A wave record taken at the same time at a nearby location shows a very different pattern but it has similar statistical properties. The records of a particular area might contain locally wind-generated waves from an existing storm superposed on lower waves having different range of periods, and these were generated by previous winds acting in a different area, even thousands of kilometers away.

The average height and period of the wind-generated waves grow as the wind speed, duration and the distance or fetch over which the wind blows increase. For a given wind speed, and unlimited fetch and duration there is a limit to which the average wave height and period cannot overtake. That happens because at this stage the rate of energy input to the wave from the wind is balanced by the rate of energy dissipation due to wave breaking and surface water turbulence. When that energetic balance is reached by the ocean is known as the fully developed sea state. Fortunately the fully developed sea state is not commonly reached, not even in large storms.

Waves that are in middle of the generation process have crests that are short and not very well defined. The crests have not only one direction of propagation; they propagate within a span around the dominant wind direction. As the waves propagate through the area where the wind is active, they gradually grow in average height and period. After leaving the area of active wind generation, the surface profile becomes smoother and the crest gets longer and more distinguishable, these types of waves are known as swell. The swells propagates keeping almost all the energy stored in the waves, there exist minimal energy losses due to air resistance, internal friction but mainly because of angular speeding of the wave field. That makes longer waves to propagate ahead of the shorter ones in the field of swell. Once reached the surf zone, also called near-shore, the longest waves predominate above the smaller ones. It is though, in that area when some phenomena start occurring, phenomena like shoaling, refraction and diffraction due to the no longer negligible seabed's action. Finally the wave breaking occurs setting free the majority of the energy contained in the sea wave. The table presented below summarizes in a schematic way the birth-to-death process of a sea wave.





Wave type	Breaking	Shoaling	Swell	Sea
Environment	Shallow water-surf zone	Inner continental shelf	Deep water >>100m	Deep water >>100 m Long fetch= sea/ocean surface Wind velocity waves Wind duration waves Wind direction = wave direction
Distance travelled	100 m	1km	100s-1000s km	100s-1000s km
Time required	seconds	minutes	hours to days	hours to days
Wave profile				
Water depth	1.5 x water depth	<100m	>>100 m	>>100m
Wave character	wave breaks wave bore swash	higher shorter steeper same speed	regular lower longer flatter faster	variable height high short steep slow
Example; height(m) period(s) length(m) speed(km/hr) distance travelled (km/day)	2.5-3m 12 s 50-0 m 15-0	2-2.5m 12 s 220-50m 66-15	2 m 12 s 220m 66 km/h 1600 km/day	3-5 m 6-8 s 50-100 m 33-45 km/h 800-1100 km/day

Table 3.1: Birth-to-death process of sea waves. States the process since are generated in an irregular form by the wind pressure until they finish breaking against the shore losing the energy gathered in the travel, going through the swell and shoaling states.

Wind blowing over the surface of a water body will transfer energy into the water in the form of surface current and by generating waves on the water surface. There are turbulent pressings in the wind field that apply a fluctuating pressure on the water surface. These fluctuations are not strictly periodic and can quickly vary in magnitude and frequency, they move forward within a range of velocities. These fluctuations cause the water surface to undulate, develop and grow. This growth is mainly achieved as a result of a resonant interaction that takes place between the forward moving fluctuations and the free waves propagating at the same speed as the pressure fluctuations. Once the wave is born and somewhat consolidated another mechanism takes action, as the wind blows over a forward moving wave a complex air flow is formed over the wave. This flow implies a secondary air circulation that is set up around a wave crest parallel axis. Consequently, below that axis, where the wind velocity is equal to the wave celerity, the air flow is reversed relatively to the forward moving wave profile. As opposed to that point, above the axis, the air relative velocity has the same sign as the wave celerity. Therefore, a flow circulation in a vertical plane above the wave surface is created, that flow causes a pressure distribution on the surface that is out of phase with the surface displacement resulting in a momentum transfer to the wave that selectively amplifies the steeper waves i.e. the steeper is the wave the faster it grows. There are also shear effects on the growth of waves but they have been proved of minor significance. Wave to wave interaction also causes substantial effect on wave growth, being the smaller wave that transfers the energy into the bigger one under certain conditions such as the right phase and direction.

For wave prediction, wave climate analysis, design of coastal structures or design of floating devices is convenient to choose a single wave height and period to represent a full spectrum of wind-waves. If the wave heights from a wave record are ordered by size it is possible to define a height H_n , that would be the average of the highest n percent of the wave heights. E.g. H_{10} is the average of the highest 10% of the waves in the record or H_{100} is the average of the wave height of the whole record. The most commonly used representative wave height is H_{33} which is the average height of the highest one-third of the record and it is called the significant height H_s , this parameter has been chosen because it is, approximately the height that an experienced observer would report when visually estimating the height of waves at sea. The significant period T_s is the period corresponding to H_s , that is to say, the average period of the highest one-third waves in the record.

Whether the significant wave height or the significant wave period as well as the resulting spectrum, are directly related to the distance over which the wind blows, usually known as fetch F , are also related to the wind speed W and to the duration of that wind t_d . Some other factors such as the fetch width, the water depth, atmospheric stability, the temporal and spatial variability in the wind field or the bottom characteristics if the water depth is shallow enough can, to some extent, affect those wave defining parameters. Waves are generated with

propagation directions that cover a range of oblique angles, in other words, less than 90° from the direction of the wind. As stated before, the waves propagate through the fetch increasing their period whereas their range of directions decreases proportionally. For this reason, the narrower the fetch is the fewer the possibilities are that a short wave has to remain within the fetch limits and grow in size. The water depth affects the water surface shape and its kinematics, hence its energy transfer from the wind. Bottom friction it also dissipates energy thus retarding the rate of growth and the ultimate wave size and the atmospheric stability affects directly the wind field affecting in turn the wave generation. But, except for some specific cases, all these factors are usually neglected due to their small contribution to the wave formation and growth. The only parameters left to be considered are the fetch length F , the constant wind speed W , and the duration of the blowing wind t_d . If the wind duration exceeds the time required for the waves to travel the whole fetch length i.e. $t_d > F / C_g$ the waves will grow continuously and their characteristics at the end of the fetch will depend on F and the wind speed W , this is known as fetch limited condition and would be represented by the line OAB in the figure 3.1. On the contrary, if the duration of the wind doesn't allow the waves to travel along the whole fetch, the waves reach a certain size and then become stable, which is what is known by the term duration limited and in figure 3.1 is represented by the line OAC. If the fetch length is extremely big and the wind duration permits the wave to go along the entire fetch, note that the line AOB, in figure 3.1, would tend to be horizontal and then the conditions of fully developed sea would have been reached, but as previously said that rarely occurs, not even with the biggest storms in the middle of the ocean. Outside the generation area or for bigger distances than F , the waves propagate as swell reducing its height and increasing its period minimizing their energy losses (See Fig. 3.1).

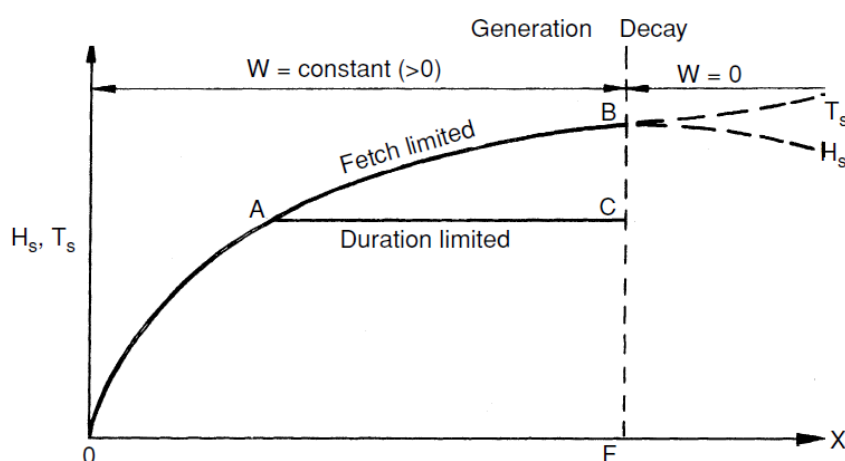


Figure 3.1: Graphical representation of the wave generation.

The characteristics of waves generated by a given wind condition may also be defined by a wave spectrum, which is a plot of the wave density of energy at each component period or frequency versus a range of component periods or frequencies. Figure 3.2 shows a series of typical wave spectra at successive point along the fetch. Note that the peak frequency decreases as the wave spectrum grows along the fetch. The total area under the spectrum curve is the total amount of energy which in turn, is related to the significant height, this area grows as the waves travel through the fetch. One of the most interesting things though, is that if the figure 3.2, which is function of the position in the fetch, was done at the same point but in five different consecutive time lapses, the pattern of the spectra wouldn't change that much or, in other words, the wave spectrum, apart from being position-dependent it is also time-dependent.

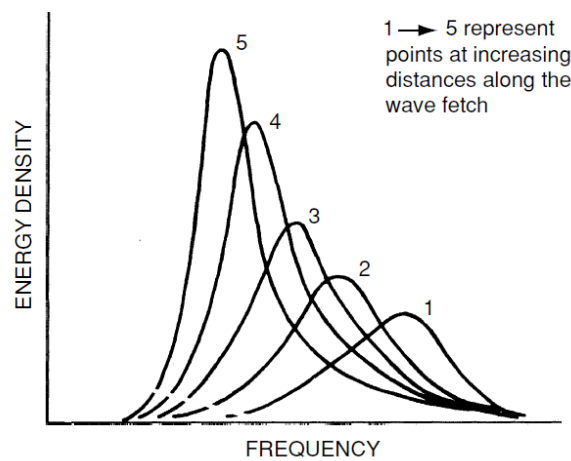


Figure 3.2: Variation of the Wave Spectrum depending on which point of the Fetch the measurement is done.

3.1.2 WAVE ANALYSIS AND STATISTICS

The general understanding of wind-generated waves comes mostly from the analysis of wave records. Most of these records are point measurements of the water surface in a fixed point at different time lapses during a period of several minutes, even hours in some cases. There are mainly two ways to perform these analyses. The first way consists of identifying individual waves in the record and statistically analyzing the heights and periods of these waves. The second and not widely used technique is based on conducting a Fourier analysis of the wave record to develop a full wave spectrum. Both ways will be shown in this chapter following the previous order.

Figure 3.3 is basically a graphical representation of a short fragment of a typical wave record. The most commonly used analysis procedure is called the zero-crossing, which has two variants, the so called zero-up-crossing and the zero-down-crossing, both variants have exactly the same validity and the results will be totally equivalent but usually and by default the most commonly used is the zero-up-crossing (Pierson, 1954). A mean water surface elevation is set and each point that crosses that zero elevation in the upward direction is noted down. The elapsed time between two consecutive points is the wave period and the maximum vertical distance between the wave crest and trough is the wave height. The zero-down-crossing follows the exact same procedure but following the downward direction to mark the points. Note that small fluctuations are left apart from the counting, that way high frequency components are directly filtered out.

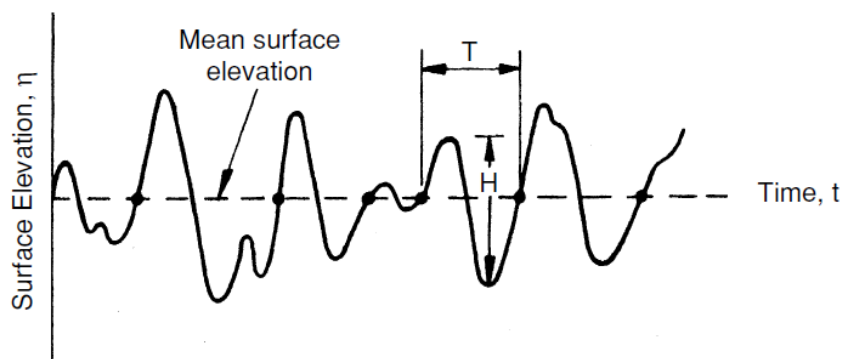


Figure 3.3: Illustration of a wave record representing the sea surface elevation over the time.

A major concern in the analysis is the distribution of heights in the record. If those wave heights are plotted as a height-frequency distribution, note that in this case frequency means frequency of occurrence; that is probability. Figure 3.4 represents an example of that distribution where $p(H)$ is the frequency of occurrence and H is the wave height. The shaded area is the upper one-third of the wave height and its average gives the significant height.

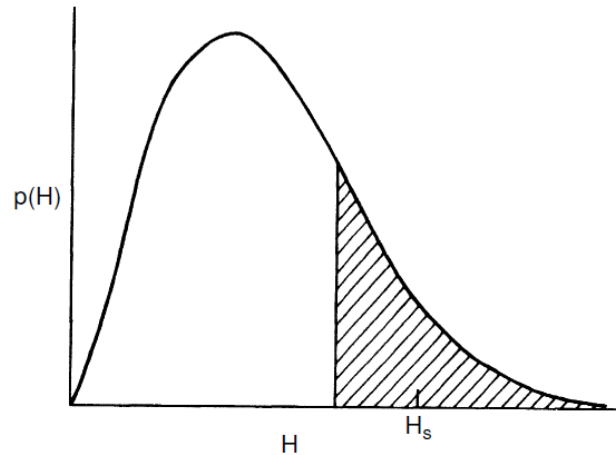


Figure 3.4: Graphic of the probability distribution of the different wave heights registered in a wave record.

For engineering purposes the most important distribution of wave heights is the one generated by a storm for obvious reasons. Longuet-Higgins (1952) proved that this kind of distribution is well defined by a Rayleigh's probability distribution.

The Rayleigh's distribution can be written by the following expression:

$$p(H) = \frac{2H}{(H_{rms})^2} e^{-\left(\frac{H}{H_{rms}}\right)^2} \quad (3.1)$$

Where the root mean square height H_{rms} is given by

$$H_{rms} = \sqrt{\frac{\sum H_i^2}{N}} \quad (3.2)$$

Where H_i is the individual wave among N waves that the wave record contains. From the Rayleigh distribution some useful relationships can be extracted:

$$H_S = 1.416H_{rms} \quad (3.3)$$

$$H_{100} = 0.886H_{rms} \quad (3.4)$$

The cumulative probability distribution results in:

$$P(H) = \int_0^H p(H)dH = 1 - e^{-\left(\frac{H}{H_{rms}}\right)^2} \quad (3.5)$$

For engineering purposes is much more interesting to know the percentage of waves which have greater heights that the given height

$$1 - P(H) = e^{-\left(\frac{H}{H_{rms}}\right)^2} \quad (3.6)$$

From equation (3.3) the following expressions is deduced

$$1 - P(H_s) = e^{-(1.416)^2} = 0.135$$

So the 13.5% of the waves in a storm record might have higher heights than the significant height. Figure 3.5 is a very useful adapted form of the Rayleigh's distribution, line a gives the probability P that any wave height will exceed the height rate (H/H_{rms}) and line b gives the average height of the n highest fraction of waves.

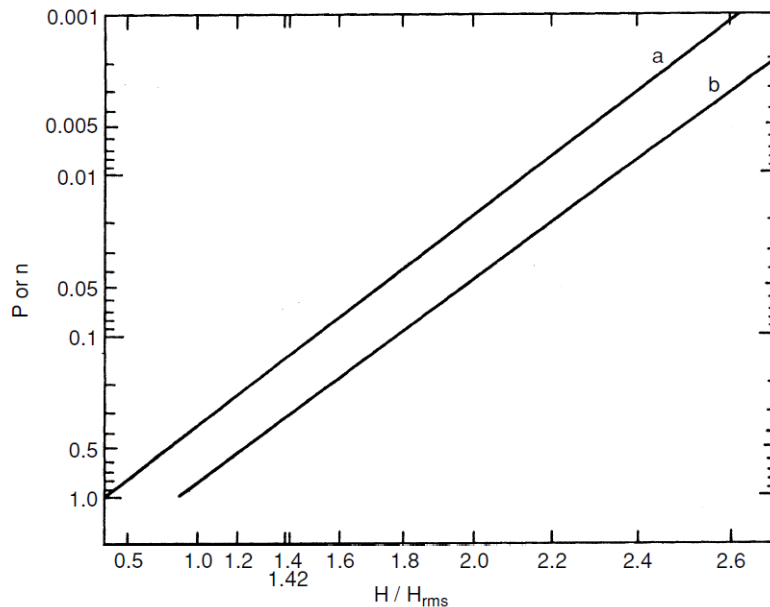


Figure 3.5: Logarithmical adapted version of the Rayleigh distribution made by the U.S. Naval Forces.

When a spectrum of waves reaches the shore, wave breaking limits the wave's height distribution at a higher end. Some authors have modified the Rayleigh's distribution to explain that behavior. There is no upper limit to the wave heights specified by the Rayleigh's distribution. Longuet-Higgins (1952) demonstrated that for a storm with relatively large number of waves N, the expected value of the height of the highest waves would be

$$H_{max} = 0.707H_s\sqrt{\ln N} \tag{3.7}$$

That equation is valid in the offshore areas where the waves are not affected by the seabed and there are no breaking conditions which due to its highly non-linear behavior void the validity of the expression.

The joint wave's height-period probability distribution can be of some interest. Figure 3.6 shows the shape of that distribution, it shows the distribution of the wave height versus the wave period of a typical record, note that the values are non-dimensionalized by diving them by the average wave's height and period from the record. The contour lines are lines of equal probability of occurrence for that couple height-period to happen. The significant period T_s is considered to be more statistically stable than average period and therefore, is preferred to

represent the records. When using a spectral approach to analyze a wave record another parameter comes to surface, the peak period T_p . As the name tells that is the period of the most energetic wave from the spectrum and it is a crucial parameter when designing sea structures and other devices. Its value can be calculated through the following expression:
 $T_s = 0.95T_p$.

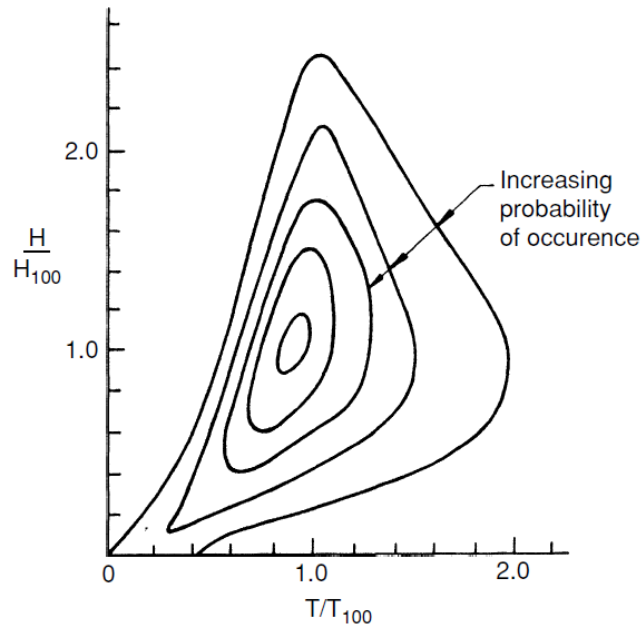


Figure 3.6: Non-dimimensionalized graphic which shows the curves of equal-probability of waves' heights over the waves' periods.

Another way to analyze a wave record is by determining the resulting wave spectrum for that record. A water surface profile can be reproduced by a series of sine waves with different periods, amplitudes, phases and propagation directions. A directional wave spectrum is produced when the sum of the energy density in these component waves at each wave frequency $S(f, \theta)$ is plotted versus wave frequency f and direction θ . A specific version of it is plotted at a single direction and only versus the frequency $S(f)$ or in the alternate version in which the energy density is plotted versus the period, the inverse function of the frequency, $S(T)$. From the linear wave theory the energy density of a wave is $\rho g H^2 / 8$, leaving apart the fluid density ρ and the acceleration of gravity g the following expression for directional wave spectrum is developed:

$$S(f, \theta) df d\theta = \sum_f^{f+df} \sum_{\theta}^{\theta+d\theta} \frac{H^2}{8} \quad (3.8)$$

Where H is the wave height in the record, this expression is simplified for the one-dimensional spectrum as:

$$S(f) df = \sum_f^{f+df} \frac{H^2}{8} \quad (3.9)$$

The expression for the one-dimensional spectrum dependent on the wave period is:

$$S(T) dT = \sum_{T}^{T+dT} \frac{H^2}{8} \quad (3.10)$$

The relation between both spectra is the following:

$$S(f) = S(T)T^2 \quad (3.11)$$

The exact scale and shape of a wave's spectrum depends on the generating factors, previously stated in the first section of that chapter such as the wind speed, the duration of the wind and the fetch. Nonetheless, a general form of a spectral model equation is:

$$S(f) = \frac{A}{f^5} e^{\frac{-B}{f^4}} \quad (3.12)$$

Where A and B are scale adjusting factors and can be written as functions of the generating factors or as functions of the representative wave parameters such as the significant wave height and period (H_s and T_s). An important way to define a wave spectrum can also be by the moments of that spectrum, the n^{th} moment of a spectrum can be defined as:

$$m_n = \int_0^{\infty} S(f) f^n df \quad (3.13)$$

For instance, the zeroth moment is the area below the spectral curve of the plot and since a spectrum shows the density of energy at each frequency versus a range of frequencies, the area below that curves equals to the total energy of the wave spectrum.

From the linear wave theory, the total energy density is twice the potential energy density of a wave and it can be written as:

$$\bar{E} = 2\bar{E}_p = \frac{2}{T_*} \int_0^{T_*} \rho g \eta \left(\frac{\eta}{2} \right) dt \quad (3.14)$$

Where T_* is the length of the analyzed wave record and the bar over the E denotes the energy density. The equation 14 can be rewritten as:

$$\bar{E} = \rho g \bar{\eta}^2 = \frac{\rho g \sum \eta^2}{N_*} \quad (3.15)$$

In that occasion the bar over the E denotes the average sum of N_* water surface values from a wave record of length T_* . From the definition of H_{rms} and H_s the energy density can also be expressed as:

$$\bar{E} = \frac{\rho g H_{rms}^2}{8} = \frac{\rho g H_s^2}{16} \quad (3.16)$$

If the zeroth moment of a spectrum equals the total energy density divided by the fluid density and the gravity's acceleration; combining the equations 3.15 and 3.16 the following expression is obtained:

$$\bar{E} = \rho g m_0 = \frac{\rho g \sum \eta^2}{N_*} = \frac{\rho g H_s^2}{16} \quad (3.17)$$

Reorganizing the equation 3.17, the expression of the significant height for a wave spectrum is deduced as:

$$H_s = 4\sqrt{m_0} \quad (3.18)$$

Where, from now on H_s will be named as H_{m0} for semantic reasons since H_s was directly obtain from a wave record and H_{m0} it has been obtain from a wave spectrum analysis.

The Rayleigh's distribution is a useful model for the expected distribution of wave heights for stormy conditions, but it is not enough. It is also useful to have other models to determine that wave spectrum. Several one-dimensional wave spectra have been proposed and they all generally derive from the main equation presented above, the equation 3.12. The two most commonly used models will be presented and described in the following lines. The first one is the Pierson-Moskowitz Spectrum Model (Pierson and Moskowitz, 1964). The authors analyzed wave and wind records from British weather ships operating in the north Atlantic and selected records representing, in the majority of the cases, fully developed seas for wind speeds between 20 and 40 knots to generate the spectrum shown below:

$$S(f) = \frac{\alpha g^2}{(2\pi)^4 f^5} e^{-0.74\left(\frac{4g}{2\pi W f}\right)^4} \quad (3.19)$$

Where W is the wind speed measured at 19.5 meters of altitude which is usually from 5% to 10% higher than the speed measured at the standard elevation of 10 m above the sea level. Other formation parameters such as the fetch or the duration are not taken into account due to the fully developed sea conditions which allows neglecting them. The alpha coefficient equals to 8.1×10^{-3} . At much higher speeds than 20 to 40 knots, that spectrum shouldn't be used because it is thought for fully developed seas and at that wind speeds it is highly improbable for those conditions to be reached. The following expressions derive from the Pierson-Moskowitz spectrum formulation:

$$H_{mo} = \frac{0.21W^2}{g} \quad (3.20)$$

$$f_p = \frac{0.87g}{2\pi W} \quad (3.21)$$

The other widely used spectrum model it's called JONSWAP (Hasselmann et al., 1973) and comes from Joint North Sea Wave Project and it was elaborated by laboratories from four different countries. Wave and wind measurements were taken with sufficient wind durations to produce a deep water fetch limited model spectrum. The model development begins with a simple association, if the wind speed W is isolated from equation 3.21 and then substituted to the general equation of the Pierson-Moskowitz model, equation 3.19, the result is the following:

$$S(f) = \frac{\alpha g^2}{(2\pi)^4 f^5} e^{-1.25\left(\frac{f_p}{f}\right)^4} \quad (3.22)$$

The JONSWAP's spectral equation is a slight modification of that last equation, equation 3.22, and is achieved by developing relationships for α and f_p in terms of wind speed and fetch. Finally, enhancing the spectrums peak by a factor γ , the JONSWAP spectral equation looks like that:

$$S(f) = \frac{\alpha g^2}{(2\pi)^4 f^5} e^{-1.25 \left(\frac{f_p}{f}\right)^4} \gamma^a \quad (3.23)$$

Where

$$a = e^{-\left[\frac{(f-f_p)^2}{2\sigma^2 f_p^2}\right]}$$

$$\sigma = 0.07 \text{ when } f < f_p$$

$$\sigma = 0.09 \text{ when } f \geq f_p$$

In the JONSWAP spectrum, the parameter γ has a range of values from 1.6 to 6 but for general usage is recommended to use the value 3.3. The coefficient α , γ and f_p for the JONSWAP spectrum are given by:

$$\alpha = 0.076 \left(\frac{gF}{W^2}\right)^{-0.22} \quad (3.24)$$

$$f_p = \frac{3.5g}{W} \left(\frac{gF}{W^2}\right)^{-0.33} \quad (3.25)$$

$$\gamma = 7 \left(\frac{gF}{W^2}\right)^{-0.143} \quad (3.26)$$

Nowadays the JONSWAP spectrum has become the most commonly used spectrum for engineering design and for laboratory irregular wave experiments. Figure 3. 7 plots the generic form of both spectra, Pierson-Moskowitz and JONSWAP; depending on the chosen γ coefficient, the form of the JONSWAP accentuates its energy density peak value.

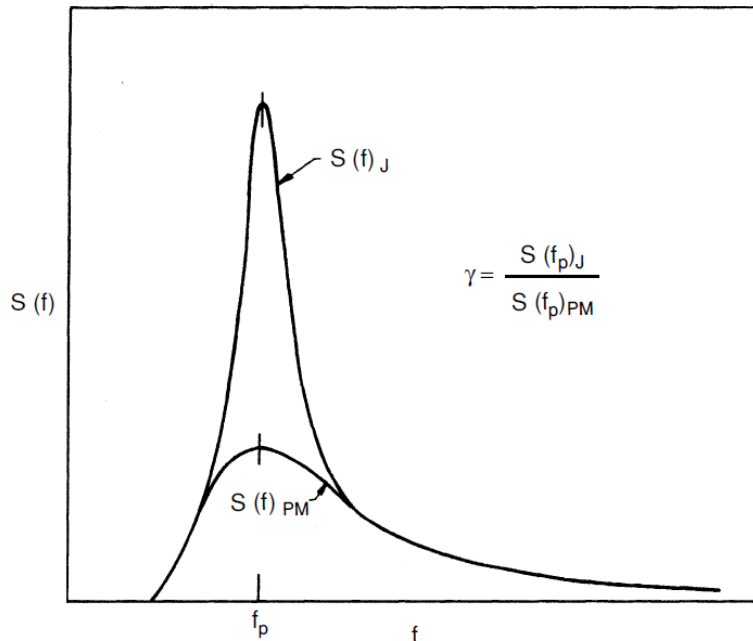


Figure 3.7: Difference from the wave spectrum obtained via the JONSWAP method or through the Pierson-Moskowitz method.

3.1.3 LINEAR WAVE THEORY

Introducing the velocity potential concept into the theory, which is the integrated form of the velocity itself, the motion equations are reduced to the Laplace's equation (3.27) and to the Bernoulli's equation (3.28).

$$\nabla^2 \phi = \frac{\partial^2 \phi}{\partial x^2} + \frac{\partial^2 \phi}{\partial y^2} + \frac{\partial^2 \phi}{\partial z^2} \quad (3.27)$$

$$\frac{\partial \phi}{\partial t} + \frac{1}{2} |\nabla \phi|^2 + \frac{p}{\rho} + gz = 0 \quad (3.28)$$

Those equations with the right boundary conditions become the basis of the irrotational wave motion theory and the hypothesis in which are based are the following:

1. Non viscous ideal fluid
2. Conservative forces
3. Irrotational motion

Furthermore, experimental studies have determined that another constrain has to be added to maintain the theory's validity. The period of the sea waves must be within the following range $1.1s < T < 30s$ but that is not a major problem because practically the totality of the sea waves generated by the wind which are relevant for engineering purposes are within that range.

In the following paragraphs will be developed the linear wave theory also known as first order theory. Firstly, the boundary condition regarding to the free water surface must be set linear. This constrain is composed by two different equations, the kinematic equation (3.29) and the dynamic equation (3.30), which closely analyzed make perfectly sense in terms of velocity for the former and in terms of energy the for latter:

$$\frac{\partial \zeta}{\partial t} + \frac{\partial \phi}{\partial x} \frac{\partial \zeta}{\partial x} + \frac{\partial \phi}{\partial y} \frac{\partial \zeta}{\partial y} - \frac{\partial \phi}{\partial z} = 0 \quad \text{for } z = \zeta(x, y, t) \quad (3.29)$$

$$g\zeta + \frac{\partial \phi}{\partial t} + \frac{1}{2} \left[\left(\frac{\partial \phi}{\partial x} \right)^2 + \left(\frac{\partial \phi}{\partial y} \right)^2 + \left(\frac{\partial \phi}{\partial z} \right)^2 \right] = 0 \quad \text{for } z = \zeta(x, y, t) \quad (3.30)$$

The non linearity of the equations is obvious for the unknown parameters of ζ and ϕ but there is another implicit non linear condition for $z = \zeta(x, y, t)$ which is part of the solution and therefore, another unknown parameter. The linearization of those equations requires the introduction of new constrains.

Figure 3.8 fully describes a progressive periodic wave and all its parameters; this wave propagates in a flat-bottomed channel and is mainly defined by its period T , inverse function of the frequency, its wave length L and its wave height $H=2a$. Analyzing the figure, the proportion among the different parameters is clear and the orders of magnitudes can securely be determined.

$$\zeta = O(H) ; \quad \frac{\partial \zeta}{\partial t} = O\left(\frac{H}{T}\right) ; \quad \frac{\partial \zeta}{\partial x} = O\left(\frac{H}{L}\right)$$

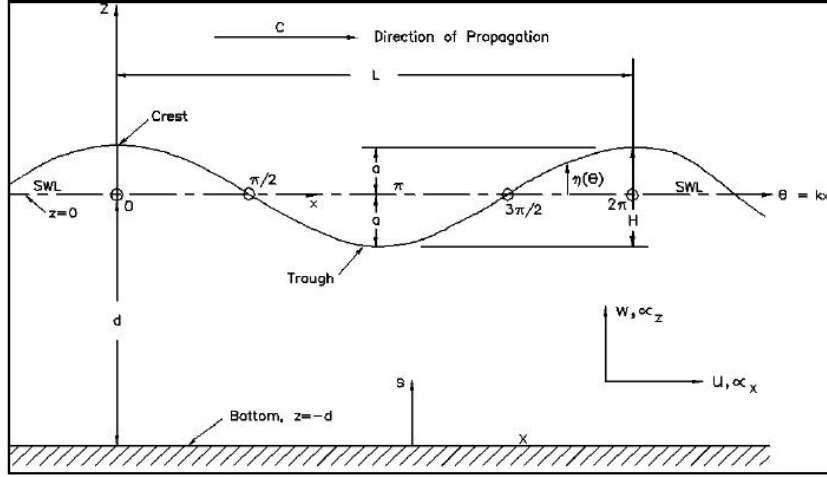


Figure 3.8: Spatial and frequency description of a linear wave with all its parameters.

The maximum velocity of the water particles can be approximated to $\pi H/T$ which leads to the next expression.

$$(u)_{max} = (v)_{max} = (w)_{max} = \left(\frac{\partial \phi}{\partial x}\right)_{max} = \left(\frac{\partial \phi}{\partial y}\right)_{max} = \left(\frac{\partial \phi}{\partial z}\right)_{max} = \frac{\pi H}{T} = O\left(\frac{H}{T}\right) \quad (3.31)$$

Knowing that, in addition $c=L/T$, the non linear terms of the equations (3.29) and (3.30) have the following orders of magnitudes:

$$\frac{\partial \phi}{\partial z} = O\left(\frac{H}{T}\right) = O\left(c \frac{L}{T}\right) \quad (3.32)$$

$$\frac{\partial \zeta}{\partial t} = O\left(\frac{H}{T}\right) = O\left(\frac{\partial \phi}{\partial z}\right) \quad (3.33)$$

$$\frac{\partial \phi}{\partial x} \frac{\partial \zeta}{\partial x} = \frac{\partial \phi}{\partial y} \frac{\partial \zeta}{\partial y} = O\left(c \frac{H^2}{L^2}\right) = \frac{H}{L} O\left(\frac{\partial \phi}{\partial z}\right) \quad (3.34)$$

These relations proof that the non linear terms have an order of magnitude H/L times that of the linear terms and assuming that the wave slope $\varepsilon=H/L \ll 1$ is rather small, the non linear terms of the free surface boundary condition can be eliminated due to its small influence in the whole expression. Once the quadratic terms have been suppressed there is still the implicit non-linearity to be taken care of. If the free water surface elevation is taken to zero, the critical condition can be expanded using the Taylor polynomial form and the final result is:

$$\zeta \frac{\partial^2 \phi}{\partial z^2}(x, 0, t) = O\left(\frac{H}{T} \frac{H}{h}\right) = O\left(c \frac{H}{L} \frac{H}{h}\right) \quad (3.35)$$

As previously commented the term $\varepsilon=H/L \ll 1$ and $H/h \ll 1$ make the order of magnitude close to zero, so this term is also negligible. So after all the analysis and the pertinent transformations the boundary condition expressions are linearized and under the form of:

$$\frac{\partial \zeta}{\partial t} - \frac{\partial \phi}{\partial z} = 0 \quad \text{for} \quad z = 0 \quad (3.36)$$

$$g\zeta + \frac{\partial \phi}{\partial t} = 0 \quad \text{for} \quad z = 0 \quad (3.37)$$

To simplify even more these boundary conditions, both expressions can be merged into a single equation to form only one boundary condition at the free water surface. The mathematical problem in its linearized form is governed by the following expressions:

$$\nabla^2 \phi = \frac{\partial^2 \phi}{\partial x^2} + \frac{\partial^2 \phi}{\partial y^2} + \frac{\partial^2 \phi}{\partial z^2} \quad \text{in the fluid} \quad (3.38)$$

$$\frac{\partial \phi}{\partial n} = \frac{\partial \phi}{\partial z} = 0 \quad \text{for } z = -h \quad (3.39)$$

$$\frac{\partial^2 \phi}{\partial t^2} + g \frac{\partial \phi}{\partial z} = 0 \quad \text{for } z = 0 \quad (3.40)$$

The previous equations are valid when the following hypotheses are respected:

1. Constant depth.
2. Small width waves.

At that point, adding a few more constraints, it is possible to solve the problem based in the variable ϕ , the velocity potential, once this is found the velocity field in the fluid domain is easily studied. Moreover, the free water surface profile can be obtained from a derivate of the boundary condition's equation. The pressure induced by this on the fluid field, can also be easily calculated by the linearized form of the Bernoulli's equation:

$$p^+ = p + \rho g z = -\rho \frac{\partial \phi}{\partial t} \quad (3.41)$$

Where p^+ is the pressure's excess induced by the wave in the fluid.

The next logical step is to find the solution for the velocity potential and the velocity field. In order to achieve that goal some new hypothesis must be introduced:

1. Constant period of the waves.
2. Constant shape of the waves.
3. Bidimensional flat waves (x,z) .

As a consequence of the last hypothesis the Laplace equation for the motion of the fluid, which can only have components of velocity in the x and z directions of the plane, becomes:

$$\nabla^2 \phi = \frac{\partial^2 \phi}{\partial x^2} + \frac{\partial^2 \phi}{\partial z^2} = 0 \quad \text{in the fluid} \quad (3.42)$$

Assuming that the wave is constant-shaped, that means that always has the same length L and mathematically speaking is expressed in the following way:

$$\frac{\partial \phi}{\partial x}(x, z, t) = \frac{\partial \phi}{\partial x}(x + L, z, t) \quad (3.43)$$

The previous reasoning works also for the second hypothesis, being a constant period wave implies:

$$\frac{\partial \phi}{\partial t}(x, z, t) = \frac{\partial \phi}{\partial t}(x, z, t + T) \quad (3.44)$$

Taking into account that those two relations together with the relation of the phase celerity, previously stated $c=L/T$ is constant, and a new way of representing the equations is deduced. Instead of expressing $\zeta(x,t)$ and $\phi(x,z,t)$ why not introducing a new variable that simplifies the expressions? The result is the new variable θ which is defined by the following expression:

$$\theta = 2\pi \left(\frac{x}{L} - \frac{t}{T} \right) \quad (3.45)$$

So now the result is $\zeta(\theta)$ and $\phi(\theta,z)$ and by introducing two new parameters the equations are fully described in this new simpler system of coordinates. These two new parameters are the wave number k and the angular frequency w . The equation of Laplace looks like the following way:

$$k = \frac{2\pi}{L} \quad (3.46)$$

$$w = \frac{2\pi}{T} \quad (3.47)$$

$$\theta = kx - wt \quad (3.48)$$

$$\frac{\partial^2 \phi}{\partial z^2} + k^2 \frac{\partial^2 \phi}{\partial \theta^2} = 0 \quad \text{in the fluid} \quad (3.49)$$

$$\frac{\partial \phi}{\partial z} + \frac{w^2}{g} \frac{\partial^2 \phi}{\partial \theta^2} = 0 \quad \text{for the free water surface} \quad (3.50)$$

$$\frac{\partial \phi}{\partial \theta} \left[\theta = -2\pi \frac{t}{T}, z \right] = \frac{\partial \phi}{\partial \theta} \left[\theta = 2\pi \left(1 - \frac{t}{T} \right), z \right] \quad \text{for periodicity} \quad (3.51)$$

Once all this changes have been applied and through lots of somewhat complicated mathematical passages, such as ODE solution and sinusoidal wave theory, the final result is reached giving the following expressions for free water surface's elevation and for the velocity potential:

$$\zeta = a \cos(kx - wt) = \frac{H}{2} \cos(kx - wt) \quad (3.52)$$

$$\phi(x, z, t) = \frac{ag}{w} \frac{\cosh [k(h+z)]}{\cosh (kh)} \sin(kx - wt) \quad (3.53)$$

Once reached the expression of the velocity potential (3.53), seems obvious that the next step is to calculate the velocity field, but there is a step in the middle in which without it, the computing of the velocity field is not feasible. The fact is that the wave number still is an arbitrary number, given that there is no expression to calculate the wave length for a fixed period yet. Using the boundary condition at the free water surface (3.29) and the following derivates of the equation (3.53) it is obtained that:

$$\left[\frac{\partial \phi}{\partial z} \right]_{z=0} = \frac{ag}{w} \tanh(kh) \sin(kx - wt) \quad (3.54)$$

$$\left[\frac{\partial^2 \phi}{\partial t^2} \right]_{z=0} = -agw \sin(kx - wt) \quad (3.55)$$

Which substituted into the equation (3.30) gives the relation of dispersion, the intermediate step to find the velocity field. The physical meaning of the relation of dispersion is quite complicated. Essentially its meaning is no other than the relation of wave energy loss in wave propagation depending on its frequency and its mathematical form is:

$$w^2 = gk \tanh(kh) \quad (3.56)$$

Once the relation of dispersion is found the velocity field and trajectory of the water particles can easily be calculated. The only operations required to find their expressions are derivatives of the velocity potential, respecting to the x axis to find the horizontal velocity u and respecting to the z axis to find the vertical velocity w:

$$u(x, z, t) = \frac{\partial \phi}{\partial x} = \frac{ag}{w} k \frac{\cosh [k(h+z)]}{\cosh(kh)} \cos(kx - wt) \quad (3.57)$$

$$w(x, z, t) = \frac{\partial \phi}{\partial z} = \frac{ag}{w} k \frac{\sinh [k(h+z)]}{\cosh(kh)} \sin(kx - wt) \quad (3.58)$$

Three different groups can be distinguished in the equations (3.49) and (3.50), the first group expresses the wave characteristics i.e. wave width, wave number and wave angular frequency; the second group reflects the velocity variation depending on the vertical position and the third group states the harmonic behavior of a sea wave. See Fig 3.9.

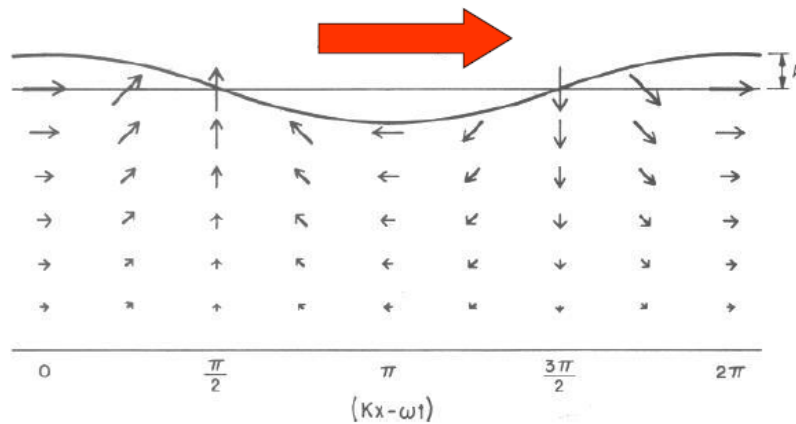


Figure 3.9: Water particle velocities in a wave.

Finding the trajectory of a particle if its velocity field is known has no secret, it is universally known that the position is the velocity integral form or on the contrary the velocity is the derivate in the time of the position. Knowing that, the next step seems obvious, the velocity field must be integrated in the time.

$$x_p(t) = x_0 + \int u[x_p(t), z(t)] dt \quad z_p(t) = z_0 + \int w[x_p(t), z(t)] dt \quad (3.59)$$

Once integrated and simplified the expressions of the particle trajectories on the horizontal and vertical axis look like that:

$$x_p(t) = x_0 - a \frac{\cosh [k(h+z_0)]}{\sinh(kh)} \sin(\omega t - kx_0) \quad (3.60)$$

$$z_p(t) = z_0 + a \frac{\sinh [k(h+z_0)]}{\sinh(kh)} \cos(\omega t - kx_0) \quad (3.61)$$

Using the terms:

$$\alpha = a \frac{\cosh [k(h+z_0)]}{\sinh(kh)} \quad (3.62)$$

$$\beta = a \frac{\sinh [k(h+z_0)]}{\sinh(kh)} \quad (3.63)$$

If the equations (3.60) and (3.61) are divided by α and β respectively, squaring them and finally adding them term by term, the result is a very known type of equation:

$$\frac{[x_p(t)-x_0]^2}{\alpha^2} + \frac{[z_p(t)-z_0]^2}{\beta^2} = 1 \quad (3.64)$$

This is the ellipse equation and it varies its parameters depending on the conditions. If the seabed is deep enough to be dismissed, i.e. deep water conditions, then this ellipse is turned into a perfect circumference which radius decreases with the depth until a limit when tends to zero. See Figure 3.10. If the sea bed is close enough to the water surface to have influence in the behavior of the wave, i.e. shallow water conditions, then the ellipse remains ellipse and its secondary radius also decreases with the depth until seabed surface, where the velocity has only horizontal component in order to respect the bottom boundary condition. See Figure 3.11.

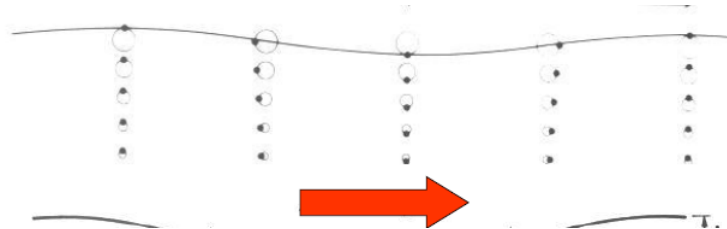


Figure 3.10 Water particle orbits in deep water.

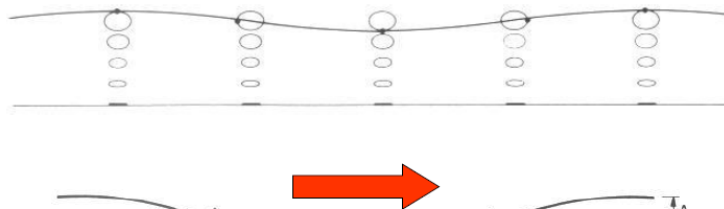


Figure 3.11: Water particle orbits in shallow water.

The distribution of the pressure in the fluid mass is obtained through the linearized Bernoulli's equation:

$$p^+ = -\rho \frac{\partial \phi}{\partial t} = \rho a g \frac{\cosh [k(h+z)]}{\cosh (kh)} \cos(kx - \omega t) = \rho g \zeta(x, t) \frac{\cosh [k(h+z)]}{\cosh (kh)} = \rho g K_p \zeta(x, t) \quad (3.65)$$

Where K_p is the pressure response factor and its value is always equal or smaller than one and depends on the value of z . If the equation (3.65) substituted into the equation (3.41) the entire pressure profile in the water is obtained:

$$p = p^+ - \rho g z = \rho g (K_p \zeta - z) \quad (3.66)$$

When $z = 0$ then $K_p = 1$ thus resulting in a pressure $p = \rho g \zeta$ so in the crest of a wave the pressure is $p = \rho g a$ and in the trough of a wave the pressure is $p = -\rho g a$. Then the pressure profile keeps growing as the depth point of study is also increasing. See Figure 3.12.

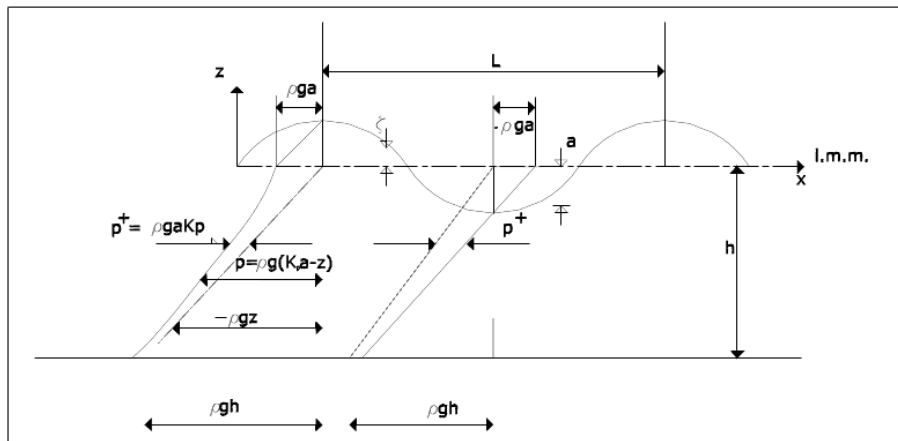


Figure 3.12: Pressure distribution along the depth in the wave crest and the wave trough.

In the linear wave theory all dissipative phenomena are neglected, so the energy linked to wave motion is made only by potential energy and kinetic energy. As an oscillating motion, the energy in a certain point (x,y) is time dependent. However, the energy contained at a point in a certain time is not really a matter of major interest in the engineering world, a much more used term is the specific energy, defined as mean energy (in time) per surface unit or, in other words, the density of energy which applications have been exposed in detail at previous sections of this chapter. In the following paragraphs the expressions of potential and kinetic energy will be developed separately and finally merged together.

Figure 3.13 shows the schematic geometric basis to calculate potential energy. An elementary fluid column is the studied area. That column has a unitary width (perpendicular to the sheet plane), a differential length dx and a height of $h+\zeta$. The elementary potential energy is:

$$d\bar{E}_{p1} = g h_G dm \quad (3.67)$$

The mass of the fluid column is equal to:

$$dm = \rho(h + \zeta)dx \quad (3.68)$$

This can be substituted into equation (3.67):

$$d\bar{E}_{p1} = \frac{1}{2}\rho g(h + \zeta)^2 dx \quad (3.69)$$

Which in turn is implicitly time dependent, owing to the variable $\zeta(x,t)$. The final step to get the potential energy density is to integrate the equation (3.69) over the variables x and t , from x to $x+L$ and from t to $t+T$:

$$\bar{E}_{p1} = \frac{1}{LT} \int_t^{t+T} \int_x^{x+L} d\bar{E}_{p1} dt = \frac{\rho g}{2LT} \int_t^{t+T} \int_x^{x+L} (h + \zeta)^2 dx dt \quad (3.70)$$

Operating mathematically and trigonometrically the equation (3.70) results in the final and simplest form of:

$$\bar{E}_p = \rho g \frac{a^2}{4} \quad (3.71)$$

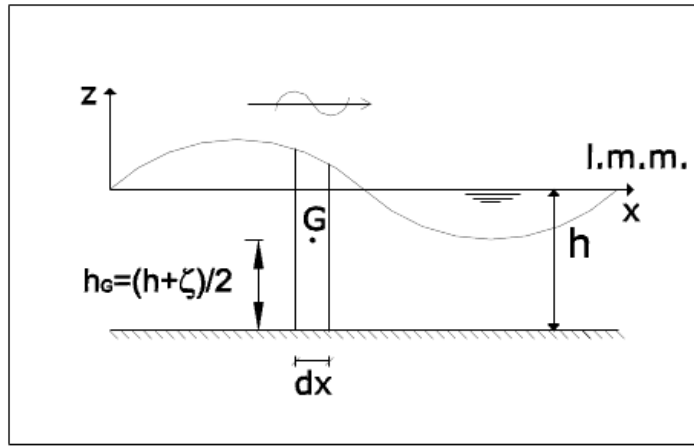


Figure 3.13: Geometric configuration to compute the Potential Energy.

To develop the kinetic energy expression the figure 3.14 is used. The study area is again an elementary region of fluid mass, which length and height are respectively dx and dz and it has a unitary width. The resulting expression is:

$$d\bar{E}_C(t) = \frac{1}{2}(u^2 + w^2)dm = \frac{\rho}{2}(u^2 + w^2)dx dz \quad (3.72)$$

Making the mean on the wave period and length and integrating on the vertical, the following expression is obtained:

$$\bar{E}_C = \frac{1}{LT} \int_x^{x+L} \int_{-h}^0 \int_t^{t+T} d\bar{E}_C dt dx dz = \frac{\rho}{2LT} \int_x^{x+L} \int_{-h}^0 \int_t^{t+T} (u^2 + w^2) dx dz dt \quad (3.73)$$

After long passages of mathematical and trigonometric operations the final and simplified expression of the kinetic energy density is:

$$\bar{E}_C = \rho g \frac{a^2}{4} \quad (3.74)$$

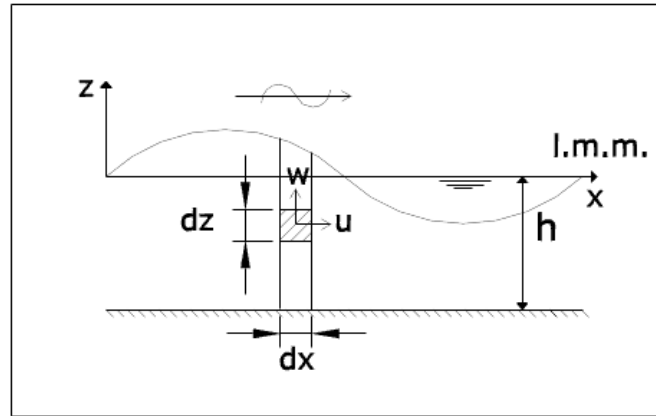


Figure 3.14: Geometric configuration to compute the Kinetic Energy.

Astonishingly, the exact same quantity than the other kind of energy, the potential energy. By adding both term the total amount of energy density in a wave is obtained:

$$\bar{E} \equiv \bar{E}_c + \bar{E}_p = \frac{1}{8} \rho g H^2 \quad (3.75)$$

It is important to remind that this expression is valid for a unitary horizontal section, that is why is called energy density. Another interesting fact to keep in mind when designing in the sea engineering world is that the energy contained in a wave is not function of its period or length but of its height, that's why the wave height is the most important parameter when building marine structures.

At this point, the bases of the linear wave theory have been exposed. For this Master Thesis purpose, the already described part is mainly the whole needed theory so the rest of the linear wave theory will be describe in a very brief way. As stated above the real sea water surface is not made of one monochromatic wave, the reality is that, even a small portion of the sea surface is composed by hundreds or thousands of waves, which have different heights, directions, periods and phases. Groups of waves and reflected waves will be treated in the next paragraphs.

The principle of superposition of the effects is also valid within the linear wave theory premises. That principle is as simple as the sum of each different component:

$$\zeta(x, t) = \sum_n \zeta_n = \sum_n a_n \sin(k_n x - \omega_n t + \delta_n) \quad (3.76)$$

There are some particular cases such as:

A- Waves that propagate in the same direction and have same periods

A.1- If their phase is the same

$$\zeta(x, t) = (a_1 + a_2) \sin(kx - \omega t + \delta) \quad (3.77)$$

A.2- If their phase is opposed π rad

$$\zeta(x, t) = (a_1 - a_2) \sin(kx - \omega t + \pi) \quad (3.78)$$

B- Waves that propagate in the same direction and have different periods

$$\zeta(x, t) = 2a \{ \cos[\delta k - \delta \omega t - \delta] \sin(kx - \omega t) \} \quad (3.79)$$

C- Waves that propagate in opposed direction

C.1- If $a_i = a_r$ is called total reflection

$$\zeta(x, t) = 2a_r \cos(kx) \cos(\omega t) \quad (3.80)$$

C.2- If the wave amplitudes are different

$$\zeta(x, t) = 2a_r \cos(kx) \cos(\omega t) + (a_i - a_r) \cos(kx - \omega t) \quad (3.81)$$

The minimum and maximum values of the free elevation surface corresponding respectively to the trough and the crest are:

$$|\zeta_{min}| = a_i - a_r \quad |\zeta_{max}| = a_i + a_r \quad (3.82)$$

And the Reflection coefficient is $R = \frac{a_r}{a_i}$ (3.83)

When describing groups of waves a new concept rises up. The group celerity, physically the group celerity is the velocity in which the totality of the energy contained in a group of waves propagates. Do not forget the fact that in a group of waves, each wave can propagate at different speeds but their energy is shared and unique of that group, this is why is called a group of waves. To find the group celerity the relation of dispersion is used and its final expression can be simplified depending on the depth, shallow water or deep water.

$$c_g = \frac{c}{2} (1 + G) \quad (3.84)$$

Where G is obtained from the relation of dispersion:

$$G = \frac{2kh}{\sinh(2kh)}$$

$$c_{g0} = \frac{1}{2} c_0 \quad \text{for deep water} \quad (3.85)$$

$$c_g = c = \sqrt{gh} \quad \text{for shallow water} \quad (3.86)$$

Once the group celerity has been introduced the next logical step is to describe the energy propagation in a group of waves. It is easily understandable, once known the physical meaning of the group celerity, that the flux of energy in a wave group is nothing else than the energy contained in the wave multiplied by the group celerity:

$$\bar{E}_f = c_g \bar{E} = \frac{1}{16} \rho g H^2 c \left[1 + \frac{2kh}{\sinh 2kh} \right] \quad (3.87)$$

When approaching to the shoreline, in the area called near-shore, the seabed starts having a significant influence in the wave's behavior. The first wave response at the seabed presence is called Shoaling. When the wave reaches that area the depth decreases as the wave propagates so the water has less space to move forward with the same amount of energy, lets remind that until wave breaking there is no energy loss in the linear wave theory, resulting in an initial smooth decrease completed by a sudden substantial increase of the waves height (See Figure 3.15). The Shoaling degree is represented by a coefficient called shoaling coefficient K_s , defined by the following expression:

$$K_S = \frac{H}{H_0} = \sqrt{\frac{c_0}{2c_g}} = \frac{1}{\sqrt{\tanh(kh)(1+G)}} \quad (3.88)$$

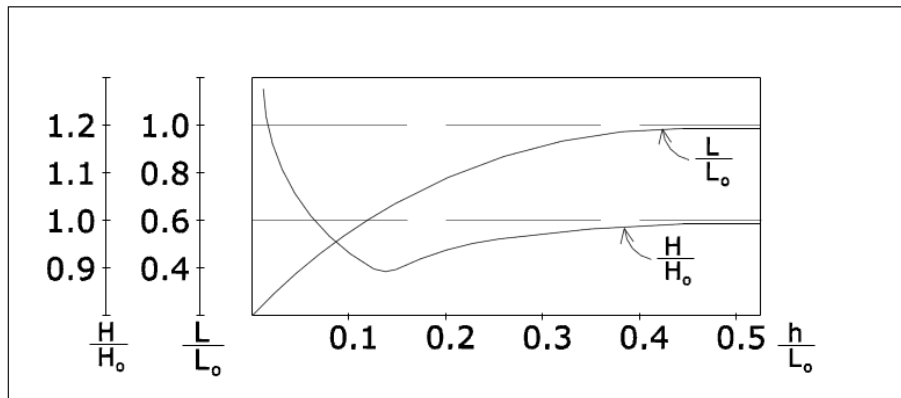


Figure 3.15: Evolution of the shoaling coefficient over the ratio sea depth by wave length in deep waters.

The waves usually don't reach the near-shore area propagating perpendicularly to the coast line but when observing wave breaking, their direction of propagation is always perpendicular to the coast, this occurs because of refraction. It is the same kind of refraction to which the light waves are submitted, it works the same way and the same principles can be applied. Actually, the law of Snell, developed for light waves is also used in sea waves to calculate the refraction coefficient. Figure 3.16 illustrates in fully detail how is the law of Snell applied in the sea wave field.

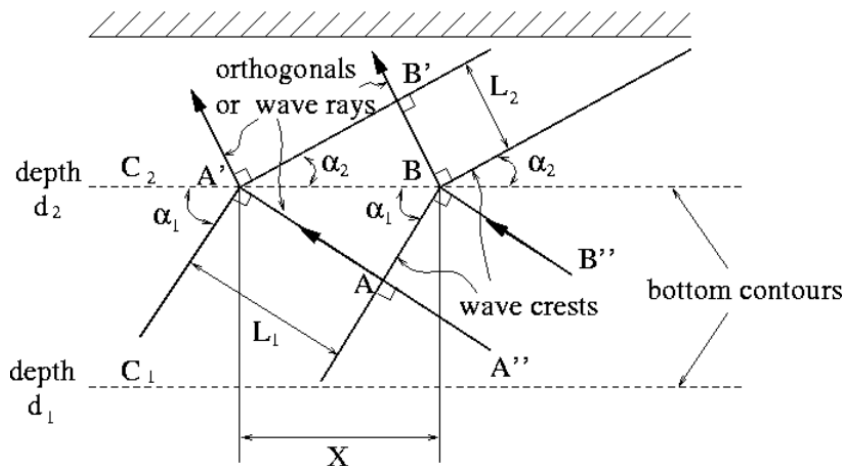


Figure 3.16: Geometric representation of the Snell's law applied in sea waves in the near-shore area.

Resulting in a refraction coefficient expression:
$$K_r = \sqrt{\frac{L_1}{L_2}} \quad (3.89)$$

Depending on the coastline form, the wave height can increase or decrease when refracted i.e. if the coast is a bay, concave form, waves will tend to spread into a wider area and therefore, their height will decrease. On the contrary, if the coast is a cape, convex form, the

waves will tend to concentrate towards the outer cape point and their height will increase (See Figure 3.17). The height can be computed through the following expression:

$$K_r K_S = \frac{H}{H_0} = \sqrt{\frac{c_0}{2c_g}} \sqrt{\frac{L_1}{L_2}} \quad (3.90)$$

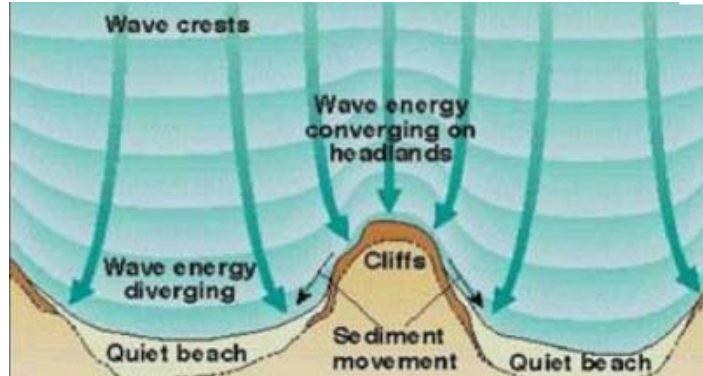


Figure 3.17 Representation of the wave behavior when waves are refracting.

Finally, the last part of the linear wave theory is based on another particular phenomenon, also found in light waves, called diffraction. When a wave finds an obstacle when propagating throughout the oceans, an unusual phenomenon occurs. Immediately after over passing the obstacle the wave propagation direction changes abruptly following the obstacle main direction. For that behavior to occur, the obstacle dimensions must be similar than the waves dimensions. In other words, the main dimension of the obstacle must be whether the same or under one order of magnitude as the wave length. The mathematical representation of this phenomenon is by no means easy and its understanding is of complicated nature. The equation proposed by the German mathematician is an adaptation of the Laplace equation by introducing complex numbers in it:

$$\phi(x, y, z, t) = Im\{f(z)\Phi(x, y)e^{-tiw}\} \quad (3.91)$$

$$\zeta(x, y, t) = Re\{\eta(x, y)e^{-tiw}\} \quad (3.92)$$

Where: $f(z) = \frac{\cosh [k(h+z)]}{\cosh (kh)}$ (3.93)

After some mathematical operations like partial derivation and simplification the Helmholtz version of the Laplace Equation is the following expression:

$$\frac{\partial^2 \Phi}{\partial x^2} + \frac{\partial^2 \Phi}{\partial y^2} + k^2 \Phi = 0 \quad (3.94)$$

This equation which results in the elliptic form it has been proved valid for the following cases:

- Straight hurdle of semi-infinite length.
- Finite gap in an infinite length straight hurdle.
- Isolated obstacle made of a straight hurdle of finite length.
- Isolated obstacle which horizontal section is circular.

The last of these cases could be the floating body of the device studied in this Master Thesis. So diffraction is an element which has to be seriously considered when designing a Wave Energy Converter. In the particular case of this Master Thesis work, diffraction can be neglected due to the fact that the main dimension of the floating body is about two orders of magnitude smaller than the typical wave length and only in some rare occasion would occur. Moreover, if occurred, the energy contained in the incident wave would be extremely low due to its reduced dimensions. Figure 3.18 illustrates the typical behavior of waves when finding an obstacle and diffracting.

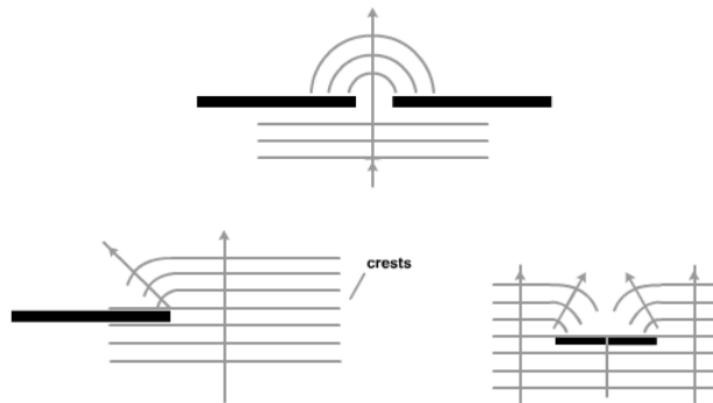


Figure 3.18 Wave diffraction behavior depending on the obstacle.

3.2 ELECTROMAGNETICS OF LINEAR GENERATOR

As previously stated, this Master Thesis studies the performance of point absorber wave energy converters. Among the different kind of this type of devices, this work is going to be focused on heaving floating body devices with a specific power take-off system, the electrical linear generators.

To achieve a full understanding of how these generators work, the fundamental concepts of electromagnetism need to be introduced. Electromagnetic laws are well represented by the Maxwell's equations:

$$\nabla \cdot D = \rho_c \quad (3.95)$$

$$\nabla \cdot B = 0 \quad (3.96)$$

$$\nabla \times E = -\frac{\partial B}{\partial t} \quad (3.97)$$

$$\nabla \times H = J + \frac{\partial D}{\partial t} \quad (3.98)$$

Where B is the magnetic flux density or magnetic induction, D is the displacement field, E is the electric field and H is the magnetizing field or magnetic field intensity. On the other side of the equations there are ρ_c which refers to the charge density and J which is the free current density. The equation (3.96) states that the flux of the magnetic induction must be zero in the whole dominium of the body. In spite of electrical fields, magnetic fields must complete a close loop. Equation (3.101) expresses that the curl of the electric field must be equal to the negative time derivative of the magnetic field. The magnetic field intensity can also be expressed by the following equation and is expressed in amperes per meter (A/m):

$$\underline{H} = \frac{1}{4\pi} I \int_C \frac{\overline{dl} \times \overline{r}_l}{r^2} \quad (3.99)$$

The integration is carried out over the circuit C that carries a current I. This current gives place to an H-field in the point P. The unitary vector r_l and the distance r determine the direction and distance from the circuit C to the point P. See Figure 3.19.

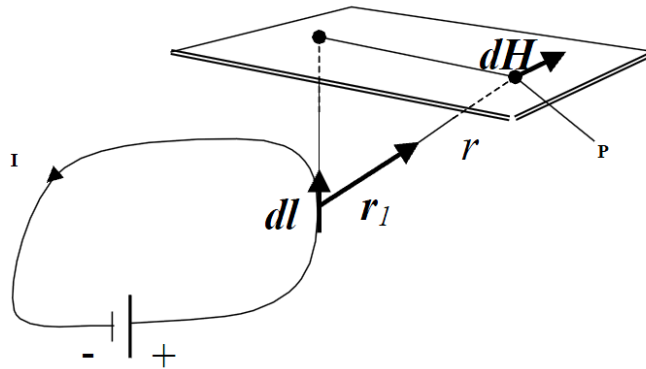


Figure 3.19: Conceptual Scheme of the magnetic induction.

Magnetic field induction is closely related to the force exerted on a conductor carrying an electrical current and also to the magnetizing field by the following expression:

$$B = \mu H \quad (3.100)$$

Where μ is the permeability constant of the medium in which the magnetic induction is generated. Magnetic induction is expressed in Tesla (T).

The magnetic flux through a surface S is measured in Webbers (W) and defined by:

$$\Phi = \int_S \underline{B} d\vec{a} \quad (3.101)$$

Another important concept is the magnetization. Namely, the magnetic moment per unit of volume at a point in a given medium, it has the same units as the magnetic field intensity H and contributes to the magnetic induction in the following way:

$$\underline{B} = \mu_0(\underline{H} + \underline{M}) \quad (3.102)$$

Where μ_0 is the permeability of free space, the vacuum. Using the Stokes' theorem, equation (3.98) can be reformulated as follows:

$$\oint_C \underline{H} d\vec{l} = \int_S \underline{J} d\vec{a} \quad (3.103)$$

Equation (3.103) is the Ampere's law and states that the integral of the magnetic field intensity over a closed loop equals the integral of the density of current going through the inner surface surrounded by c. This is the theoretical origin of the solenoids or coil turns, the final total current in a coil is the obtained in equation (3.103) multiplied by the number of turns. Equation (3.97) can also be reformulated applying the Stokes' theorem in the left hand side and the equation (3.101) in the right hand side resulting in:

$$e = - \frac{d\Phi}{dt} \quad (3.104)$$

This is known as the Faraday's law for induction. The e is the induced voltage by the total flux bound by the circuit. The direction of the induced current in the circuit is what generates the opposition against the flux change by the magnetic field. As in the case of the Ampere's law, the induced voltage for the circuit is multiplied by the number of turns of the coil. None of this behaviors and laws would be like that without the existence of a kind of materials with unique properties, the ferromagnetic materials. This type of materials are magnetic dipoles that can reach very high levels of magnetization, this ability is expressed through the previously introduced relative permeability μ . Equation (3.100) can be combined with equation (3.102) to show the dependence between the relative permeability μ and the magnetization M, both parameters are strictly related with the material nature.

$$\mu \equiv \frac{B}{H} = \mu_0 \left(1 + \frac{M}{H} \right) \quad (3.105)$$

The relative permeability of ferromagnetic materials is very high and thus, those are used to build magnetic devices to guide the magnetic flux. Each material has a curve of magnetization, in which depending on the applied magnetic field; a magnetic induction is achieved to a greater or lesser extent depending on the material characteristics such as the

magnetization or relative permeability. When the ferromagnetic material reaches the saturation means that the magnetic induction stabilizes and the magnetization no longer increases. See figure 3.20.

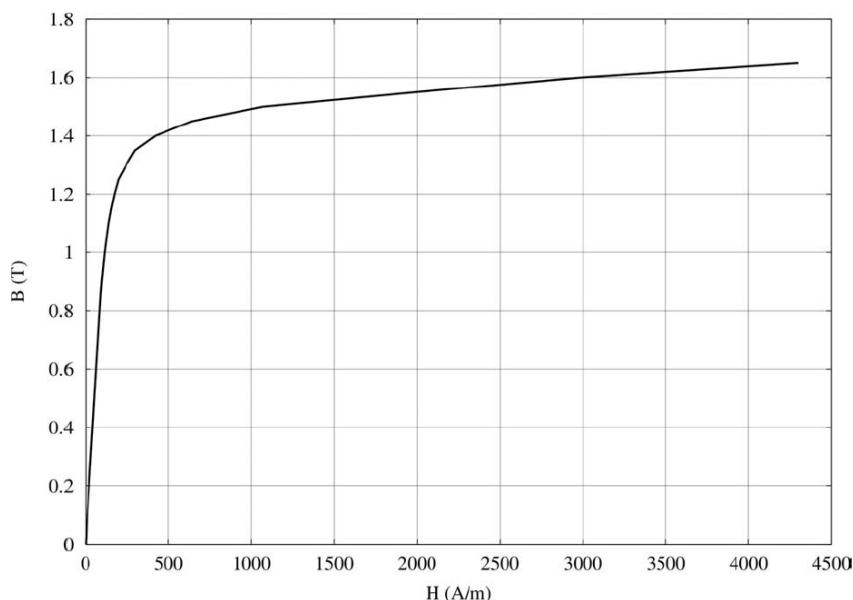


Figure 3.20: Magnetization curve for a ferromagnetic material.

Once the theoretical bases have been introduced it's time to focus on the practical problem, the electrical linear generator. A linear generator is a brand new form of an induction generator, it hasn't reached the commercial stage yet and therefore, a lot of research study has to be done in the field in order to optimize its performance. A good proof of that is that only few prototypes have been built and most of the research is still in the computer based simulations. An induction generator is composed of two main parts: the rotor and the stator. The terminology of those terms is due to its main function, the rotor is the piece of the generator that rotates to generate the magnetic flux changes and the stator is the piece which is static and gathers the induced currents. In the present case, the rotor no longer rotates, in fact, follows an alternative motion of translation, so from now on will be treated as translator; the stator keeps being static so there is no need to change its name. Between the translator and the stator there is a small distance called the air gap, so the translator and rotor are not directly in contact. Without the air gap the mechanics of the system would be much more complicated and the solution would be too costly to make it profitable.

The translator is mounted with permanent magnets between pole shoes. Pole shoes are steel bars with the poles placed face to face which serve to conduce the magnetic flux towards the air gap and over the stator. The stator consists of coil windings placed inside a steel block, which is the stator structure. Once the magnetic flux has crossed the air gap is led through the stator-tooth to the stator-yoke where the flux is divided into two parts and sent back to

the translator to close the loop according to the Maxwell's equations. The previous process is illustrated in the figure 3.21.

As the translator moves relatively to the stator a time varying magnetic field is created in the stator coils, this variation can be measured by an angle due to its periodicity. This angle is called the electric angle.

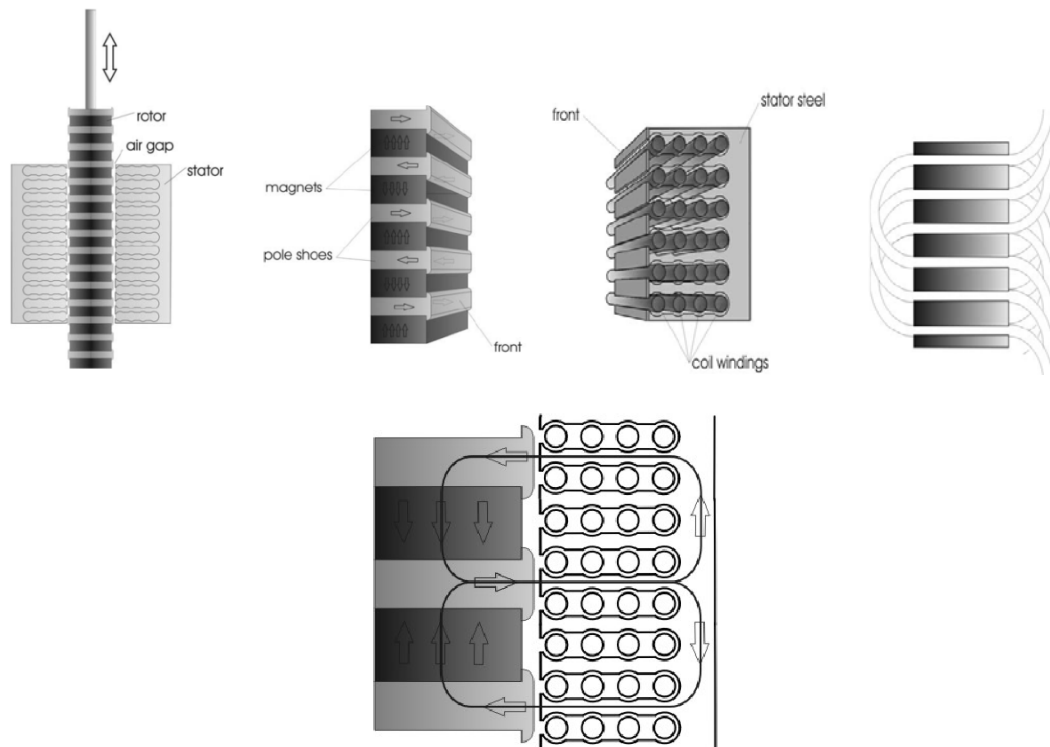


Figure 3.21: Physical description of the translator and stator parts of the linear Generator and its conceptual function.

The majority of the generators have a multi phase system which means that the coil windings are composed of several parallel circuits. A single circuit is called a phase, the most used system is the three-phase system in which each phase is shifted $2\pi/3$ electrical radians from the other ones. The property of the three-phase system is that allows a constant power production. That's not 100% true in the linear generator's case, it is true when the relative motion of the rotor from the stator is constant and in linear generators the translator is not always moving at the same speed compared to the stator. Actually, there are the so called end-stop points (crest and trough of the waves) where the translator does not move and thus the power output at that instant is zero.

The induction generator uses the same principle of the equation (3.104) where a time varying electromagnetic field induces an electromagnetic voltage in the coil windings. The induced voltage in the generator is the sum of all voltages induced separately in each coil per phase.

The magnetic induction is assumed to be sinusoidal and monochromatic so as wave propagation is, and thus not being constant.

$$B = \hat{B} \sin(x - \omega t) \quad (3.106)$$

Where \hat{B} is the maximum amplitude, x is the reference point in the stator and ω is angular velocity of the translator. The single flux related to a coil at a certain time t is described by the following expression:

$$\Lambda = \frac{\omega}{2\pi} N l \hat{B} \int_{-\frac{\pi}{2}}^{\frac{\pi}{2}} \sin(x - \omega t) dx = \frac{\omega}{\pi} N l \hat{B} \sin \omega t \quad (3.107)$$

Where, in this case, ω is the pole width, N the number of turns and l the length of a coil turn. The induced voltage is:

$$e = -\frac{d\Lambda}{dt} = \omega \frac{\omega}{\pi} N l \hat{B} \cos \omega t = 2f\omega N l \hat{B} \cos 2\pi f t \quad (3.108)$$

So the effective or root mean square voltage E is defined as:

$$E = \frac{\hat{e}}{\sqrt{2}} = \sqrt{2} f \omega N l \hat{B} \quad (3.109)$$

Where \hat{e} is the maximum voltage.

Each generator has a magnetic equivalent, which has been described in full detail above and also an electrical equivalent, which is usually known as the equivalent circuit, illustrated in figure 3.22. The induced voltage is the E_{nl} , this is referred to as a no load voltage and is the measurable voltage at the coil ends when no electric intensity is flowing through the generator. X_s is the synchronous reactance and R_c is the resistance of the coil windings. R_{load} can be purely resistive, reactive or a combination of both, in this case will be considered as purely resistive for simplicity reasons, the physical meaning of the load is the useful interface in which the output power will be used, could be an appliance, a house or simply the national grid. Finally, U is the voltage used by that interface and is in phase with the current in the armature I_a .

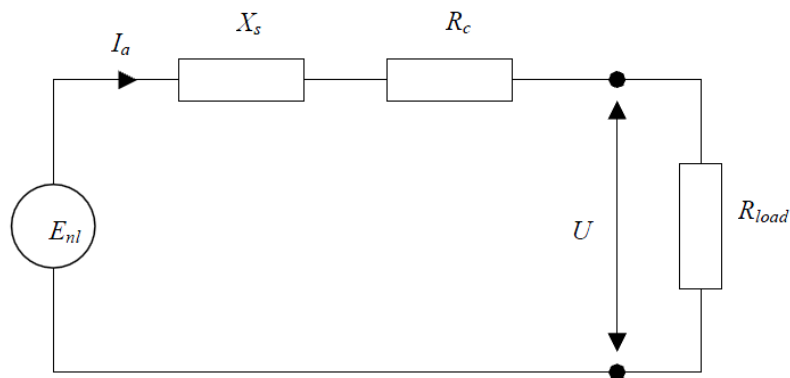


Figure 3.22: Equivalent Electric Circuit.

The equivalent circuit equation for the voltage U can be deduced as function of the induced voltage E_{nl} , the armature current I_a , the coil resistance R_c , and the synchronous reactance X_s :

$$U = E_{nl} - (R_c + jX_s)I_a \quad (3.110)$$

$$U = R_{load} I_a \quad (3.111)$$

Although the simple appearance of this equation is rather complicated due the introduction of imaginary numbers and the electrical angular velocity, to solve that problem another schematic way is used, rather trigonometric than electric or magnetic, it is a helpful way to operate with imaginary numbers. The diagram works in the following way: imaginary numbers can only be drawn in the vertical axis and in proportion with the real numbers which can only be represented along the horizontal axis. Figure 3.23 illustrates a phasor diagram describing the relations between the different parts of the equivalent circuit. The resulting equation is a simple trigonometric relation:

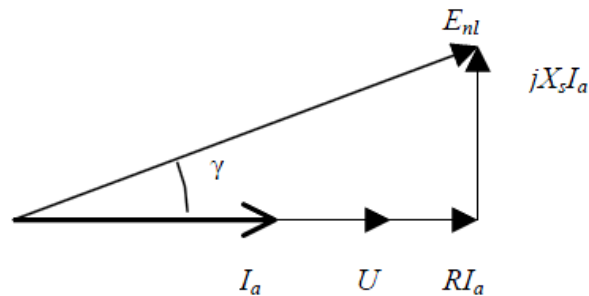


Figure 3.23: Conceptual representation of the load angle.

The angle γ between the purely resistive load voltage and the real load voltage is called load angle and it's an easy way to know the degree of reactance of the equivalent circuit, electric theory states that the lower the load angle is the higher the useful extracted power will be.

$$U = E_{nl} \cos \gamma - RI_a \quad (3.112)$$

The term RI_a represent the losses by the Joule effect, that loss of energy is translated into heat power. In an induction generator there are losses that in this work will be neglected due to its small entity and for simplicity reasons. The main characteristic energy losses given in an electric induction generator are:

- Losses due to the changing magnetic field.
 - Hysteresis losses.
 - Eddy currents losses.
- Resistive losses in the coil windings (Joule Effect).
- Mechanical losses due to friction and deformation.

3.3 FLOATING BODY DYNAMICS

The purpose of the last part of this chapter is to describe the interaction between the sea waves and oscillating floating bodies. Body oscillations and wave forces on bodies will be studied in detail as well as the theory hidden behind and the equations that shape mathematically this behavior.

The first step when studying the floating body dynamics is to create a reference coordinate system for obvious reasons, without the coordinate system would be impossible to write the equations that govern the oscillating motion or describe the forces acting on that body. The system has its z axis through the gravity center of the body, being the origin of the coordinate system the center of gravity point. See Figure 3.24.

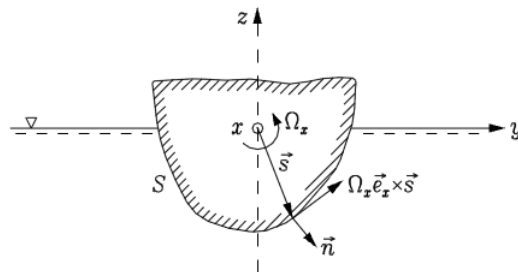


Figure 3.24: Floating body full coordinate system.

If the floating body is not fixed to any anchor or mooring system, the body has six degrees of freedom, three of them translational and the other three rotational. For a ship or a well distinguishable body shape are named as shown in figure 3.25 and table 3.2. For axisymmetric bodies the mode numbers (1 and 2) and (4 and 5) are ambiguous and its semantic determination is left anyone free will. In the case studied in this work, although being axisymmetric bodies like spheres and cylinders, this problem has not even been considered because the used floating bodies have been restricted to only one degree of freedom, they can only oscillate along the z axis and thus, they are only in heaving mode.

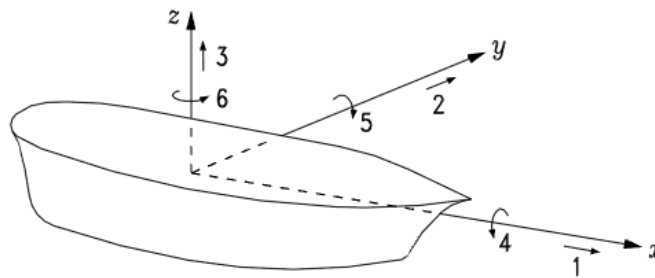


Figure 3.25: Illustration of the six degrees of freedom of a floating body

Mode No.	Component	Mode Name
1	$u_1=U_x$	Surge
2	$u_2=U_y$	Sway
3	$u_3=U_z$	Heave
4	$u_4=\Omega_x$	Roll
5	$u_5=\Omega_y$	Pitch
6	$u_6=\Omega_z$	Yaw

Table 3.2: Description of the six degrees of freedom of a floating body given a reference coordinate system.

After introducing the coordinate system, the next step is to derive expressions for the forces and moments which act on a free floating body, in terms of a given velocity potential \emptyset . Firstly, the vertical force component F_z , which acts in heave mode will be considered. The vertical force acting on a body of wet surface S is initially deduced from its hydrodynamic pressure:

$$p(-n_z)dS = -pn_3dS \quad (3.113)$$

Integrating over the wet surface the result is the total heave force :

$$F_3 \equiv F_z = - \iint_S pn_3dS \quad (3.114)$$

Analogous expressions are derived for the surge and sway forces, F_1 and F_2 respectively. When the forces have been derived, it's time for the moments following exactly the same procedure:

$$dM_x = s_y dF_z - s_z dF_y = (pn_y s_z - pn_z s_y) dS \quad (3.115)$$

Integrating over the wet surface:

$$M_x = - \iint_S (pn_y s_z - pn_z s_y) dS = - \iint_S p(\vec{s} \times \vec{n})_x dS = - \iint_S pn_4 dS \quad (3.116)$$

Again like in the forces case, analogous expression are derived for the pitch and yaw modes giving place at generalized force vector:

$$F \equiv (F_1, F_2, F_3, F_4, F_5, F_6) \equiv (F_x, F_y, F_z, M_x, M_y, M_z) = (\vec{F}, \vec{M}) \quad (3.117)$$

The first three components of the vector have SI units N and the following three ones have Si units Nm. Once the general forces and moments have been stated, what comes next and directly is the power expressions, which as commonly known, is the product of the force applied on a body by its velocity:

$$P(t) = \vec{F}(t) \cdot \vec{U}(t) + \vec{M}(t) \cdot \vec{\Omega}(t) = \sum_{j=1}^6 F_j \cdot U_j \quad (3.118)$$

When the body is fixed, a certain velocity potential $\hat{\phi}$ is the consequence of an incident wave. The F_j introduced above, in that case is called the excitation force, the excitation moment

when $j=4,5,6$, and the sub index e is used to express this kind of force, which is described by the following expression:

$$F_{e,j} = i\omega\rho \iint_S (\hat{\phi}_0 + \hat{\phi}_d)n_j dS \quad (3.118)$$

Where $\hat{\phi}_0$ represents the undisturbed incident wave and $\hat{\phi}_d$ the diffracted wave. Note that the velocity potential due to a diffracted wave won't be considered in this work. As stated previously, in the linear wave theory, the diffraction term originated in the studied devices is so small that can be neglected without affecting the validity of the results. Equation (3.118) is a very complicated equation to solve due to its intrinsic variation depending on many factors as seen on the linear wave theory section. Even though it has been already simplified by working in the frequency domain instead of working in the time domain. For the purpose of this work is very interesting to show the example of the simplified equation for a floating heaving cylinder in infinitely deep waters:

$$\begin{aligned} \hat{F}_{e,3} &= i\rho\omega \int_0^{2\pi} \int_0^a \phi(r, \theta, 0)n_3 r dr d\theta = \\ &= -i\rho\omega \sqrt{\frac{2}{\pi}} \int_0^{2\pi} \int_0^a \int_0^\infty P_m(\zeta) \frac{I_m(\zeta r)}{I_m(\zeta a)} d\zeta r dr \cos(m\theta) d\theta = \\ &= 2\pi i\rho\omega a \int_0^\infty P_0(\zeta) \frac{I_1(\zeta r)}{\zeta I_0(\zeta r)} d\zeta \end{aligned} \quad (3.120)$$

Where I_m is the modified first Bessel function of order m , $P_m(\xi)$ is an unknown coefficient and a is the cylinder radius. Figure 3.26 illustrates the normalized heave excitation force, in the frequency domain, as a function of $k_0 a$ ($k_0 = \omega^2/g$) for various draft (b) to radius (a) ratios.

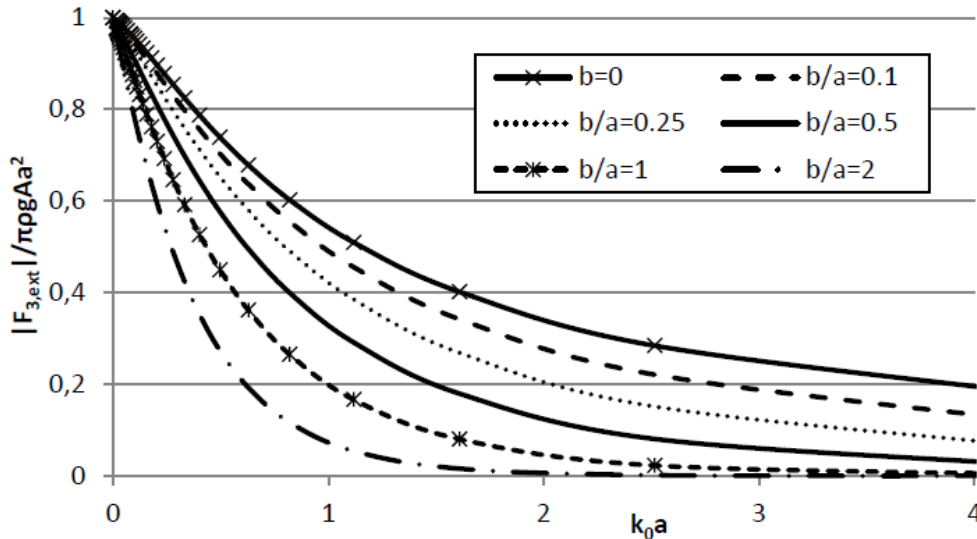


Figure 3.26: Excitation Force restricted in heave mode depending on the wave frequency and the radius of the sphere floating body.

In the following paragraphs the case of an oscillating body with no incident wave has been treated. The body's oscillation results in the generation of secondary waves, usually called radiated waves which have a considerable effect on the body's dynamics, this force is called the radiation force. The radiated wave is associated with the velocity potential as follows:

$$\hat{\phi}_r = \varphi_j \hat{u}_j \quad (3.121)$$

$$\hat{F}_{r,j} = i\omega\rho \iint_S \varphi_j \hat{u}_j n_j dS \quad (3.122)$$

Where φ_j is a coefficient of proportionality and \hat{u}_j is a constant under the integration conditions, for this reason the radiated force can be reformulated in the following way:

$$\hat{F}_{r,j} = -Z_{j',j} \hat{u}_j \quad (3.123)$$

$$Z_{j',j} = -i\omega\rho \iint_S \varphi_j n_j dS \quad (3.124)$$

Where $Z_{j',j}$ is the radiation impedance matrix which SI units are Ns/m for $Z_{p',p}$ when $p',p=1,2,3$, Nsm for $Z_{q',q}$ for $q',q=4,5,6$ and Ns for $Z_{q',p}$ and $Z_{p',q}$. Using the boundary condition in the wet surface the following expression is obtained:

$$Z_{j',j} = -i\omega\rho \iint_S \varphi_j \frac{\partial \varphi_{j'}}{\partial n} dS \quad (3.125)$$

Note that the term φ_j is complex while the term $\frac{\partial \varphi_{j'}}{\partial n}$ is real on S because n is real. If the boundary condition has to be respected, can be deduced from equation (3.125) that $-Z_{j',j}$ is the component j' of the reaction force which is caused by the radiated wave in mode j, and when oscillating with the unit amplitude must be equal to the j component of the reaction force due to wave radiation from mode j', also oscillating with the unit amplitude causing a reciprocity relation. Given that the dimension of the radiation impedance is 6 x 6 it becomes a symmetric matrix:

$$Z_{j',j} = Z_{jj'} \quad (3.126)$$

Several simplifications can be done in the impedance matrix depending on the analyzed body's geometry. For instance, if the plane $y=0$ is a symmetry plane then n_2 , n_4 and n_6 are odd functions of y in equation (3.124) whereas φ_1 , φ_3 , and φ_5 are even functions. Thus, $Z_{21}=Z_{23}=Z_{25}=Z_{41}=Z_{43}=Z_{45}=Z_{61}=Z_{63}=Z_{65}=0$. Furthermore, if the plane $x=0$ is also a symmetry plane then n_1 , n_5 and n_6 are odd functions of x while φ_2 , φ_3 , and φ_4 are even functions. Hence, $Z_{12}=Z_{13}=Z_{14}=Z_{52}=Z_{53}=Z_{54}=Z_{62}=Z_{63}=Z_{64}=0$. Taking also into account equation (3.126), the only remaining non zero off-diagonal elements of the radiation matrix impedance, when $y=0$ and $x=0$ are symmetry planes are $Z_{15}=Z_{51}$ and $Z_{24}=Z_{42}$. Given that ω is real, it is convenient to separate $Z_{j',j}$ into real and imaginary parts:

$$Z_{j',j} = R_{j',j} + iX_{j',j} = R_{j',j} + i\omega m_{j',j} \quad (3.127)$$

Where analogously to an electrical equivalent $R_{j',j}$ is named the radiation resistance, that contains the so called radiation damping coefficient, and $X_{j',j}$ is called the radiation reactance

where $m_j'j$ is the added mass coefficient. Both, radiation damping and added mass are fundamental parameters to reproduce accurately the floating body dynamics.

The only force which has not been described yet to complete the description of the forces acting on a floating body is the hydrostatic force, which is by far the simplest force acting on a floating body. The hydrostatic force F_H is the combined action of the gravity W and the buoyancy force F_B , which is strictly related to the hydrostatic pressure. Its expression is the following one and follows closely the Archimedes's principle:

$$F_B = V_s \rho g \quad (3.128)$$

$$W = mg = V_b \rho_b g \quad (3.129)$$

$$F_H = (V_s \rho - V_b \rho_b) g \quad (3.130)$$

Where V_s is the submerged volume of the body, V_b the total volume of the floating body and ρ_b is the body's density.

After describing all the forces acting on a floating body the final equation is:

$$F_F(t) = F_e(t) + F_r(t) + F_H(t) \quad (3.131)$$

Once all the forces acting on a floating body have been described it's time analyze the response of the body on the force's action. Following the pattern developed in the previous work in this Master Thesis, simplifications will be done in the motion modes, restricting the motion only to the third mode; namely, the heaving mode and therefore, the motion of the body in this single mode can be written as:

$$Z(t) = Re\{\xi e^{-i\omega t}\} \quad (3.132)$$

Where ξ is a complex constant the magnitude of which corresponds to the magnitude of the oscillation and the phase, it is remarkable to state that these parameters might differ, and commonly do, from those contained within the incident wave. The derived velocity field acceleration fields are respectively equations (3.133) and (3.134):

$$\dot{Z}(t) = U(t) = Re\{\mathbb{U} e^{-i\omega t}\}, \quad \mathbb{U} = -i\omega \xi \quad (3.133)$$

$$\ddot{Z}(t) = \dot{U}(t) = A(t) = Re\{\mathbb{A} e^{-i\omega t}\}, \quad \mathbb{A} = i\omega^2 \xi \quad (3.134)$$

Last but not least, to fully explain the floating body dynamics there is the need to merge forces and motions into one expression that states:

$$m\ddot{X} = F_F(t) + F_{ext}(X, \dot{X}, t) = F_e(t) + F_r(t) + F_H(t) + F_{ext}(X, \dot{X}, t) \quad (3.135)$$

Where m is the mass of the body and F_{ext} are the forces produced due to external elements such as mooring systems, end-stop system or power take-off systems. Equation (3.135) which is written in time domain can also be rewritten in the ordinary differential equation form (3.136) and in the frequency domain (3.137) as:

$$(m + A)\ddot{X} + B\dot{X} + CX = Re\{\mathbb{X} e^{-i\omega t}\} + F_{ext}(X, \dot{X}, t) \quad (3.136)$$

$$Re\{[-\omega^2(m + A) - i\omega B + C]\xi e^{-i\omega t}\} = Re\{\mathbb{X} e^{-i\omega t}\} + F_{ext}(X, \dot{X}, t) \quad (3.137)$$

Where A is the added-mass coefficient B is the radiation damping coefficient and C is the hydrostatic force coefficient.

CHAPTER 4: MATHEMATICAL MODELING

A model is a simplified representation of a system, which purpose is to enable reasoning within an idealized framework and also to allow testable predictions of what might happen under new circumstances. Done properly, the representation is based on explicit simplifying assumptions that give place to acceptably accurate simulations of the real system. A compact overview of the model building and evaluation process is presented in Figure 4.1. The process begins by interacting with reality through observation and experiment (through our senses and measurement device extensions of our senses). From qualitative and quantitative observations of the environmental system, progressive mental understanding of what seems important and how things work is gained. This forms a subjective ‘perceptual model’, unique to each person and influenced by previous experience and education.

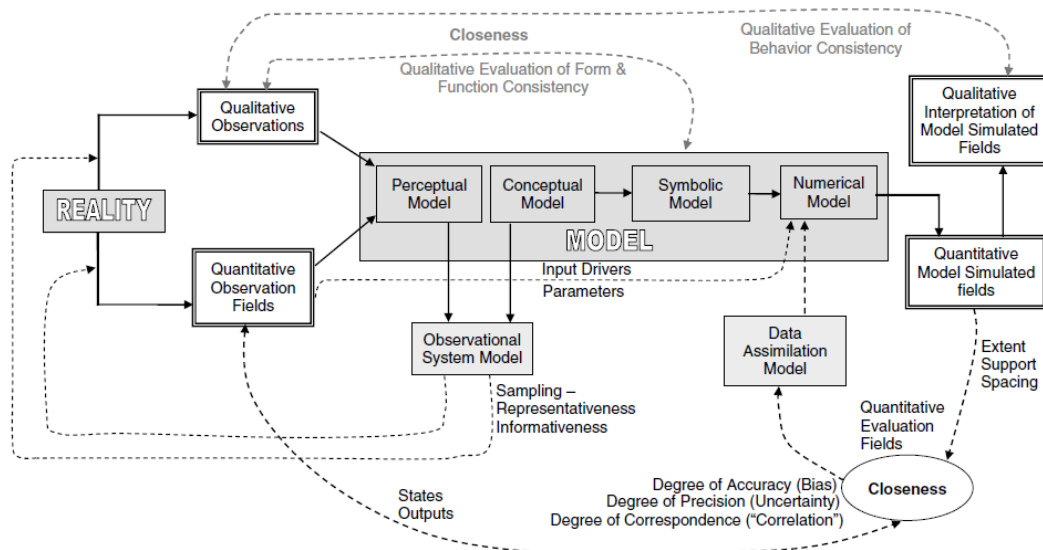


Figure 4.1: Stages of the model creation process and factors that have some kind of influence in that process.

As this perceptual understanding through contemplation and discussion is organized, one or more 'conceptual models' emerge, represented usually in the form of verbal and pictorial descriptions that enables to specify, summarize and discuss the gained understanding with other people. A complete conceptual model will include a clear specification of the following system elements; system boundaries, relevant inputs, state variables and outputs, physical and/or behavioral laws to be obeyed, facts to be properly incorporated uncertainties to be considered and the simplifying assumptions to be made. The relationships among these elements need not be rigorously specified, but should be conceptually explained through drawings, maps, tables, papers, reports, oral presentations, etc. Therefore, the conceptual model summarizes the abstract state of knowledge about the structure and workings of the system. Furthermore, it defines the level at which communication actually occurs between scientific colleagues or between scientists and policy/decision makers. Alternative conceptual models represent competing hypotheses about the structure and functioning of the observed system, conditioned on the perceptually acquired qualitative and quantitative observations and on the prior facts, knowledge and ideas. Taken together, the perceptual and conceptual models of the system along with the conditioning prior knowledge form the basic levels of the 'theory' about the system.

The need to a better understanding of the system and a better discrimination between competing hypotheses leads to the formulation of an 'observational system model' to guide effective and efficient acquisition of further data. The observation model should, of course, be derived from the theory and be designed to maximally reduce the uncertainty in our knowledge. Moreover, it should also be designed to detect flaws in the theory. Observational model design should accommodate observations on boundary conditions, conventional and extreme modes of system behavior, the issue of poorly observable system states, clarification of assumptions, and so on. Design issues will include sufficiency of sampling, representativeness of observations, informativeness, quality of data and measurement extent, support and spacing. Clearly, acquisition of knowledge via the observational system model is complementary to the formation of hypotheses via the theory.

The next steps in model development include the formulation of 'symbolic' and 'numerical' models. A symbolic model formalizes the understanding represented by a conceptual model using a mathematical system of logic that can be manipulated to enable rigorous reasoning and to facilitate the formulation of testable predictions. It is common to use the related systems of algebra and calculus for this purpose, although other logical systems are possible. Finally, because mathematical intractability often precedes explicit derivations of the dynamic evolution of system trajectories, it is common to build a numerical model approximation using a computer.

4.1 MODEL OF THE FLOATING BODY

There is a wide variety of mathematical models that describe the floating body dynamics, there are models in all forms and aspects: models working in the time domain, models working in the frequency domain, first order models also known as linear models, non-linear models of a higher order such as second or third order models and so on. In this work a non-linear model and more specifically a second order model has been chosen. Is a model that works in the time domain and has its origins in the Morison's Equation. This was introduced in a scientific paper in 1950 by Morison itself, O'Brien, Johnson and Schaaf. The model takes the name of its principal equation and it is therefore called, the Morison's Model. This model has been chosen due to its simplicity, low computational costs and accurate results and of course because it is especially efficient when talking about the description of offshore oscillating floating bodies dynamics, which is specially the case this Master Thesis work is about. The mathematical instrument used to carry on the simulation and modeling processes is the computer software MATLAB.

The Morison's equation which describes the forces acting on a floating body due to an incident wave is:

$$F = \rho_w V \dot{u} + \rho_b C_a V (\dot{u} - \dot{v}) + \frac{1}{2} \rho_w C_d A (u - v) |u - v| \quad (4.1)$$

Where V is the body's volume, u and v are the flow and body velocities respectively. \dot{u} and \dot{v} are their time derivative, so their accelerations, ρ_w is the sea water density, A is the area in which the force is applied, C_a is the added-mass coefficient and C_d is the drag or radiation force coefficient, both of them seen in the previous chapter in the floating body dynamics section. The first group of terms in equation (4.1) represents the Froude-Kyrlov force, equation (4.2), which represents the inertial term or as treated in the previous chapter, the excitation force. The second group of terms represents the real part of the radiation impedance directly related to the added-mass effects on a body. Finally, the third group of terms represents the imaginary part of the radiation impedance also known the radiation reactance which states the drag made by an incident wave.

$$\vec{F}_{FK} = - \int \int_S p \vec{n} dS \quad (4.2)$$

Where \vec{F}_{FK} is the Froude-Kyrlov force, S is the wet surface of the body p is the undisturbed pressure and \vec{n} is the normal vector of the incident wave. The Froude-Kyrlove force in its simplest form helps understand its intrinsic behavior:

$$F_{FK} = A p_{dyn} = A \rho g \frac{H}{2} \quad (4.3)$$

Where A is the wet area of a floating body, ρ is again the sea water density, g is the acceleration of gravity and H is the wave height. Once the fundamentals of the model have been stated its time to introduce the model's equation:

$$m(1 + c_a)\ddot{z} = F_B - W + \frac{1}{2}\rho C_d A(\dot{\eta} - \dot{z})|\dot{\eta} - \dot{z}| \quad (4.4)$$

Where m is the mass of the floating body, c_a is the added-mass coefficient, F_B is the buoyancy force, W is the weight force, ρ is the sea water density, C_d is the drag coefficient, A is the incident surface of the floating body, \ddot{z} is the body's acceleration and, $\dot{\eta}$ and \dot{z} are the free water surface and body's velocities respectively. It is extremely relevant to note that, whether the position, sea water velocity, body's velocity and body's acceleration are restricted to the vertical axis, that is why the letter z is used in their notation; thus, being coherent with the one degree of freedom restriction, specifically in heave mode.

Is generally known that the weight force is no mystery being the product of the body's mass by the gravity's acceleration:

$$W = mg = \rho_b Vg \quad (4.5)$$

Where ρ_b is the body's material density and V its volume. In this work two different geometries have been used to run the simulations, a spherical buoy and a cylinder shaped buoy:

$$V_S = \frac{4}{3}\pi r^3 \quad (4.6)$$

$$V_C = \pi a^2 b \quad (4.7)$$

Where r is the sphere radius, a is the base circle radius and b the draft of the cylinder. The buoyancy force derives directly from the Archimedes's principle as stated in the previous chapter and can be expressed in the following way:

$$F_B = \rho_f V_{sub} g \quad (4.8)$$

Where ρ_f is the density of the fluid and V_{sub} is the submerged volume of the body which in the sphere's and cylinder's cases is:

$$V_{subS} = \frac{4}{3}\pi r^3 - \frac{\pi}{6}h^2(3(2r - h) + h) \quad (4.9)$$

$$V_{subC} = \pi a^2 h \quad (4.10)$$

Being h the vertical distance from the base or the lowest point of the body to the water surface level. See Figure4.2.

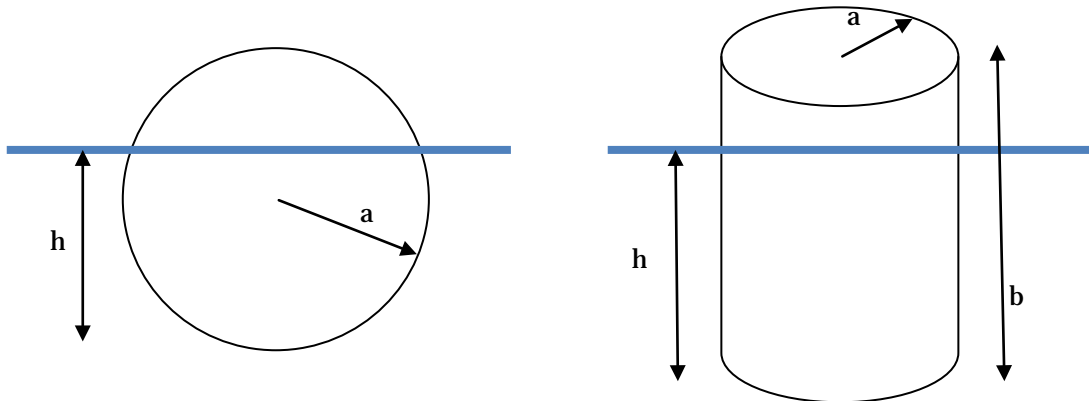


Figure 4.2: Description of the geometrical figures used as floating bodies. All the needed parameters to model them are described in the figure. Namely, the radius, draft and vertical distance where the floating body is partly submerged.

For a general geometry it is complicated to solve the radiation problem for an oscillating body, more specifically, to solve the boundary condition value problem without some numerical specialized computer software like WAMIT or AQUADYN. Unfortunately, it has been impossible to work with a software package of these characteristics in this Master Thesis, so as previously said, some general and simple geometries such as the sphere and the cylinder have been chosen. In the following paragraphs numerical calculations are presented for the radiation impedance for these particular geometries. Let's consider a sphere of radius a semi submerged on water of infinite depth. The particular geometry of the sphere allows to state with security that rotary modes ($j=4,5,6$) cannot generate any wave in an ideal fluid. Furthermore, all non-diagonal elements of the radiation impedance are equal to zero because $x=0$ and $y=0$ are both symmetry planes. Therefore, the only non vanishing terms are $Z_{11}=Z_{22}$ and Z_{33} , which can be written as:

$$Z_{jj} = \frac{2\pi\omega\rho a^3}{3}(\epsilon_{jj} + i\mu_{jj}) \quad (4.11)$$

Where ϵ and μ are non-dimensionalized radiation or drag and added-mass coefficients, respectively. The evolution of these parameters over the axis ka is illustrated in Figure 4.3, where k is the angular repetency, ω^2/g , seen on the previous chapter.

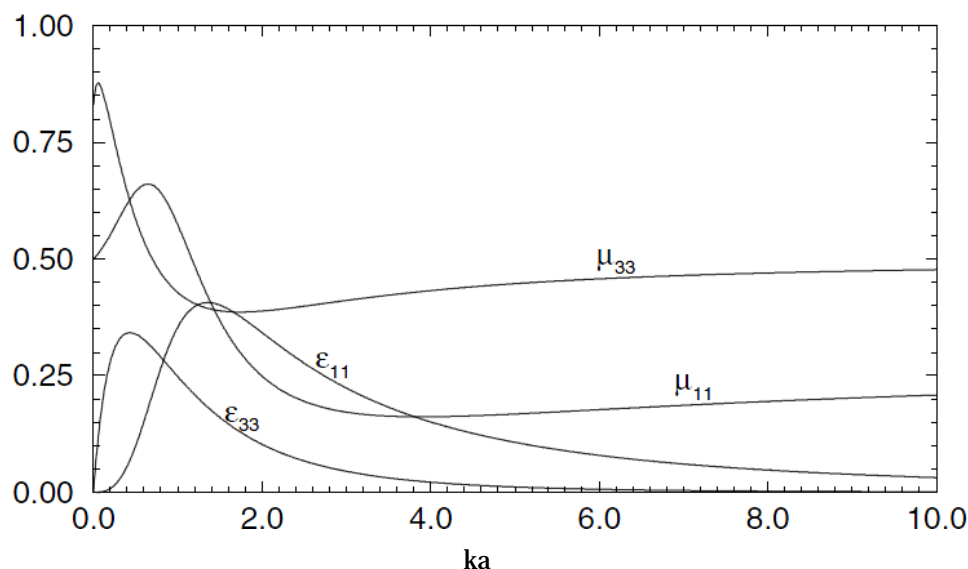


Figure 4.3: Distribution of the unitary radiation damping, ϵ , and the unitary added-mass coefficient, μ , in surge mode, $j=1$, and heave mode, $j=3$, of a spherical floating body of radius a over the product of the angular repetency, $k = \omega^2/g$, by the sphere's radius a .

May be noted that the radiation resistance tends to zero as ka approaches zero or infinite and the added mass is finite in both of these limits.

The next example shown in Figure 4.4 is the radiation impedance for the heave mode of a floating truncated vertical cylinder of radius a and draft b . The cylinder axis is the z axis ($x=0, y=0$). It may be observed that the curves shown in Figure 4.4 are qualitatively different to the corresponding curves in Figure 4.3 corresponding to the semi submerged sphere. This is because a different method has been used for the cylindrical buoy coefficients estimation. The method is called the Keulegan Carpenter method and it was designed specially for cylinders dynamics modeled with the Morison's equation, which is exactly the kind of model used in this work. Depending on the Keulegan Carpenter Number, $KC = \pi H/2a$, the plots indicate a specific value for the Drag Coefficient and for the added-mass coefficient (See Fig 4.4).

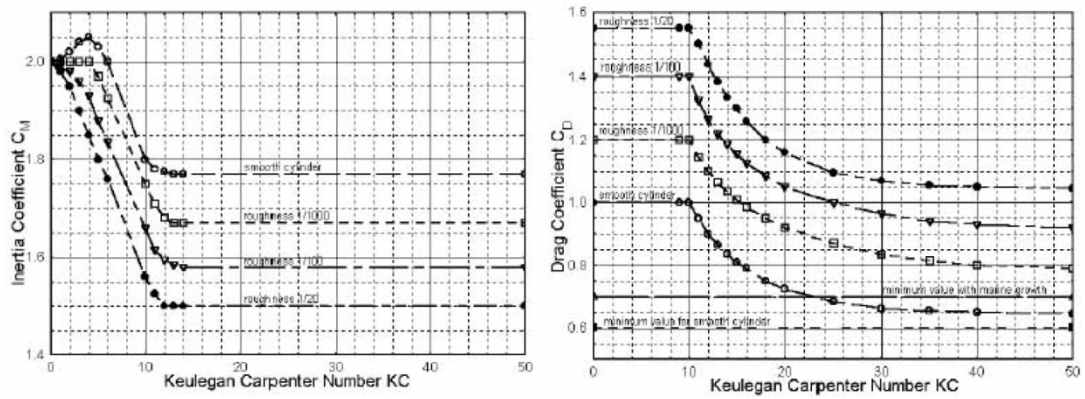


Figure 4.4: Distribution of the unitary radiation damping, C_{M_r} , and the unitary added-mass coefficient, C_D , in surge mode, $j=1$, and heave mode, $j=3$, of a cylindrical floating body of radius a over the Keulegan Carpenter Number $KC=\pi H/2a$.

The results for the given waves are:

$$H = \{0.5, 1.0, 1.5, 2.0, 2.5, 3.0, 3.5, 4.0, 4.5, 5.0, 5.5, 6.0\} [m] \quad (4.13)$$

$$T = \{2, 3, 4, 5, 6, 7, 8, 9, 10\} [s] \quad (4.14)$$

$$C_d = \{0.240, 0.340, 0.330, 0.270, 0.180, 0.095, 0.050, 0.040, 0.030\} \quad (4.15)$$

$$C_a = \{0.425, 0.640, 0.720, 0.780, 0.820, 0.825, 0.810, 0.790, 0.790\} \quad (4.16)$$

$$C_d = 1.55 \quad (4.17)$$

$$C_a = \{1.99, 1.96, 1.93, 1.89, 1.85, 1.81, 1.77, 1.74, 1.70, 1.67, 1.62, 1.58\} \quad (4.18)$$

Vectors (4.15) and (4.16) are the drag and added-mass coefficients respectively for the sphere buoy and vectors (4.17) and (4.18) are the drag and added-mass coefficients for the cylinder buoy.

Figures 4.5 and 4.6 show the reaction of the sphere and cylinder respectively, for a certain wave of $H=2$ [m] and $T=4$ [s]:

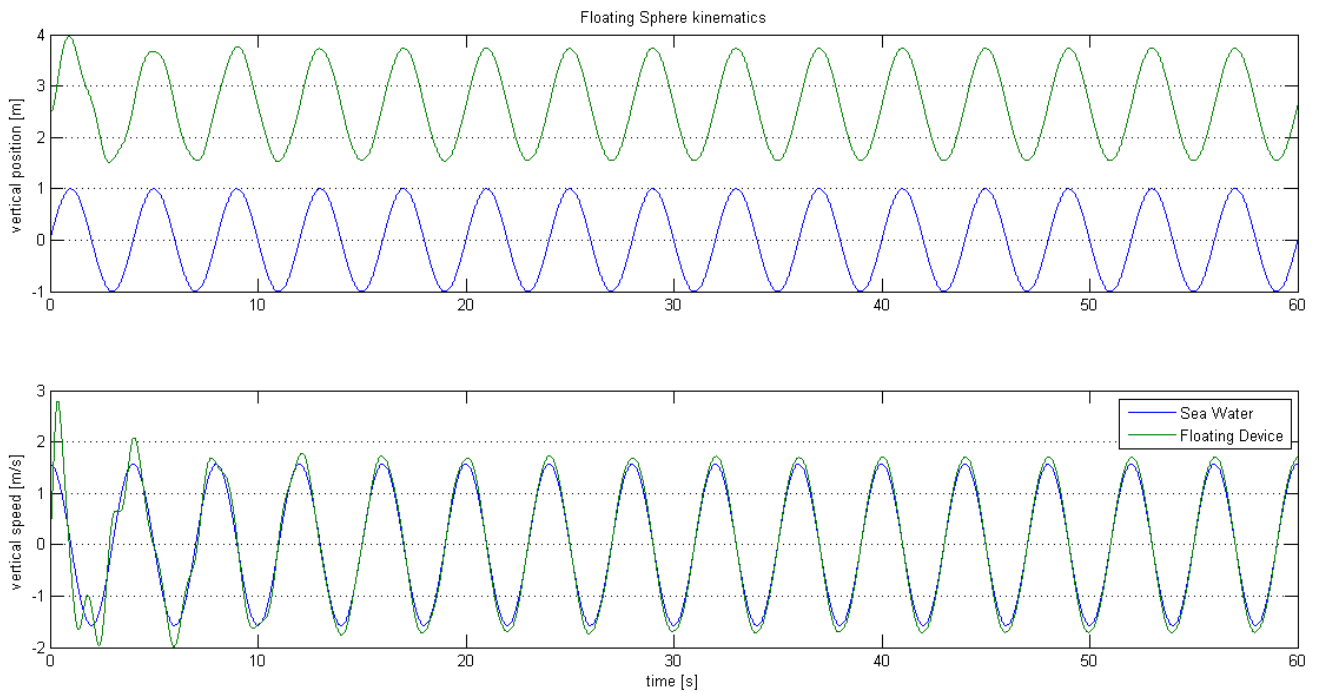


Figure 4.5: Vertical Position and vertical Speed of a spherical floating body induced by incident monochromatic waves with constant height and period over the time.

It can be noted that the previously described model reproduces accurately and coherently the behavior of a floating sphere of 1.5 meters of radius placed within a wave field.

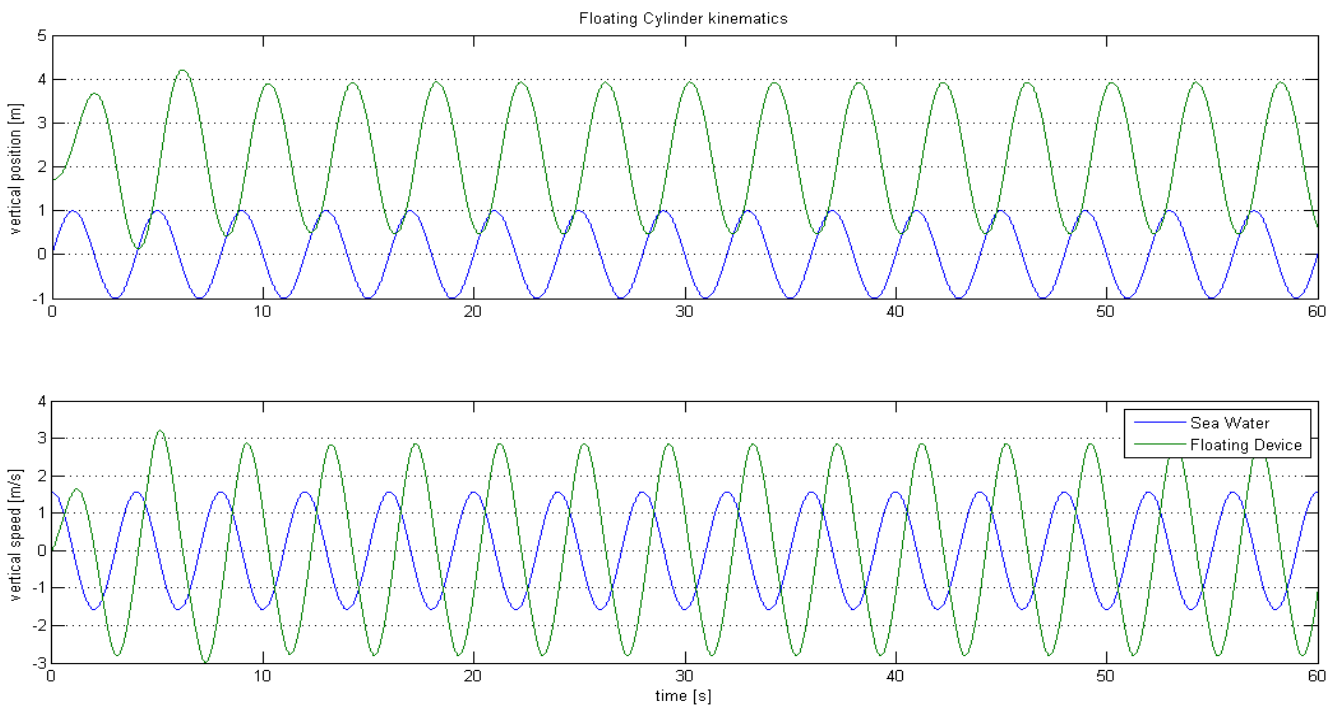


Figure 4.6: Vertical Position and vertical Speed of a cylindrical floating body induced by incident monochromatic waves with constant height and period over the time.

Same conclusion can be extracted from Figure 4.6, moreover, it may be noted that both, the floating body motion's amplitude and vertical speed are higher. As a result of a preliminary analysis it can be thought that the cylinder can have a greater power output than the sphere, but there are not enough parameters to confirm it yet and further analysis have to be done. Both figures also show clearly the transient and steady regimes of the floating body. In the firsts periods, longer or shorter number of periods depending on the variables, the floating body behavior is more instable and erratic, that is the transient regime and then gradually becomes stable and constant, at that point the system has reached the stationary regime. The stationary regime is the one used to analyze and draw the conclusions from the floating body behavior.

4.2 MODEL OF THE LINEAR GENERATOR

4.2.1 ELECTROMAGNETIC MODEL

Synchronous generator models are usually based on the hypothesis that the rotation speed is constant, a proof of that are some parameters such as the synchronous reactance in the electric equivalent circuit, $X_s = \omega L_s$ which is assumed to be a constant value; consequently, the electric frequency ω and the inductance L_s must be also constant, this is not possible in a linear generator as the translator speed is continuously varying due to the wave position. An accurate description of the linear generator is illustrated in Figure 4.7.

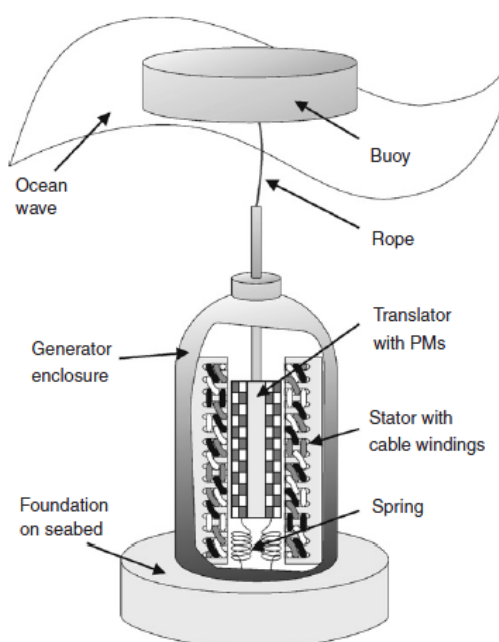


Figure 4.7: General Sketch of a point absorber wave energy converter. Main parts of the generator and the floating body are pointed down.

The proposed linear generator has permanent magnets mounted in the translator with alternating polarity. The motion of the translator can be assumed sinusoidal or closely sinusoidal, the amplitude associated with that motion is h and its frequency Ω , so the position and vertical speed of the translator can be written as:

$$z(t) = h \sin(\Omega t) \quad (4.19)$$

$$\dot{z}(t) = \Omega h \cos(\Omega t) \quad (4.20)$$

The pole pair width, ω_p , is defined as the distance from a north pole to the next one; therefore, the electric angular frequency can be expressed as: (See Fig. 4.8)

$$\omega(t) = \frac{2\pi}{\omega_p} \dot{z} = \frac{2\pi\Omega h}{\omega_p} \cos(\Omega t) \quad (4.21)$$

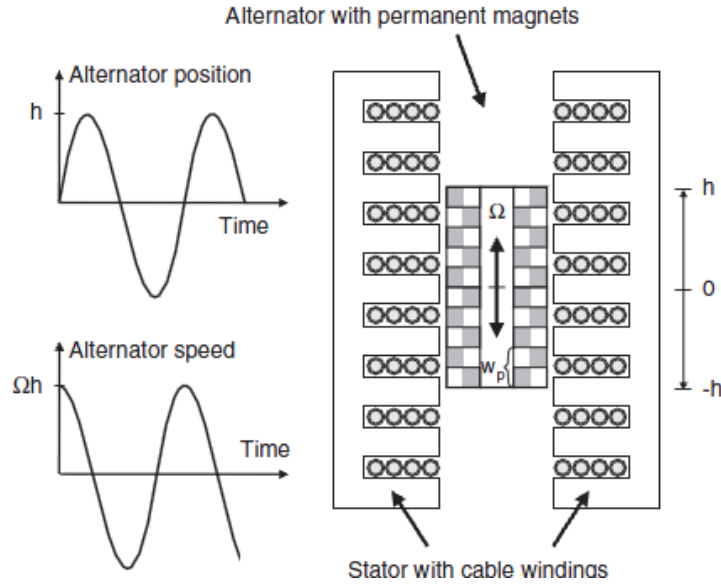


Figure 4.8: General sketch of the electric linear generator, with its main parts such as the translator and stator are illustrated in detail.

The electric position θ is obtained integrating the electric angular frequency over the time:

$$\theta(t) = \int_0^t \omega(t) dt = \frac{2\pi h}{\omega_p} \sin(\Omega t) \quad (4.22)$$

Considering the flux, Φ , slows down the motion by an angle δ , the flux can be expressed as a function of the electric position θ in the following way:

$$\Phi(t) = \Phi_t \cos(\theta + \delta) = \Phi_t \cos\left[\frac{2\pi h}{\omega_p} \sin(\Omega t) - \delta\right] \quad (4.23)$$

Where Φ_t is the flux amplitude and δ is the load angle, which has been exposed in the previous chapter, the flux amplitude can be written as:

$$\Phi_t = B_t \omega_t d p q c \quad (4.24)$$

Where B_t is the magnetic field in a given tooth, ω_t is the width of a stator tooth, where the flux line flow through its cross-sectional area. d is the width of the stator stack, p is the total number of poles, q is the number of slots per pole and phase and c is the number of cables or windings per slot. If equation (4.23) is derived, as stated by the Faraday's law, the voltage is obtained as follows:

$$e(t) = \frac{2\pi B_t \omega_t d p q c}{\omega_p} \cos(\Omega t) \sin\left[\frac{2\pi h}{\omega_p} \sin(\Omega t) - \delta\right] \quad (4.25)$$

$$e(t) = \frac{2\pi B_t \omega_t d p q c}{\omega_p} \dot{z} \sin\left[\frac{2\pi h}{\omega_p} z - \delta\right] \quad (4.26)$$

In the previous equations, equation (4.25) is adapted to a sinusoidal motion of the translator whereas equation (4.26) is expressed as a function of generic velocities and positions.

The voltage calculated in equations (4.25) and (4.26) corresponds to a phase voltage, as stated in the previous chapter, the linear generators being studied and developed for wave energy converters are three-phase generators. The reason for it is that three coils are installed instead of a single coil, making three electric equivalent circuits, the physical location of its coil is displaced from the other two a distance that in electrical terms makes them differ in 120 degrees, this is the only difference, so the voltage, expressed in V, of each phase is:

$$e_a(t) = \frac{2\pi B_t w_t dpqc}{\omega_p} \cos(\Omega t) \sin \left[\frac{2\pi h}{\omega_p} \sin(\Omega t) - \delta \right] \quad (4.27)$$

$$e_b(t) = \frac{2\pi B_t w_t dpqc}{\omega_p} \cos(\Omega t) \sin \left[\frac{2\pi h}{\omega_p} \sin(\Omega t) - \delta + \frac{2\pi}{3} \right] \quad (4.28)$$

$$e_c(t) = \frac{2\pi B_t w_t dpqc}{\omega_p} \cos(\Omega t) \sin \left[\frac{2\pi h}{\omega_p} \sin(\Omega t) - \delta - \frac{2\pi}{3} \right] \quad (4.29)$$

Following the electric equivalent circuit illustrated in the previous chapter the electric currents, expressed in A, which flow through each phase is calculated as follows:

$$I_a(t) = \frac{e_a(t) \cos(\delta)}{R_c + R_{load}} \quad (4.30)$$

$$I_b(t) = \frac{e_b(t) \cos(\delta)}{R_c + R_{load}} \quad (4.31)$$

$$I_c(t) = \frac{e_c(t) \cos(\delta)}{R_c + R_{load}} \quad (4.32)$$

What is really of interest though, is the voltage in the loads borne, because that is the useful energy output, the useful tension, in Volts, can be expressed as:

$$u_a(t) = e_a(t) * \cos(\delta) - R_c I_a(t) \quad (4.33)$$

$$u_b(t) = e_b(t) * \cos(\delta) - R_c I_b(t) \quad (4.34)$$

$$u_c(t) = e_c(t) * \cos(\delta) - R_c I_c(t) \quad (4.35)$$

Once all these parameters have been found the next logical step is to find the output power through a very simple relation, which can be expressed either in VA or W. VoltAmpere is the unit of SI for the apparent power, which is the total electrical power and W is the unit of SI for the real power, which is the useful power. In that case, apparent and real power are the same due to the power factor, $\cos(\varphi)$, which for that generator equals to one, and that means that the reactive, and useless, power is void:

$$S_a(t) = P_a(t) = u_a(t) I_a(t) \quad (4.36)$$

$$S_b(t) = P_b(t) = u_b(t) I_b(t) \quad (4.37)$$

$$S_c(t) = P_c(t) = u_c(t) I_c(t) \quad (4.38)$$

$$S_T(t) = P_T(t) = P_a(t) + P_b(t) + P_c(t) \quad (4.39)$$

The useful kind of parameters for electrical purposes are those called the root mean squared parameters and electrically represent the equivalents for direct current systems. The studied linear generator works in alternate current:

$$e_{rms} = \frac{\max(e_a(t))}{\sqrt{2}} \quad (4.40)$$

$$I_{rms} = \frac{\max[u_a(t)]}{\sqrt{2}} \quad (4.41)$$

$$u_{rms} = \frac{\max[u_a(t)]}{\sqrt{2}} \quad (4.42)$$

$$P_{rms} = u_{rms} I_{rms} \quad (4.43)$$

In order to be attractive for modeling purposes, the magnetic force generated by the linear generator has to be determined. First the magnetic power has to be found and that is achieved through a very simple step. Linear generators, as any other device, are not perfect and their energy transfer is never complete, so dividing the electric power by the efficiency of the devices the mechanic power is obtained and then, simply dividing again by the velocity of the translator, which is the generating part, the magnetic force is obtained:

$$P_M = \frac{P_T}{\eta_{el}} \quad (4.44)$$

$$F_M = \frac{P_M}{\dot{z}} \quad (4.45)$$

Figures 4.9, 4.10, 4.11 and 4.12 show the graphics of the voltage, current and power respectively over a period of a wave of $H=2$ [m] and $T=4$ [s] and table 4.1 shows the values of the simulation parameters. One may note that all these representations are also cyclic, which is logical because they come from the original energy of the wave which is also periodical.

Parameter	Name	Value	Unit
Cosφ	Power Factor	1	-
n_s	No. of Stator Sides	4	-
ω_p	Pole Pair Width	100	mm
d	Width of the Stator	400	mm
ω_t	Tooth Width	8	mm
p	Total No. of Poles	100	-
q	Winding Ratio	6/5	slot/(pole, phase)
c	No. of Cables per Slot	6	-
B_t	Magnetic Field in tooth	1.55	T
R_{LOAD}	Load Resistance	3.1	Ω
R_C	Generator Resistance	0.3735	Ω
L	Generator Reactance	11.5	mH

Table 4.1: Description of the electromagnetic parameters of the linear generator; with name, parameter, value and unit.

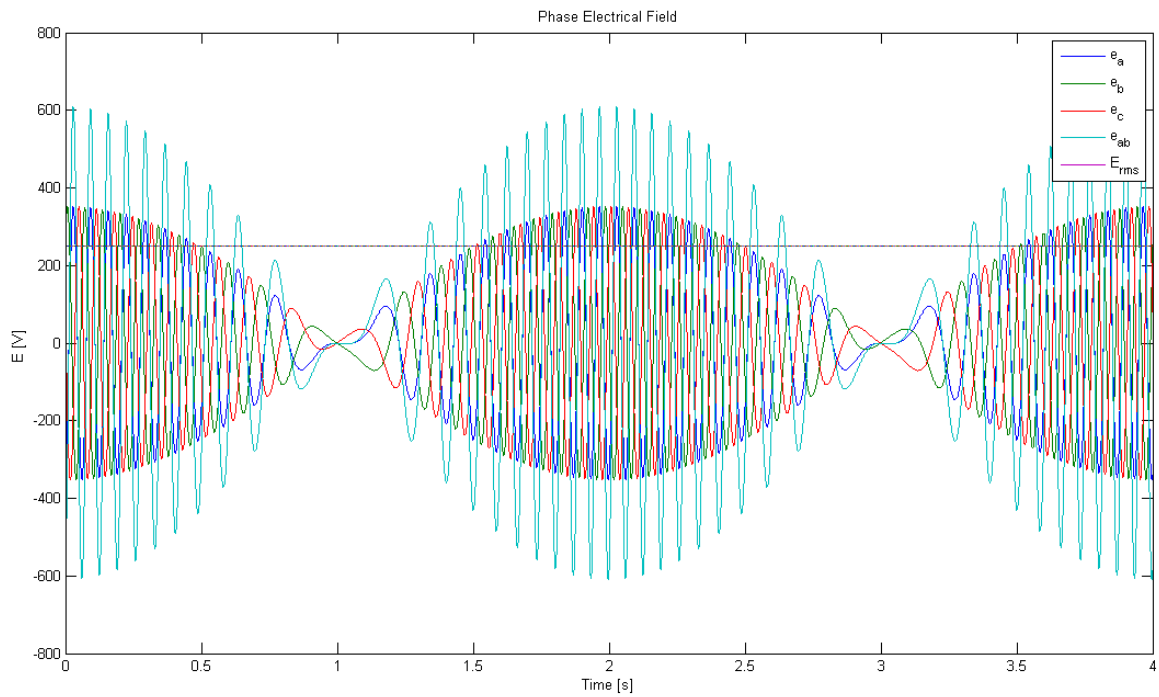


Figure 4.9: Electrical field induced by the wave motion in the stator of the generator. Phases a, b and c are represented. The voltage between two phases is also plotted and the root mean squared voltage is also marked due to its importance.

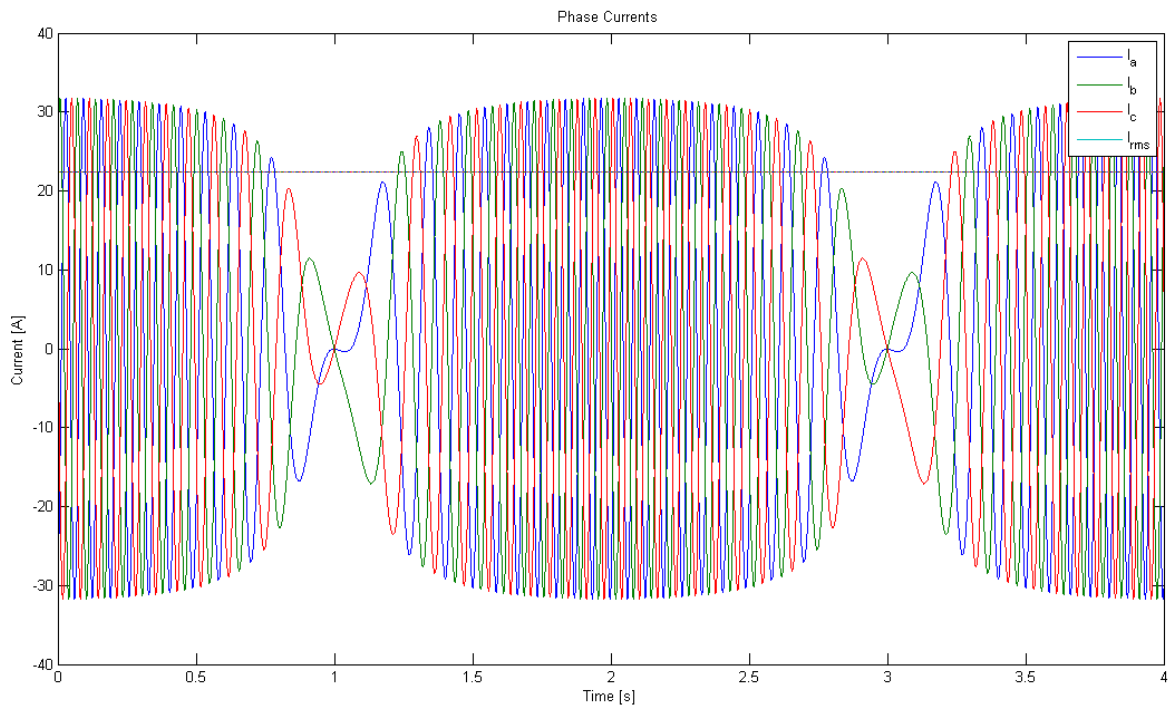


Figure 4.10: Electrical current induced by the wave motion in the stator of the generator. Phases a, b and c are represented. The root mean squared current is also marked due to its importance.

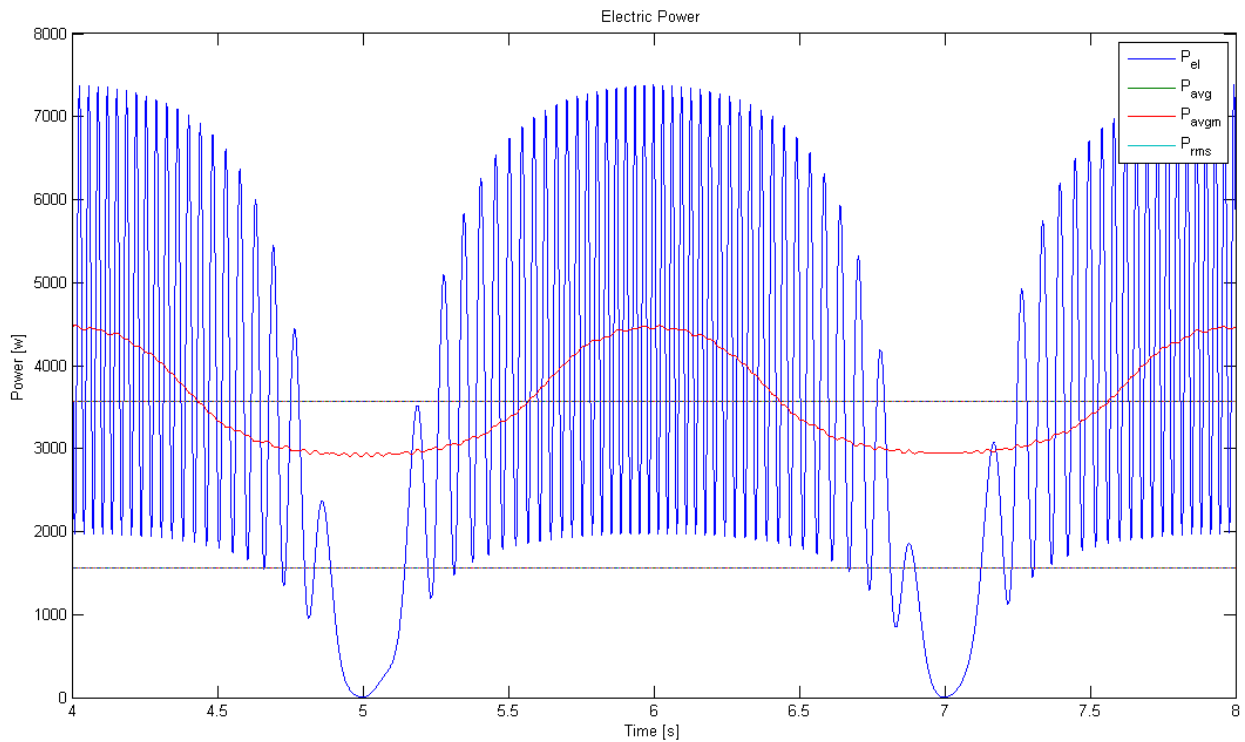


Figure 4.11: Electrical power generated by the wave motion. There are also plotted the time averaged power for the whole time and for a mobile window. The root mean squared current is also marked due to its importance.

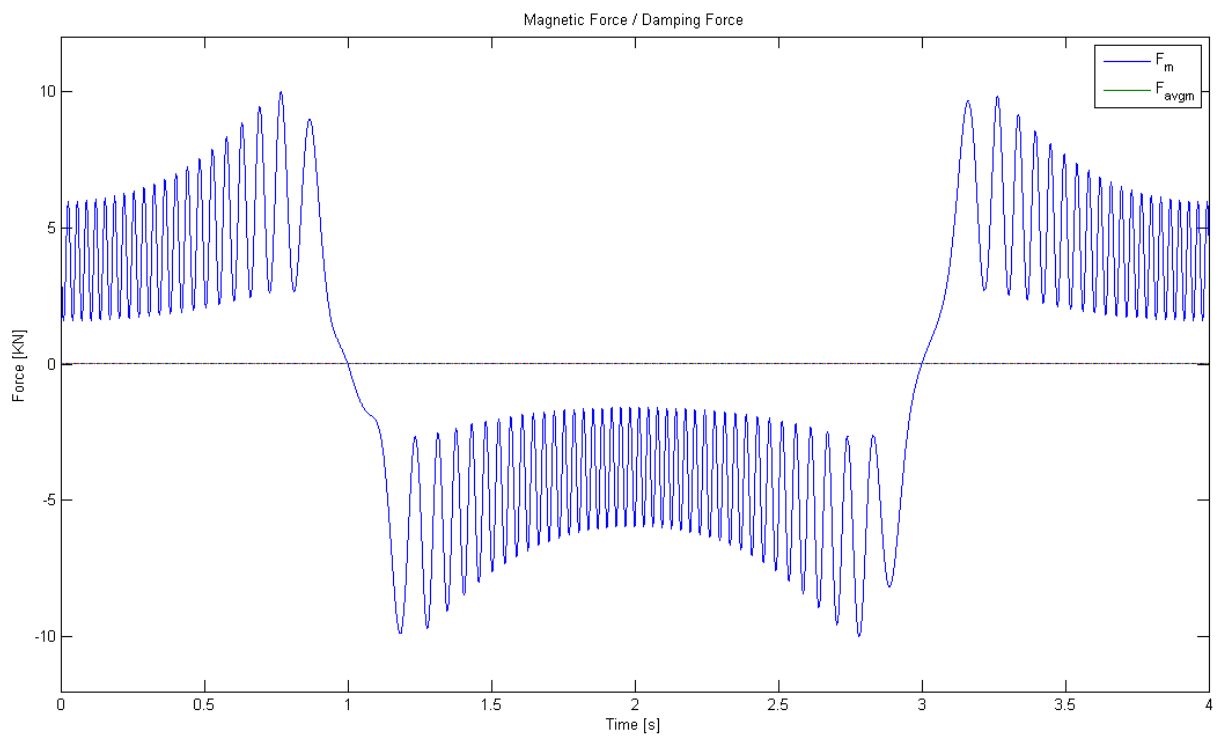


Figure 4.12: Magnetic Force generated by the wave motion in the translator of the generator. The time averaged force is also plotted.

4.2.2 MECHANICAL MODEL

An electrical linear generator can also be seen from a different point of view, from a different perspective. For obvious reasons, the electrical modeling is the most important part when developed this kind of devices but, linear generator play also a very important role in the mechanical aspect. As shown in Figure 4.13, linear generators have springs that link the translator and sea-bed. That is crucial for the proper work of the device, these springs serve as end-stop systems that prevent the device from damaging during storm periods when the wavs heights can reach considerable levels. In addition, the springs allow the translator to move in a smooth way that favors the power extraction. Their action is described as follows: when the waves pushes up the spring acts against this motion to avoid extremely high velocity peaks and when the wave level is going down to the trough, the spring assures this motion to be regular and smooth pulling the translator downwards and thus, not leaving it free to the gravity forces.

The linear generators mechanical equivalent is the well known mass-spring-damper system. This kind of systems have been very well studied for many years since are the representation of very important systems or devices like motorcycle suspensions and many others. Figure 4.13 illustrates in a mechanical way the mass-spring-damper system.

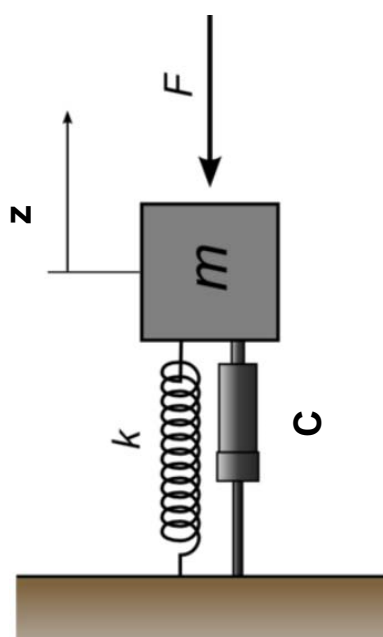


Figure 4.13: Illustration of the mechanical equivalent of the electric linear generator, a mass-spring-damper system with its parameters m , k and C as the mass, the spring coefficient and the damping coefficient respectively.

This is mainly an oscillating system; favored by the force F and the spring k and smoothed by the damper C . its governing equation can be written as follows:

$$f_{PTO} = -m_{trans} \ddot{z} - c\dot{z} - kz \quad (4.48)$$

Where the variables of this ordinary differential equation are the acceleration \ddot{z} , the velocity \dot{z} and the position z respectively. The kind of models that best describe the behavior of this systems are the so called, state-space models. The force F is considered as an input and the mass velocity \dot{z} is considered as an output of this system. The system is of second order, since it has one mass which can contain both kinetic and potential energy. A feasible selection of the states are the position z and the velocity \dot{z} , which derivate is given by Newton's second law. The state space system is indeed expressed in the following way:

$$\dot{p}(t) = Ap(t) + Bu(t) \quad (4.49)$$

$$y(t) = Cp(t) + Du(t) \quad (4.50)$$

Where $p(t)$ and $\dot{p}(t)$ are the outputs, $u(t)$ is the input and $y(t)$ is the state of the system, equations (4.49) and (4.50) derive into the following system:

$$\begin{pmatrix} \dot{p} \\ \dot{\dot{p}} \end{pmatrix} = (A) \begin{pmatrix} p \\ \dot{p} \end{pmatrix} + (B)u = \begin{pmatrix} \dot{x} \\ \dot{\dot{x}} \end{pmatrix} = \begin{pmatrix} 0 & 1 \\ -\frac{k}{m} & -\frac{c}{m} \end{pmatrix} + \begin{pmatrix} 0 \\ -\frac{1}{m} \end{pmatrix} f_{PTO} \quad (4.51)$$

$$y = (C) \begin{pmatrix} p \\ \dot{p} \end{pmatrix} + (D)u = \dot{x} = (0 \quad 1) \begin{pmatrix} x \\ \dot{x} \end{pmatrix} + (0) f_{PTO} \quad (4.52)$$

An important thing to have in mind to optimize the device behavior and maximize the power output is to reach resonance conditions. If the system is oscillating in a specific frequency ω , that analogously could perfectly be the wave frequency, by imposing the following constrain to the system resonance conditions will be reached:

$$\omega = \sqrt{\frac{k}{m}} \quad (4.53)$$

4.3 MODEL OF THE WAVE ENERGY CONVERTER

This last section of the mathematical modeling chapter is going to describe the modeling process of a wave energy converter, a point absorber device consisting of a floating body and an electric linear generator as PTO. All the knowledge acquired on the previous chapters and previous sections of this chapter is merged together to produce a complete model which allows to compute, in a realistic way, the needed values to accurately reproduce the behavior of the device in real open seas. Besides, the optimization of some parameters helps to improve, to some extent, the device's work.

The final model of the wave energy converter has and hydrodynamic part, an electromagnetic part and a mechanical part. All these concepts of very different nature are merged together and all united work in perfect harmony giving some results that permit to draw conclusions which will possibly bring to substantial improvements in the foreseeable future.

The hydrodynamic part, strictly related to the upper part of the device; in other words, the floating body is the one that traps the energy contained in the incident waves through the different mechanisms explained in full detail in the last section of the previous chapter. Both, mechanical and electromagnetic parts are referred to the power take-off mechanism and their goal is to convert the energy trapped by the floating body into a useful energy kind that can later be used by the human race. A schematic representation of the full wave energy converter is illustrated in Figure 4.14.

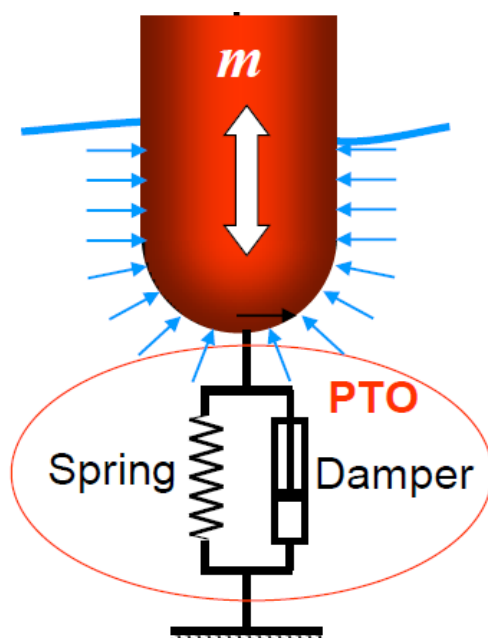


Figure 4.14: Illustration of the mechanical equivalent of the point absorber WEC, a mass-spring-damper system.

The system represented in Figure 4.14 is composed by a floating body, a spring and a damper; as stated in several occasions previously in this work, this system has only one degree of freedom in the vertical direction, allowing only the motion in heave mode and having only one coordinate in the reference coordinate system. Putting together all this concepts previously described, results in a process towards the main equation of the mathematical model of this wave energy converter in the following way:

$$m(1 + c_a)\ddot{z} = F_B - W + \frac{1}{2}\rho C_d A(\dot{\eta} - \dot{z})|\dot{\eta} - \dot{z}| \quad (4.54)$$

$$f_{PTO} = -m_{trans}\ddot{z} - c\dot{z} - kz \quad (4.55)$$

$$F_M = \frac{P_M}{\dot{z}} \quad (4.56)$$

Equation (4.54) represents the hydrodynamic aspect of the WEC. Actually, this is the floating body dynamic's equation. Equation (4.55) states the mechanical equivalent of the force generated by the power take-off mechanism and Equation (4.56) specifies the magnetic force generated by the linear generator which can also be interpreted as the mechanical damping, $c\dot{z}$, in Equation (4.55). Once the different terms of the main model's equation have been identified, this can be expressed in the following way:

$$\text{Inertial Force} = \text{Hydrostatic Forces} + \text{Hydrodynamic Forces} + \text{PTO Forces} \quad (4.57)$$

$$(m(1 + c_a) + m_{trans})\ddot{z} = F_B - W + \frac{1}{2}\rho C_d A(\dot{\eta} - \dot{z})|\dot{\eta} - \dot{z}| - F_M(\dot{z}, z) - kz \quad (4.58)$$

Where m is the mass of the floating body, m_{trans} is the mass of the translator part of the linear generator; c_a is the added-mass coefficient. \ddot{z} , \dot{z} , and z are the vertical acceleration, velocity and position of the system, respectively, F_B is the buoyancy force, W is the weight force, ρ is the fluid density, C_d is the drag coefficient, A is the wet surface of influence of the floating body. $\dot{\eta}$ is the vertical free water surface velocity, F_M is the magnetic force generated by the linear generator and k is the spring constant which states the degree of stiffness.

Furthermore, if the device performance wants to be improved and the power outtake wants to be increased, some constraints can be applied. It is commonly known that for an oscillating system the best way to maximize its energy absorption is by fulfilling its resonance conditions. In a simple system just composed of a mass and a spring of k constant, the resonance is reached by the following expression as shown by Figure 4.15:

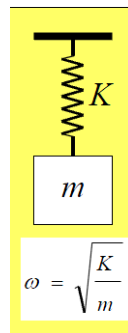


Figure 4.15: Simplification of a mass-spring system and its condition to reach resonance.

In the case of the studied wave energy converter device, its system, as shown in Figure 4.7 is a bit more complex and the resonance conditions results in:

$$\omega = \sqrt{\frac{\rho g A + k}{m(1+c_a) + m_{trans}}} \quad (4.59)$$

As a result of equation (4.59), by simply adapting the spring coefficient k , the resonance in the whole system is achieved. After applying these settings the system is optimized and the model is ready to be simulated and discover the numerical results.

CHAPTER 5:

SIMULATIONS

5.1 DESCRIPTION

After having described the mathematical model of the wave energy converter device in the previous chapter, the next logical stage is to use that model and check its performance. Subsequently, once the wave energy converter's behavior has been studied, the drawing of some conclusion will be able. Simulations will consist of reproducing the performance of two different floating bodies, a spherical buoy and a cylindrical buoy with practically the same electrical linear generator in two different locations; the coasts of Alghero, in the island of Sardinia, Italy and Mazara, in the island of Sicily, Italy.

The simulations begin with the physical determination of the wave energy converter device. In order to achieve reliable results all parameters must be set in a proper and realistic way. Table 5.1, 5.2 and 5.3 specify the physical parameters of the spherical buoy, the cylindrical buoy and the linear generator respectively.

Parameter	Name	Value	Units
R_e	External Radius	1.500	m
R_i	Internal Radius	1.485	m
A	External Area	7.068	m ²
V_e	External Volume	14.137	m ³
V_i	Internal Volume	13.717	m ³
V	Material Volume	0.420	m ³
ρ_m	Material Specific Weight: PVC	14000	N/m ³
W_m	Material Weight	5878.4	N
m_m	Material Mass	599.4	Kg

Table 5.1: Description of the physical parameters of the spherical floating body of the WEC; with name, parameter, value and unit.

Parameter	Name	Value	Units
R_e	External Radius	1	m
R_i	Internal Radius	0.850	m
b	Draft	4	m
A	External Area	3.142	m ²
V_e	External Volume	12.566	m ³
V_i	Internal Volume	8.398	m ³
V	Material Volume	4.161	m ³
ρ_m	Material Specific Weight: PVC	14000	N/m ³
W_m	Material Weight	58354	N
m_m	Material Mass	5950.4	Kg

Table 5.2: Description of the physical parameters of the cylindrical floating body of the WEC; with name, parameter, value and unit.

As it can be seen in tables 5.1 and 5.2, the spherical and cylindrical buoys respectively, are not solid bodies and they could be considered as a spherical and cylindrical shells respectively, of 15 cm of thickness. Its dimensions are relatively low in comparison to other devices which are currently being tested in different seas of the world. Since the devices, studied in this work, are thought to be deployed in the Mediterranean Sea, where the energetic regime is substantially lower than in other oceans of the world, the devices dimensions need to be reduced to maximize the energy capture.

Parameter	Name	Value	Unit
$\cos\varphi$	Power Factor	1	-
n_s	No. of Stator Sides	4	-
ω_p	Pole Pair Width	100	mm
d	Width of the Stator	400	mm
ω_t	Tooth Width	8	mm
p	Total No. of Poles	100	-
q	Winding Ratio	6/5	slot/(pole, phase)
c	No. of Cables per Slot	6	-
B_t	Magnetic Field in tooth	1.55	T
R_{LOAD}	Load Resistance	3.1	Ω
R_C	Generator Resistance	0.3735	Ω
L	Generator Reactance	11.5	mH
ρ_F	Density of the translator's Material: Ferrite	4700	Kg/m ³

Parameter	Name	Value	Unit
L_{Tr}	Length of the Translator	5.425	m
w_{Tr}	Width of the Translator	0.298	m
A_{Tr}	Area of the Translator	0.089	m ²
V_{Tr}	Volume of the Translator	0.482	m ³
m_{Tr}	Mass of the Translator	2264.3	kg
W_{Tr}	Weight of the Translator	2205	N

Table 5.3: Description of both, the electromagnetic and physical parameters of the linear generator; with name, parameter, value and unit.

In table 5.3 every parameter of the linear generator is defined. However, there is still one essential parameter of the power take-off system to be stated. The power take-off mechanism is composed by the linear generator and a system of springs that guarantee the best and smoothest performance of the wave energy converter. This set of springs can be simplified as an equivalent spring which elastic coefficient is still unknown and has to be determined. As stated in the previous chapter, for optimized power absorption levels, the resonance of the whole oscillating system has to be reached. Thereby, the properties of this spring have to be adapted in the following way:

$$k = \omega^2 m_{tot} - \rho g A \quad (5.1)$$

Where ω is the wave frequency, m_{tot} is the total mass of the device (including the added mass), ρ is the sea water density and A is the area described in tables 5.1 and 5.2 for spherical buoy and cylindrical buoy respectively.

Simulations have been run over 108 different sea states, composed of 9 different significant wave periods and 12 different significant wave heights. That is to say, for each of the 12 different significant wave heights, one simulation for each of the 9 different significant wave periods has been carried out. The specific significant wave periods and heights composing the sea states are shown below:

$$H_{s,i} = \{0.5, 1.0, 1.5, 2.0, 2.5, 3.0, 3.5, 4.0, 4.5, 5.0, 5.5, 6.0\} [m] \quad (5.2)$$

$$T_{s,j} = \{2, 3, 4, 5, 6, 7, 8, 9, 10\} [s] \quad (5.3)$$

In each simulation the optimal value for resonance condition of the spring coefficient is calculated for both WECs, the one with the spherical buoy and the one with the cylindrical floating body. After finding the optimal value for k , all parameters needed to run the simulations are already available. Consequently, a simulation of the entire WEC devices is run over a period of time of 60 seconds with a sampling interval of 0.0005 seconds, for each couple of significant wave height and period. To successfully run the simulation an initial state of the devices is needed, it has been chosen the most logical situation in which the devices are resting in the sea when the free water surface is flat, that is to say, the device is in static equilibrium in waves absence, as it can be seen in table 5.4 the vertical initial velocity is

not exactly zero, that is to avoid probable future problem during the simulation, as the simulation code is made of Ordinary Differential Equations that need to be integrated in order to find the solution, and when the sampling data contains an explicit zero it often fails due to its integrating limits :

Device / State	Vertical Position	Vertical Velocity
Spherical Buoy	2.49	0.001
Cylindrical Buoy	1.69	0.001
Units	m	m/s

Table 5.4: Initial states of the spherical buoy and cylindrical buoy when running the simulations. Describes, vertical position, vertical velocity and units.

When all data is ready, the simulation is carried out via the main equation of the model, stated in the previous chapter, equation (4.58). Once the data of the vertical positions and velocities over those 60 seconds is gathered the second half of the data is used to compute the power extraction. The last 30 seconds are used for that purpose because after a prudential time the system has become stable and reached the stationary state, this is a crucial step to avoid misleading when interpreting the results.

The results of the output power, achieved by each different spring coefficient and floating body, are organized by significant wave height and period creating what is commonly known as Power Matrix. The obtained Power Matrixes are used then to compute the performance of each different device through a new set of simulations. These reproduce each device's behavior in the virtual case of deployment in the locations of Alghero and Mazara for several years. These simulations have been run using the data available in the university department. The available data contains the wave record of both locations, Alghero and Mazara, already synthesized in sea state conditions.

The available data contains:

- Significant Wave Height, H_s [m]
- Peak Energy Wave Period, T_p [s]
- Duration of that specific sea state, Dt [h]
- Energetic wave Period, T_e [s]
- Sea State Power, P_{ss} [kW/m]
- Sea State Energy, E_{ss} [kWh/m]
- Annual Mean Power, P_y [kW/my]
- Annual Mean Energy, E_y [kWh/my]

In the location of Alghero the following years are available: 1990, 1991, 1992, 1993, 1994, 1995, 1996, 1997, 1998, 1999, 2000, 2001, 2002, 2003, 2007, 2010 and 2011. And for Mazara the available years are: 1990, 1991, 1992, 1993, 1994, 1995, 1996, 1997, 1998, 1999, 2000, 2001, 2002, 2003 and 2011. Before running the last set of simulations a slight modification has to be done, one may note that devices work with the significant wave height and period and in the data presented above the significant wave period is not given, instead, the Peak Energy Wave Period is part of that data and as seen on the third chapter, in the Wave Analysis and Statistics section, the Peak Energy Wave Period can be converted into the significant wave period through the following expression:

$$T_s = 0.95T_p \quad (5.4)$$

After running the simulations, each type of device with the best performance in each different location has been chosen as the definitive one. The term of “best performance” is quite ambiguous and it might vary depending on the wanted goal; to exemplify it, can be considered as the maximum power output, the maximum average energy output, the highest efficiency or the most stable power extraction rate among many others. For this work in specific and for the wave energy extraction world in general; the considered best performance is the most stable power output rate or, in other words the capacity factor and so, this is the performance evaluation parameter chosen in this work. The device with the highest capacity factor for each location has been selected as the optimal one.

Once the devices have been selected their entire performance is computed in the following way:

The first step is to calculate the power extraction in the sea states, which are registered in the data, and the total energy absorption for each device. Once the energy and power outputs have been obtained the efficiency of the devices can be calculated. As summarized previously, in the wave energy converters world, the efficiency is not a very important parameter since for some specific situation can be higher than the 100%. This is due to the complex hydrodynamic behavior of the floating body, radiation and overall to added-mass. Another factor to keep in mind is that the energy or power of a wave are calculated for unit of crest length i.e.: [kW/m] or [kWh/m], this is why the capture width is introduced. The capture width measures the power absorbing capability of the device and its units are meters, it can be larger than the device itself and that is the key point, it can absorb more energy than the one contained within its physical dimensions, see figure (5.1) and equations (5.5), (5.6), (5.7) and (5.9) :

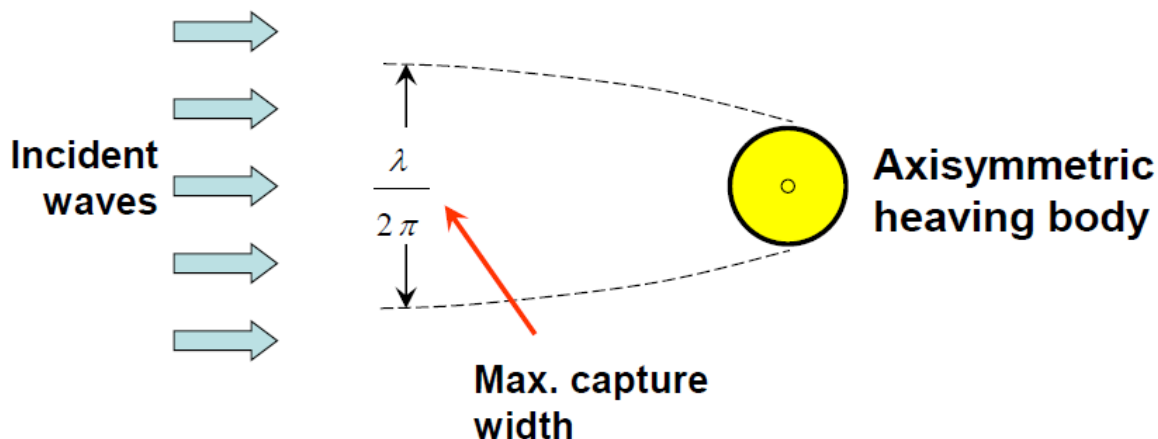


Figure 5.1: Schematic representation of the capture width concept. This figure shows how the capture width can be larger than the devices width maximizing the energy absorption.

$$P_{wave}(H_s, T_s) = \frac{1}{64} \rho g^2 H_s^2 \frac{T_s}{0.95} \quad (5.5)$$

$$E(H_s, T_s) = \frac{\rho g \omega}{4k} \left(\frac{H_s}{2} \right)^2 \left(\frac{2kh + \sinh(2kh)}{\sinh(2kh)} \right) \quad (5.6)$$

$$\eta = \frac{P_{device}(H_s, T_s)}{P_{wave}(H_s, T_s)} \quad (5.7)$$

$$C_{width} = \frac{P_{device}(H_s, T_s)}{E(H_s, T_s)} \quad (5.8)$$

Where ω is the wave frequency, k the wave number ρ the sea water density, h the depth and $E(H_s, T_s)$ is the flux energy per unit crest length. Finally, one last simulation will be done with the available data of the Alghero and Mazara's station, computing the mean annual energy and power outputs, the full load hours per year and the capacity factor for each device. As its names state, the full load hours represents the time when the device is working at full load and the capacity factor is nothing else than the full hours divided by total amount of hours contained in a year.

5.2 RESULTS

First of all, a brief comment on the computational costs is needed. As it can be seen in previous sections and chapters, the amount of different parameters used in the various fields of the model, i.e. hydrodynamic, electromagnetic and mechanical fields, is substantially high. The equations used in the model are also non trivial and with complexity levels rather elevated. All these facts mixed together with the small sampling interval $F_s=0.0005$ s or in other words $F_s=0.5$ ms, used at that levels to guarantee the accuracy of results, make the computational costs entity of relevance. Reaching, in some cases, simulation times as long as 72 hours. So it is not wrong saying that is one of the main factors to take into account when running simulations.

Once the simulation is run and completed the first thing that needs to be verified is the wave energy converter behavior, in order to detect any possible error in the programming code or structural subagent errors such as conceptual errors or theoretical misleading. The following results are presented in Figures 5.2 and 5.3:

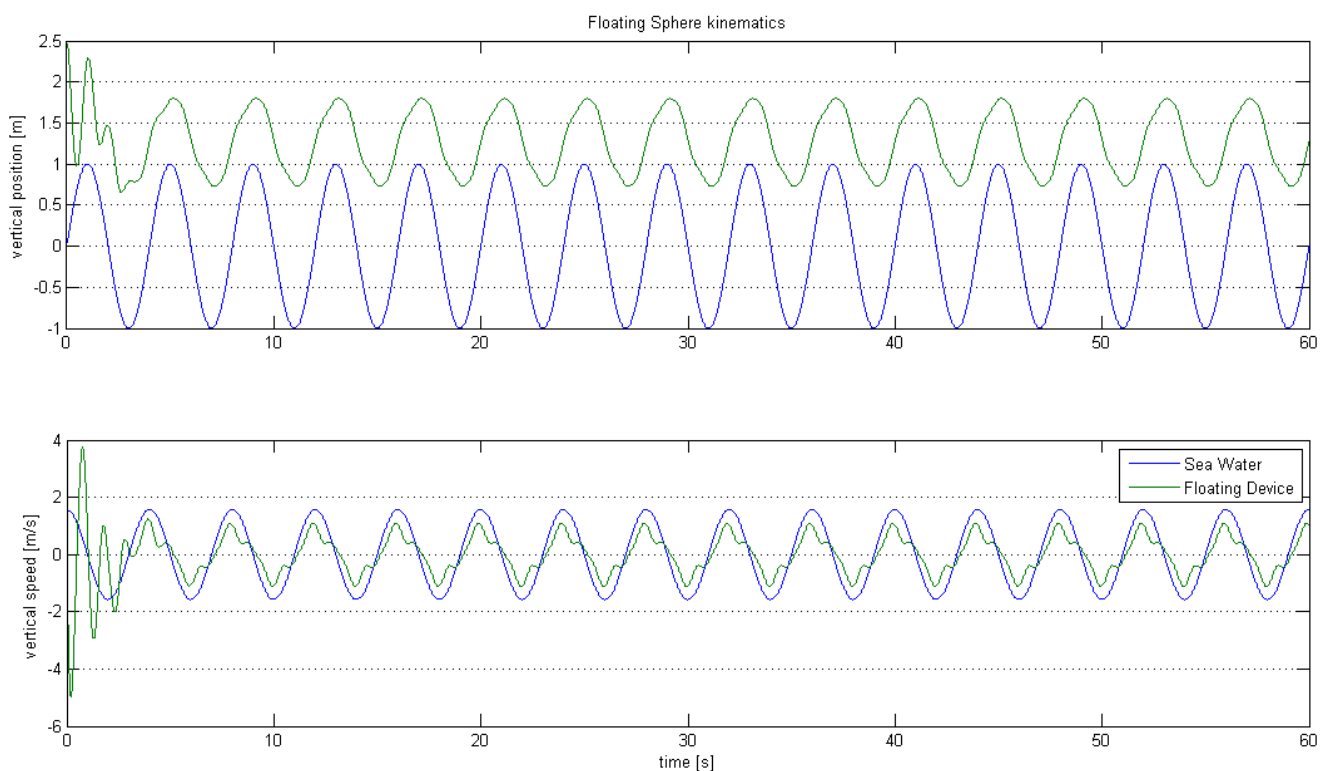


Figure 5.2: Vertical Position and vertical Speed of the spherical floating body WEC induced by incident monochromatic waves with constant height and period over the time.

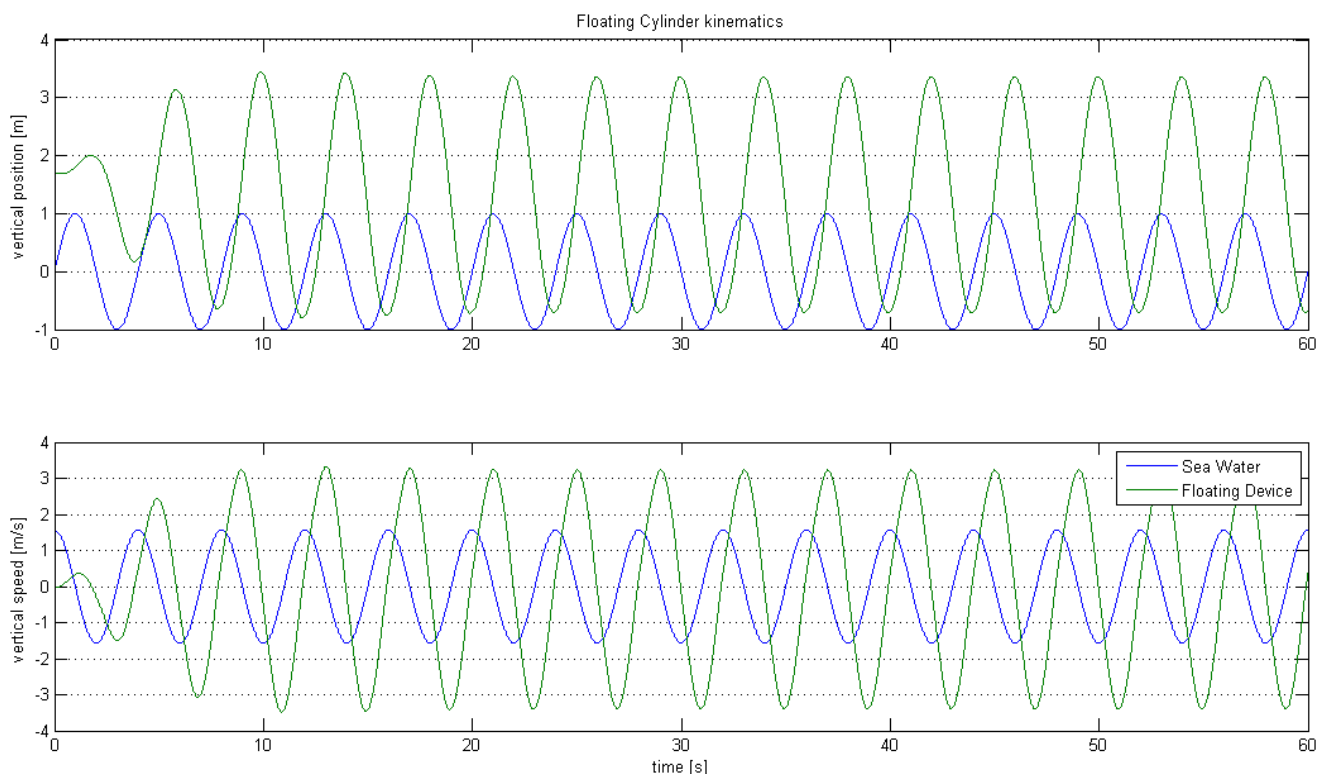


Figure 5.3: Vertical Position and vertical Speed of the cylindrical floating body WEC induced by incident monochromatic waves with constant height and period over the time.

When comparing figures 5.2 and 5.3 with figure 4.5 and 4.6 respectively, the influence of the power take-off system in the floating can clearly be seen. In figure 5.2 there are two main aspects that need to be cleared. Firstly, a very powerful transient regime can be observed in the first seconds of the simulation, approximately during the first wave period, after which the system quickly stabilizes giving place to the steady transient. Secondly, when observing the floating device's vertical velocity a clear pattern, similar to a sine wave, can be distinguished, this behavior is due to the influence of the linear generator magnetic force and its three harmonic components. In figure 5.3 it can be seen that the cylindrical wave energy converter works smoother than the spherical one, maintaining its typical features.

As seen on figure 5.2 the effect of the magnetic force modeling is reflected on the whole wave energy converter behavior so a thorough analysis of this force has to be done and the method chosen is the Fourier analysis as it can be seen in figures 5.4 and 5.5:

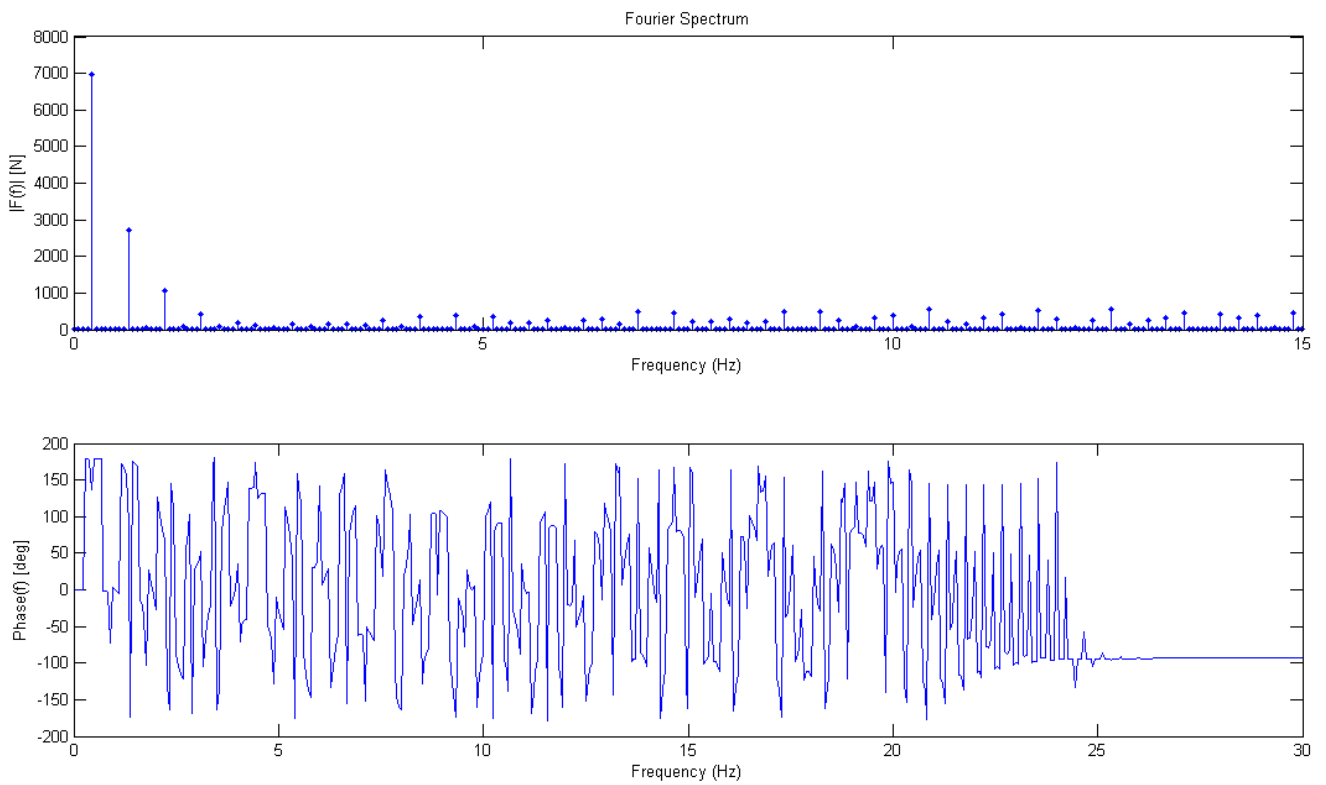


Figure 5.4: Fourier Spectrum. The upper plot shows the amplitude of the signal over a range of frequencies, and the lower plot shows the phase of the signal over a range of frequencies.

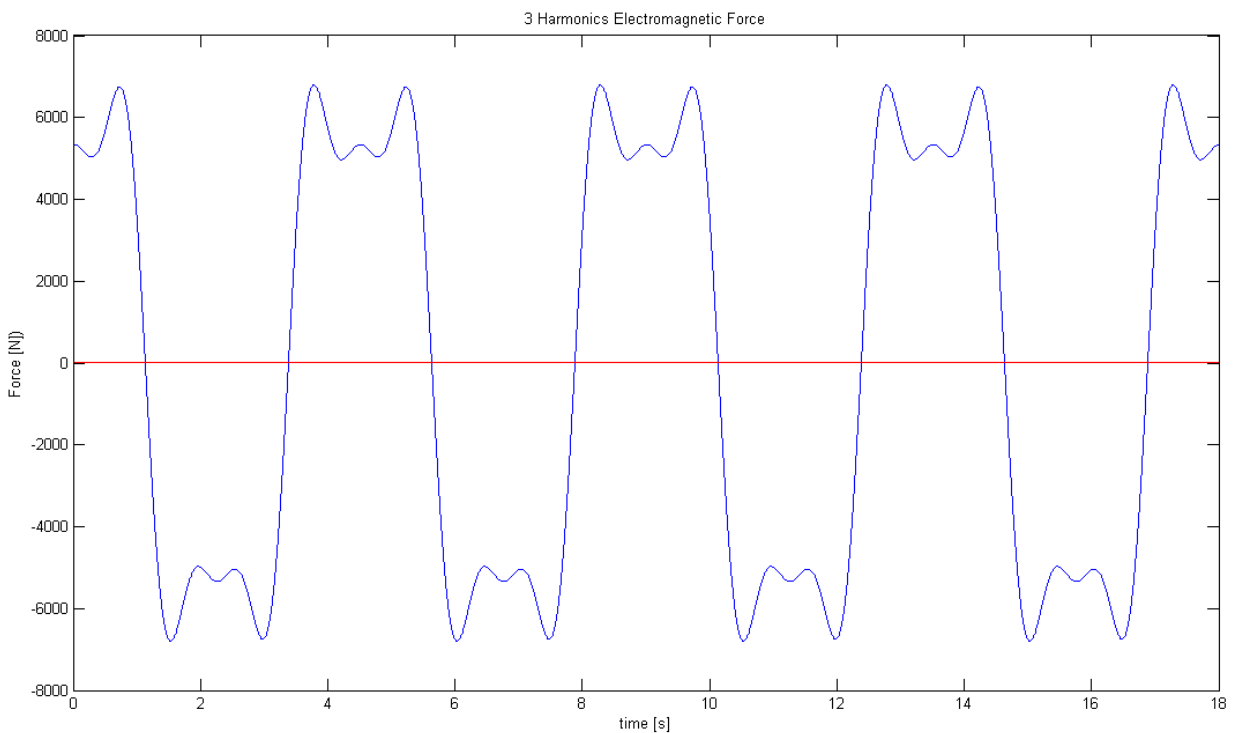


Figure 5.5: Magnetic force reduced only to its three first harmonic components.

Figure 5.4 clearly states that the Fourier spectrum of the magnetic force, shown in figure 4.12 has three main components, whose relevance in amplitude terms is much higher than the rest of the terms. This is the reason why it has been decided to reduce the force into only three harmonic components (See Fig. 5.5), because there is a substantial gain in simplicity and almost no loss in accuracy.

The next step in the simulation process, as stated in the previous section of this chapter, is to compute the optimized spring coefficient values for each device, spherical and cylindrical buoys, and for each sea state depending on the significant wave height and period, H_s and T_s respectively, as stated in equation 5.1. The following results are presented in figures 5.7 and 5.8:

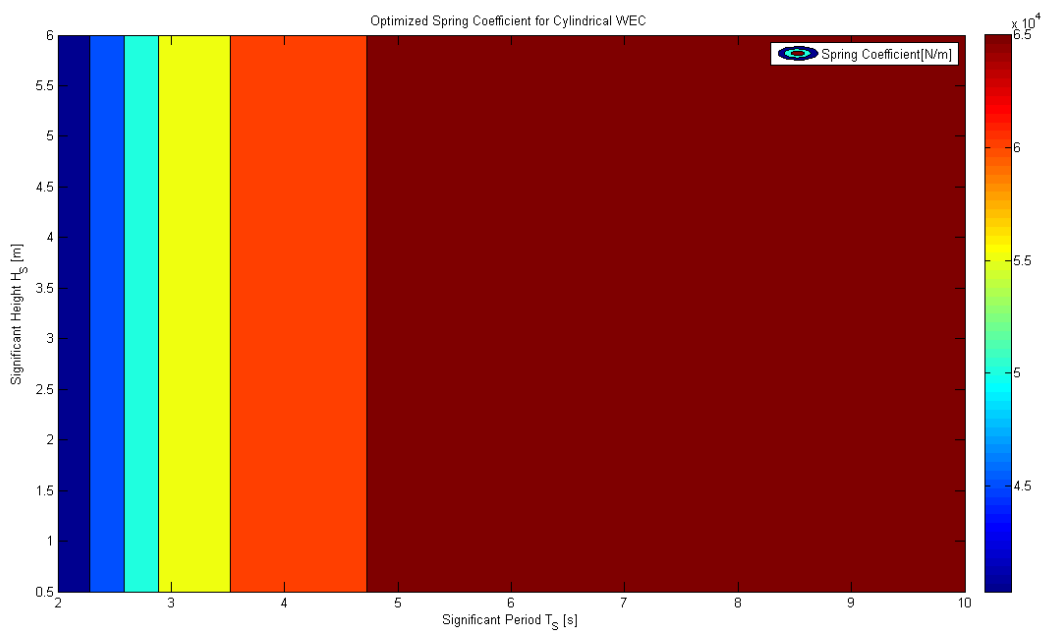


Figure 5.7: Optimized spring coefficient for the spherical floating body over different sea states.

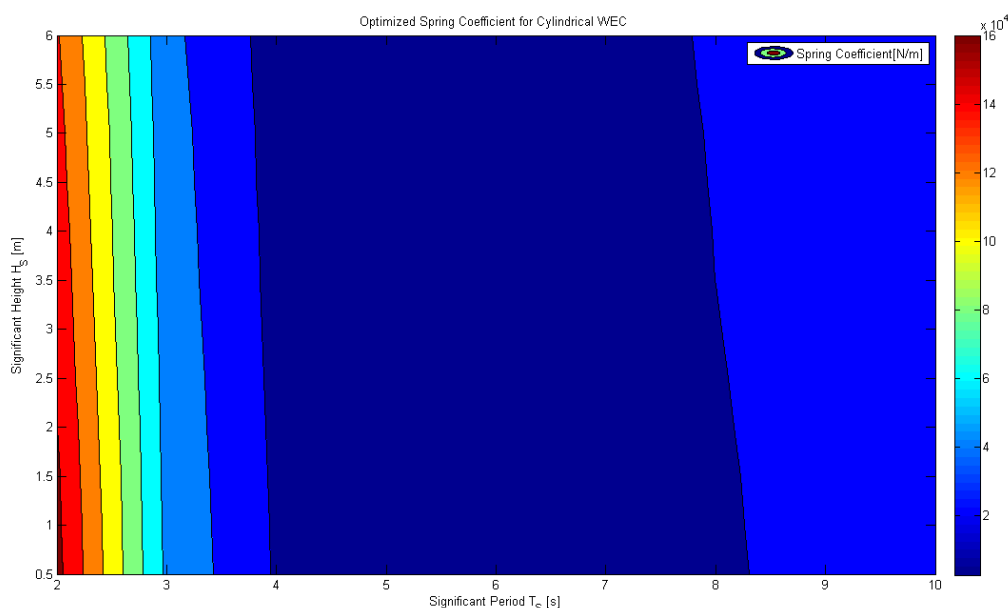


Figure 5.8: Optimized spring coefficient for the cylindrical floating body over different sea states.

According to the theoretical argument explained in the previous section, the spring coefficients vary depending on the wave frequency and mass of the system. The wave frequency in turn is dependent of the significant wave period only. The mass of the systems, which only varying component is the added-mass, it changes over the wave frequency in the case of the sphere and over the significant wave height in the case of the cylinder, as seen on the fourth chapter section one. This can be corroborated looking at figures 5.7 and 5.8, where it can be seen that in the case of the sphere the spring coefficient varies only over the significant wave period and in the case of the cylinder the spring coefficients varies bidimensionally over both, significant wave period and height.

After having found the spring coefficient matrix all the conditions to compute the power matrix for each device are satisfied. The results are presented in the figures 5.9, 5.10, 5.11 and 5.12:

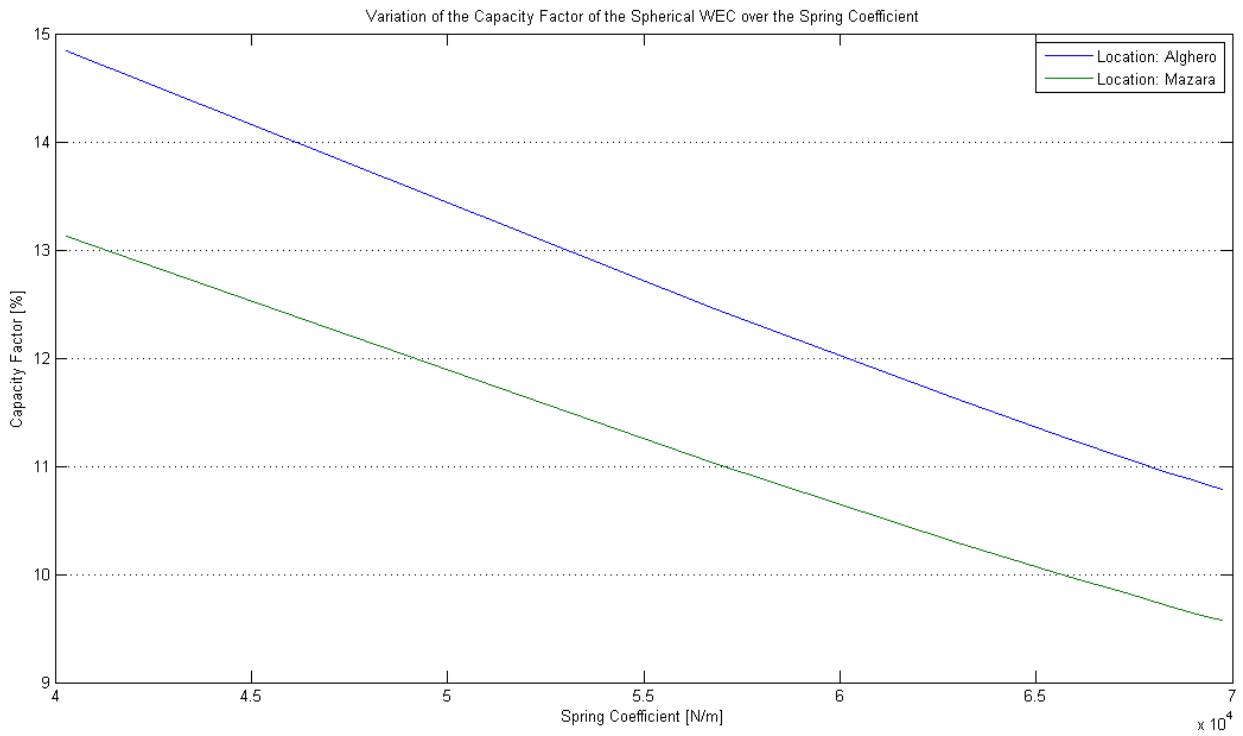


Figure 5.9: Capacity Factor vs. spring coefficient of the Spherical WEC.

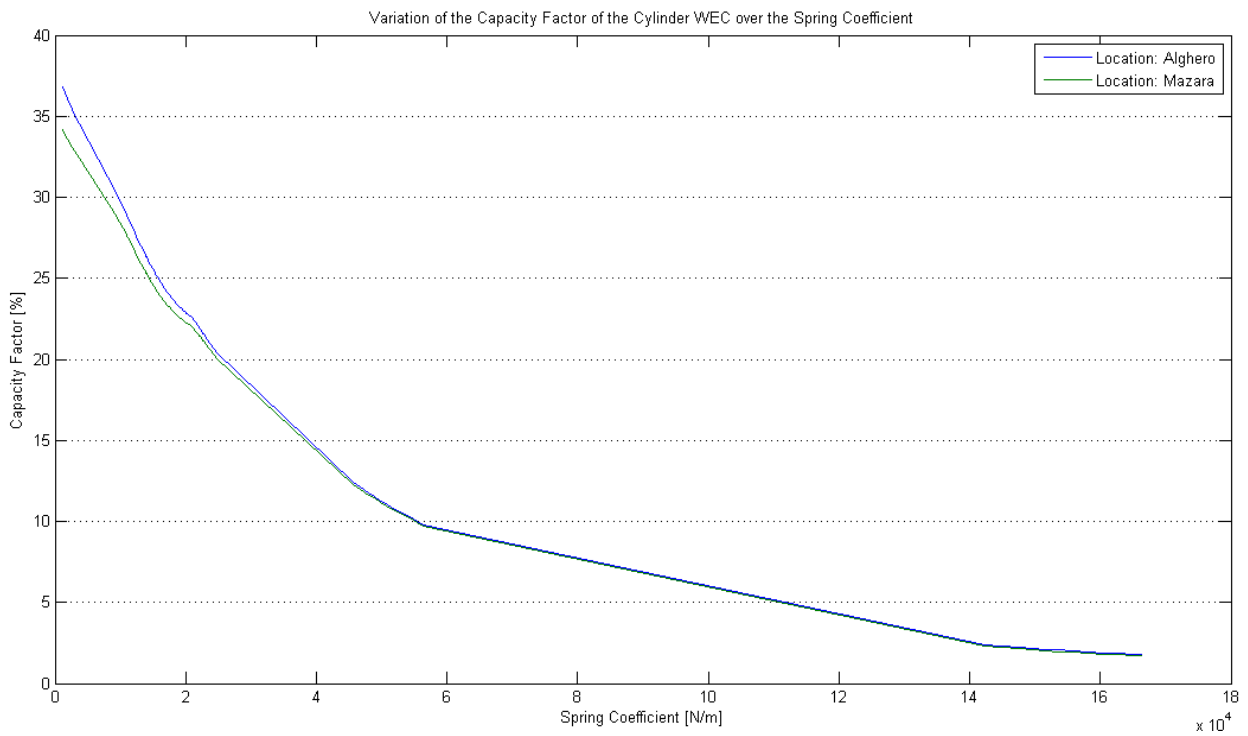


Figure 5.10: Capacity Factor vs. the spring coefficient of the Cylindrical WEC.

From the plots shown above the optimal spring coefficients are those which maximize the capacity factor for each device and location. Might be noted that for the spherical device's case (Figure 5.10), the relation between both parameters is practically linear with negative sign. Whereas, for the cylindrical device's case the relation can be better defined as multi-linear and always with negative sign. However, the selection decision must be always done within the given range of coefficients. The results of spring coefficient selection for each device and location are synthesized in table 5.5, where the significant wave height and period columns express the sea state conditions in which the device achieves resonance:

Device	H [m]	T [s]	Spring coefficient k [N/m]
Sphere Alghero	-	2	40274
Sphere Mazara	-	2	40274
Cylinder Alghero	2.5	5	1223
Cylinder Mazara	2.5	5	1223

Table 5.5: Spring coefficient determination for each device and location.

Once each spring coefficient has been determined, the devices are fully characterized. Four simulations, one per device and location, have been done including all the parameters found at this stage. The results resulting from these simulations are definitive and all the conclusions will be drawn in the basis of this stage. The first step is to compute the power matrixes of the devices. Afterwards, the rest of the performance's features are calculated. Figures 5.11 and 5.12 show the power matrix of each selected device, figures 5.13 and 5.14 illustrate the efficiency matrixes, figures 5.15 and 5.16 represent the capture width matrixes, figures 5.17 and 5.18 plot the power output and energy extraction respectively and figures 5.19 and 5.20 plot the full load hours and capacity factor respectively:

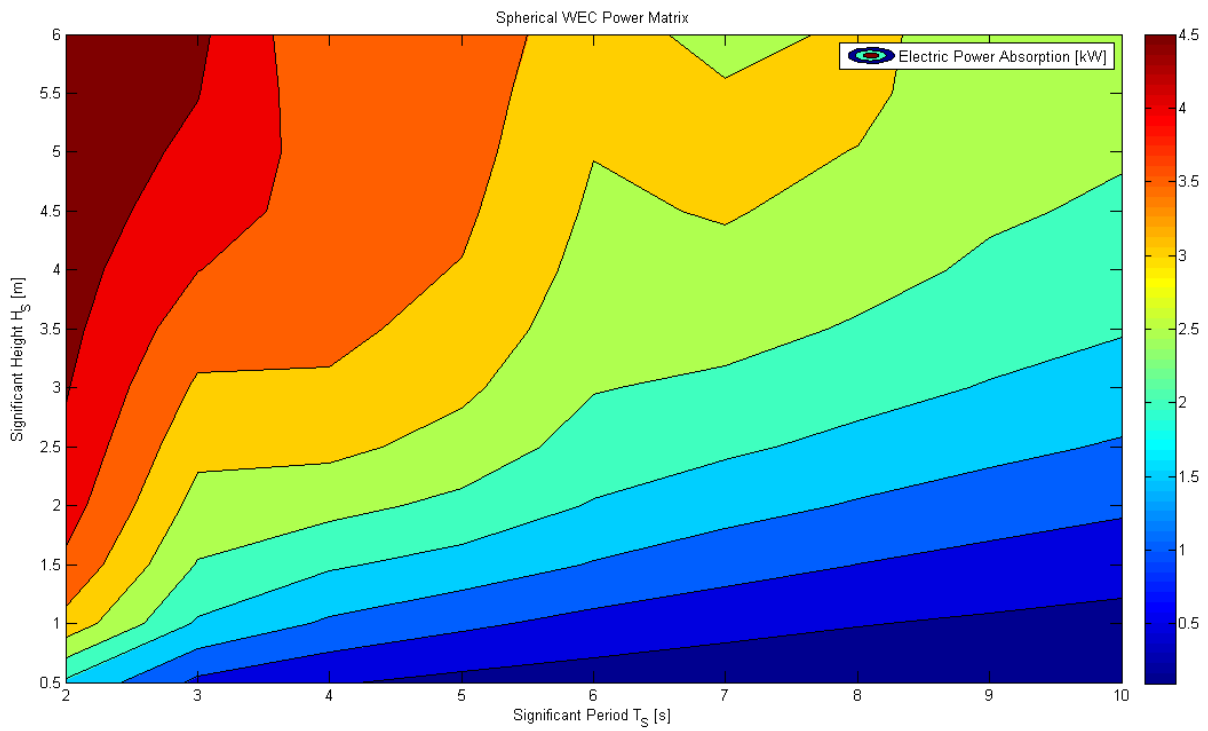


Figure 5.11: Power Matrix for the optimized Spherical device.

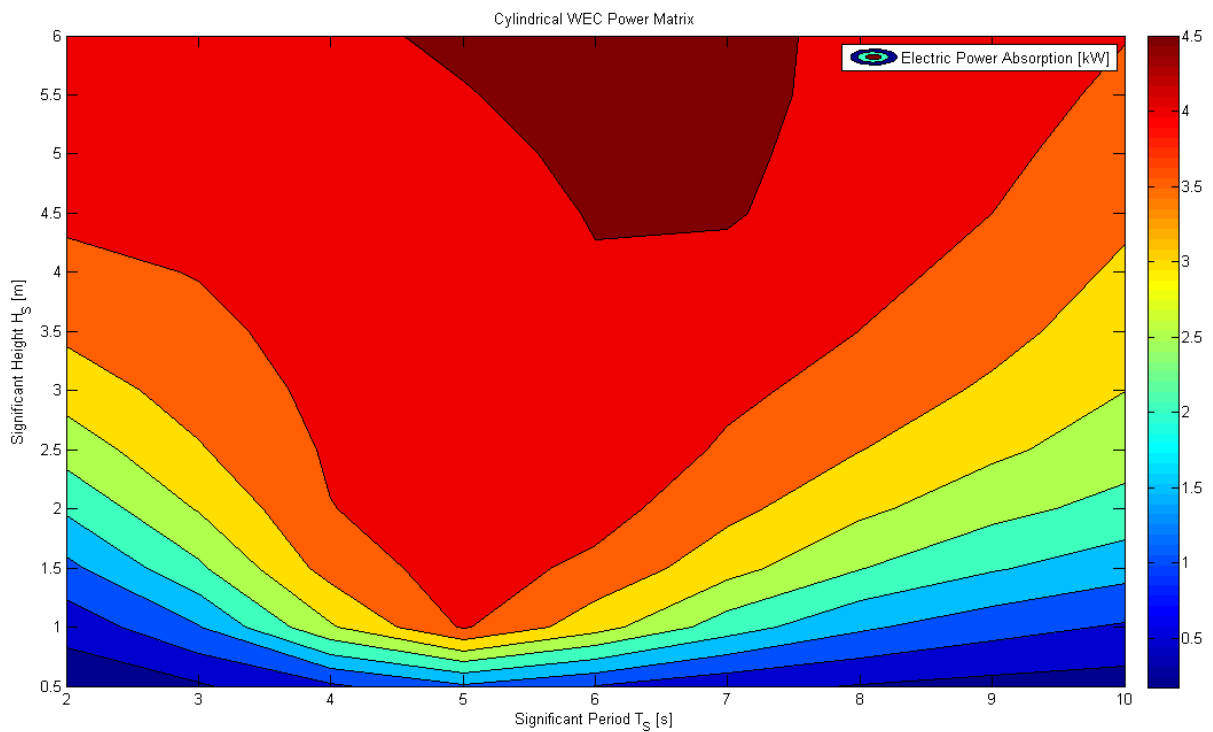


Figure 5.12: Power Matrix for the optimized Cylindrical device.

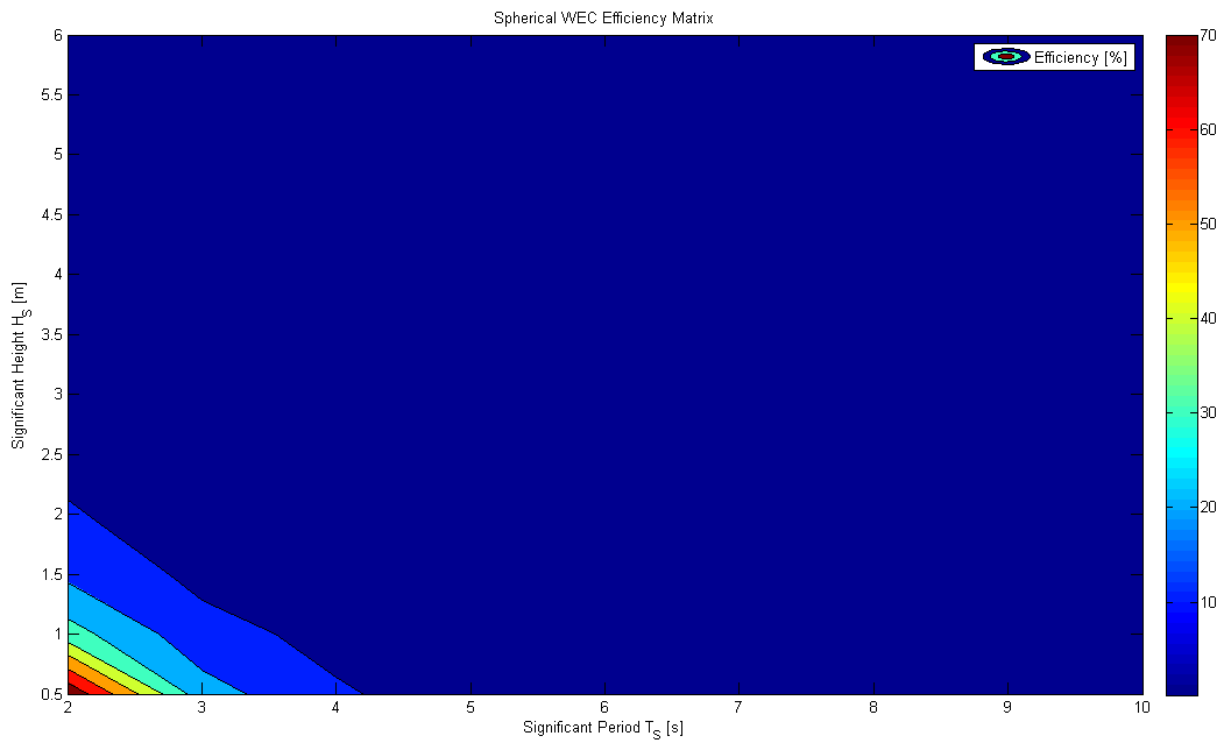


Figure 5.13: Efficiency Matrix for the optimized spherical device.

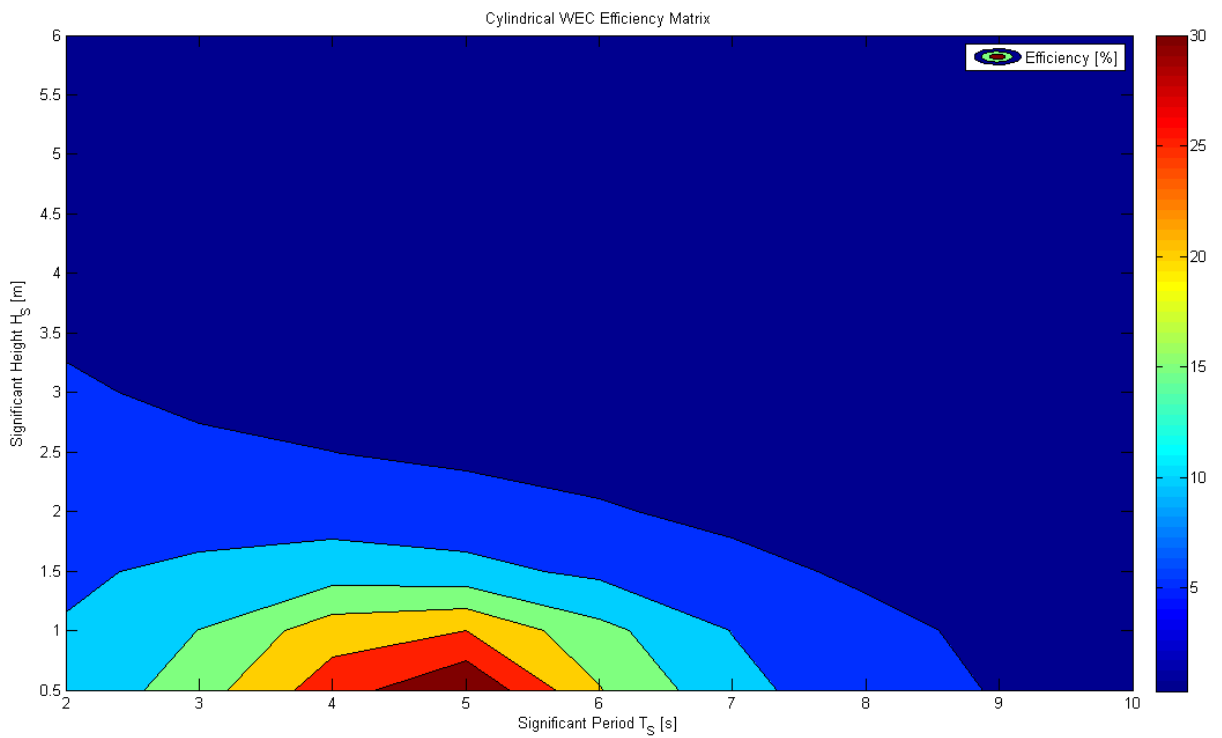


Figure 5.14: Efficiency Matrix for the optimized cylindrical device.

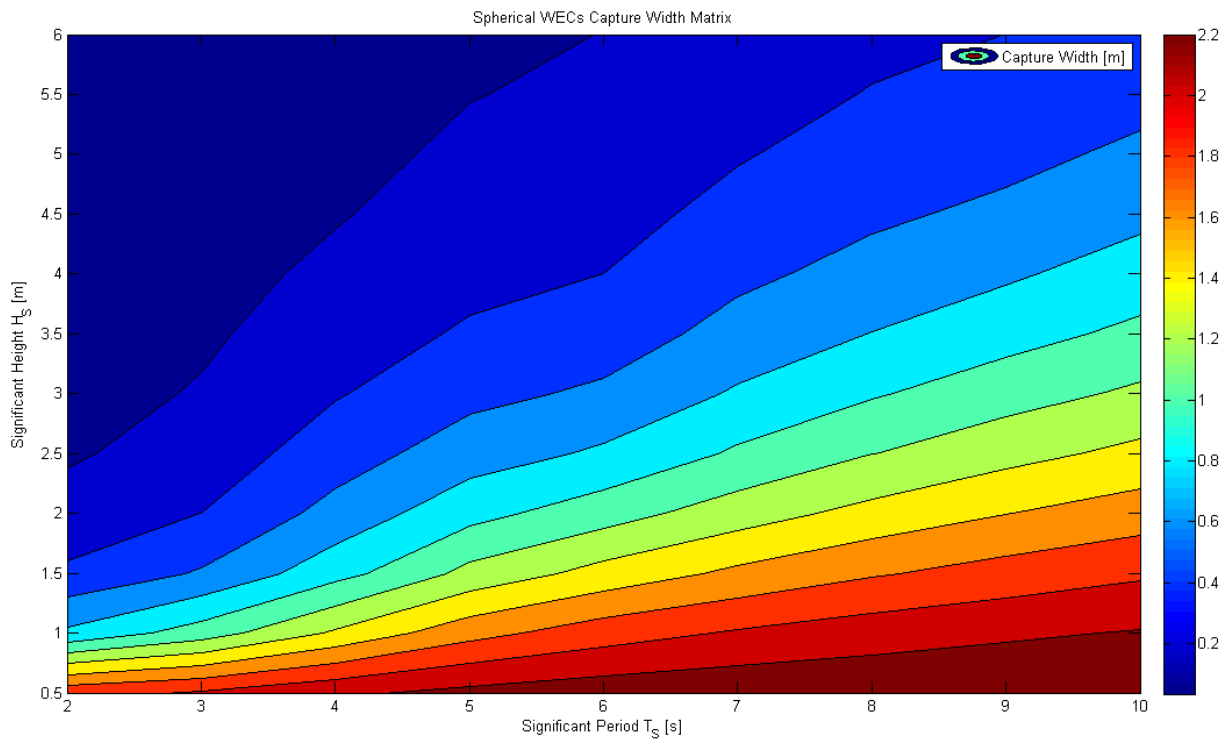


Figure 5.15: Capture Width Matrix for the optimized spherical device.

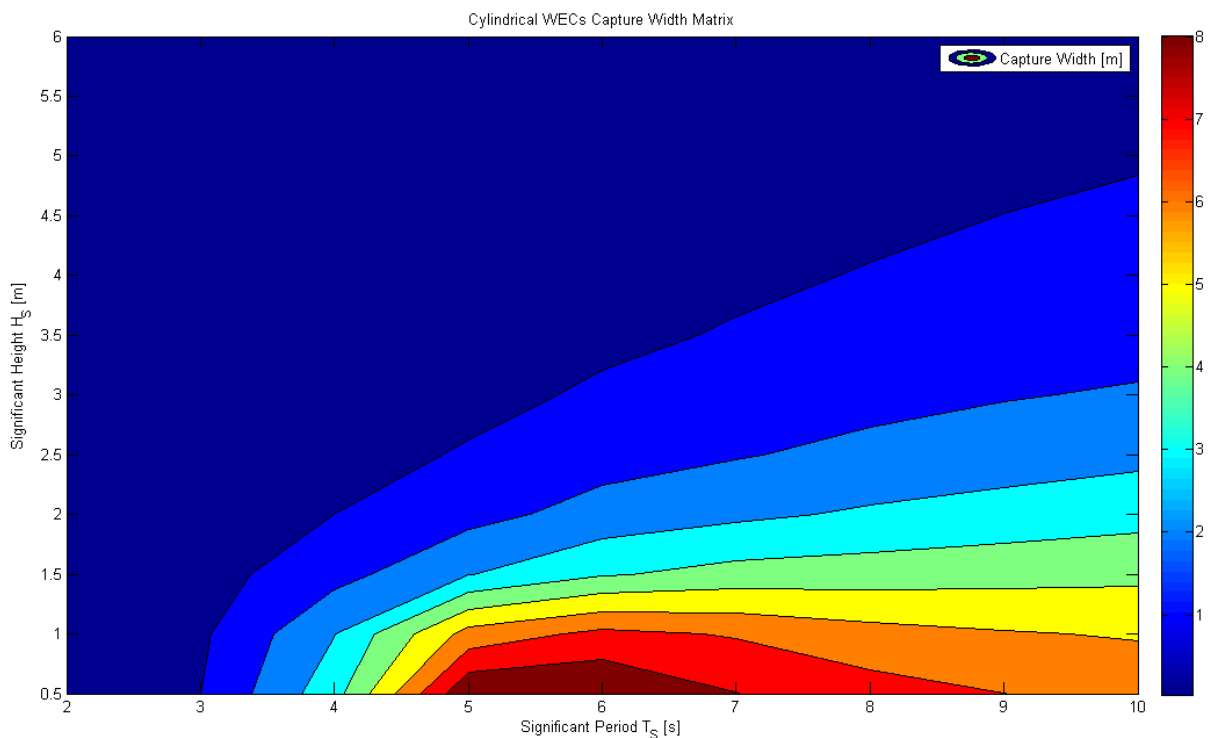


Figure 5.16: Capture Width Matrix for the optimized cylindrical device.

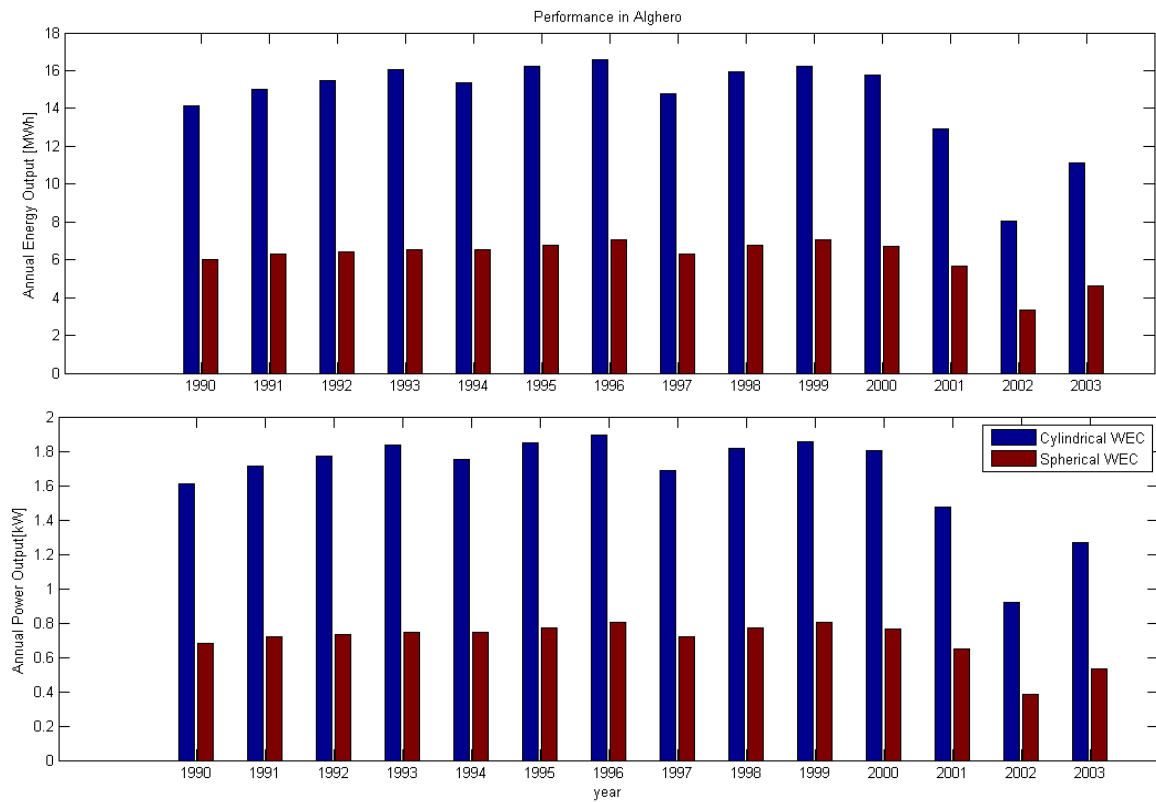


Figure 5.17: Histograms of the Energy and Power Outputs for both devices in Alghero.

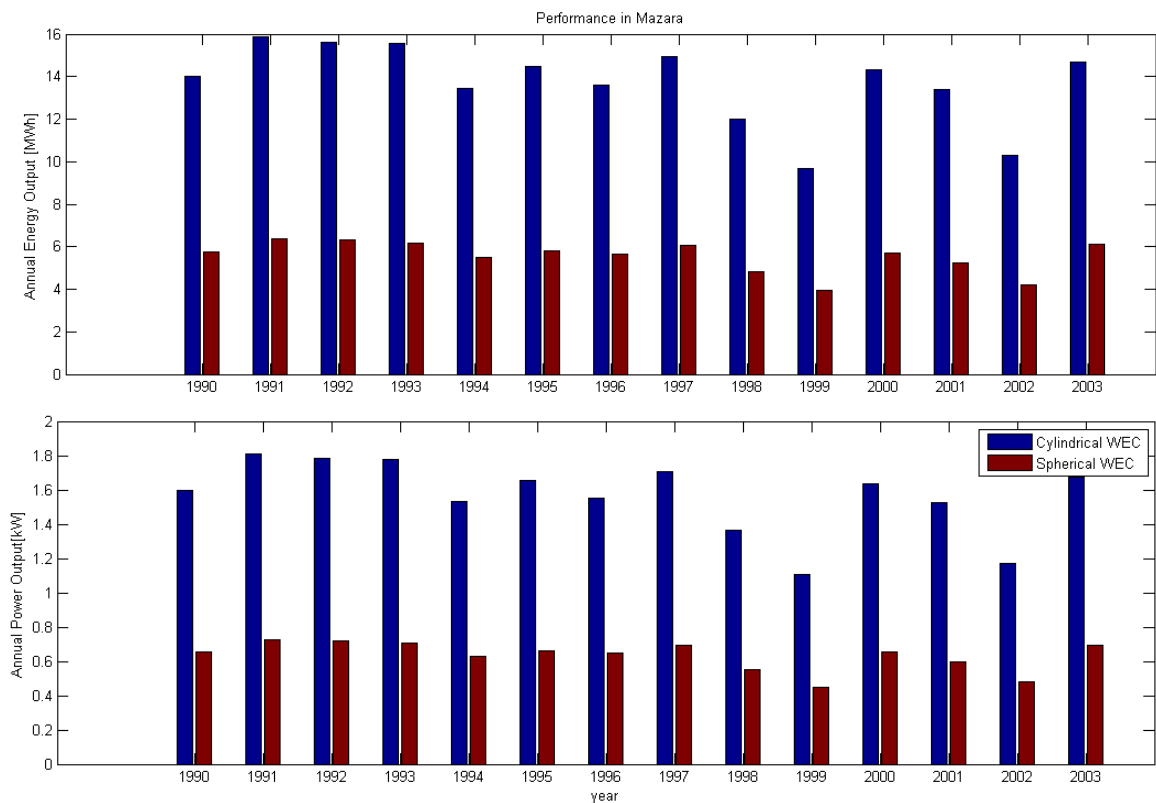


Figure 5.18: Histograms of the Energy and power Outputs for both devices in Mazara.

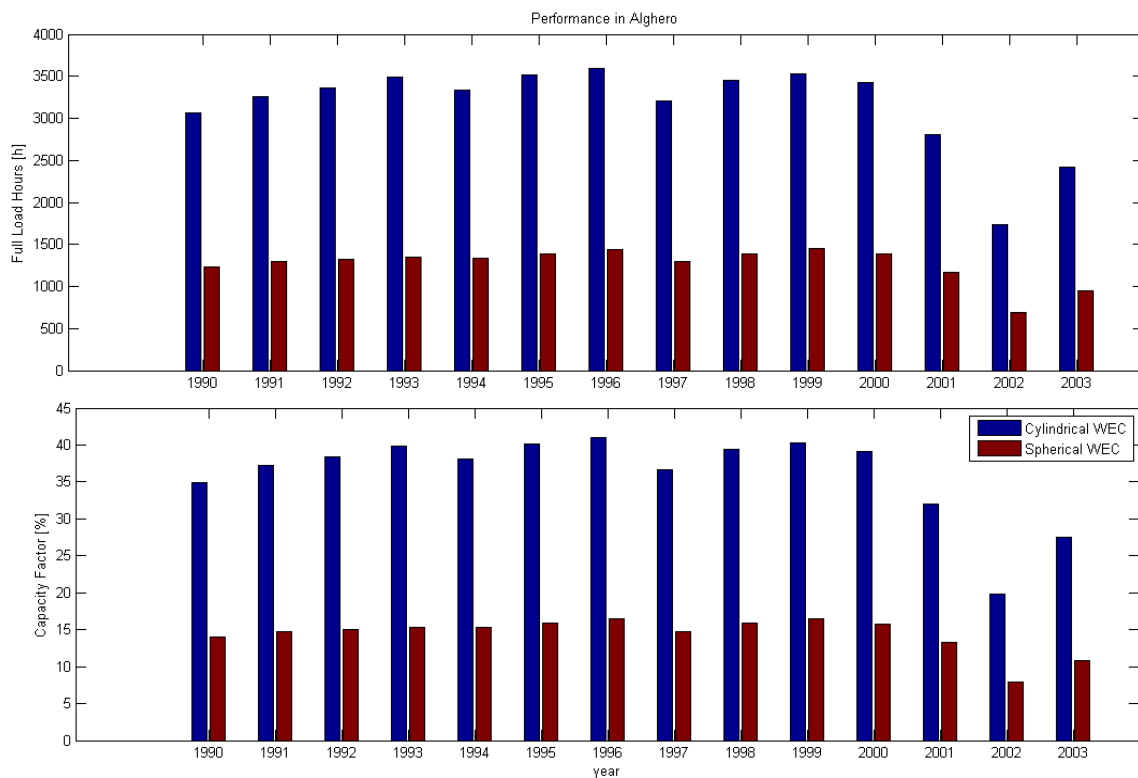


Figure 5.19: Histograms of the Full load hours and the Capacity Factor for both devices in Alghero.

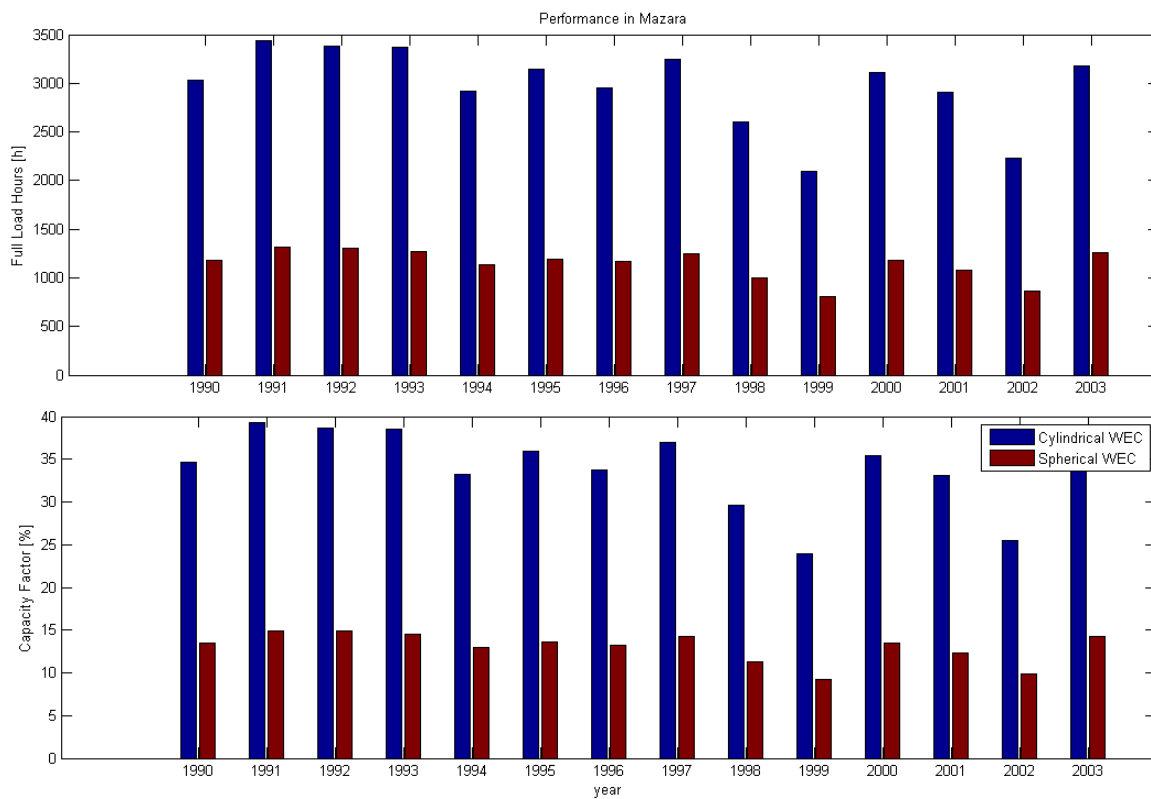


Figure 5.20: Histograms of the Full load hours and the Capacity Factor for both devices in Mazara.

With the figures presented above the devices' behaviors and characteristics are presented. The features such as power output, energy absorption, efficiency, capture width and capacity factor of each wave energy converter are synthesized in the following tables:

Device	Regular Waves			Real Waves
	H [m]	T [s]	Max. Power Output [kW]	Mean Power Output [kW]
Sphere Alghero	6	2	4.86	0.72
Sphere Mazara	6	2	4.86	0.64
Cylinder Alghero	6	7	4.61	1.70
Cylinder Mazara	6	7	4.61	1.58

Table 5.6: Wave energy converters Maximum and Mean Power output.

Device	Regular Waves			Real Waves
	H [m]	T [s]	Max. Efficiency [%]	Mean Efficiency [%]
Sphere Alghero	0.5	2	78.8	2.33
Sphere Mazara	0.5	2	78.8	5.37
Cylinder Alghero	0.5	5	34.81	8.24
Cylinder Mazara	0.5	5	34.81	19.88

Table 5.7: Wave energy converters Maximum and Mean Efficiency.

Device	Regular Waves			Real Waves	
	H [m]	T [s]	Max. Capture Width [m]	Mean Capture Width [m]	Relative Capture Width [-]
Sphere Alghero	0.5	10	2.39	0.07	0.023
Sphere Mazara	0.5	10	2.39	0.16	0.053
Cylinder Alghero	0.5	6	8.96	0.17	0.085
Cylinder Mazara	0.5	6	8.96	0.4	0.2

Table 5.8: Wave energy converters Maximum and Mean Capture Width.

Device	Mean Energy Absorption [MWh]	Mean Full Load Hours [h]	Mean Capacity Factor [%]
Sphere Alghero	6.32	1300	14.84
Sphere Mazara	5.59	1150	13.13
Cylinder Alghero	14.87	3226	36.83
Cylinder Mazara	13.80	2993	34.17

Table 5.9: Mean Annual Features for each Wave energy converter.

To sum up, both the devices, but specifically the cylindrical wave energy converter, have very interesting features. When analyzing the tables above a major difference can be found between the maxim features values and the mean ones. This denotes that the devices work much below than its full capacity as it can clearly be seen in tables 5.7 and 5.8.

Consequently, the average annual energy absorption levels (shown in figures 5.16 and 5.17 and in table 5.9) are rather low. However, the cylinder device's performance, in features like the mean power output, the mean energy absorption, the full load hours and the capacity factor, is much better than the sphere device's, achieving rates that double, at least, the sphere device's ones. This subject though, will be treated more widely in the next chapter. Another important feature to remark is the high capacity factor accomplished again by the cylindrical device which can be the key factor of its high energy and power outputs.

CHAPTER 6:

CONCLUSIONS

A mathematical model of four variants of a Wave Energy Converter has been designed, and numerical simulations have been conducted to reproduce its behavior with real seas data. The first impressions, after obtaining the results and concluding the work, have been strictly of positive sign. The numerical work reported in this thesis leads to the conclusions listed below.

Despite the fact that this has been the first attempt to model a Wave Energy Converter or, in other words, the process has been begun from zero, the results are hopeful and encouraging to carry on with the work towards further advanced stages. The performance features of the cylindrical floating body Wave Energy Converter are much higher than the spherical floating body WEC, even doubling or tripling them in some particular cases. This can be explained from the inertial terms of both devices. The spherical floating body has a total mass of approximately 600 kg, whereas the cylindrical buoy's mass is about 6000 kg, or in other words, ten times heavier. This big difference can be used to explain the reason of such diverse behaviors in the following way. The highest the inertial term is, the slower the device reacts to abrupt changes in position and velocity configurations, that is why the sphere device, with a relatively small inertial component, adapts much better to steeper waves. On the other hand, the cylinder device, with a higher inertial term, has a much lower frequency response and thus, it hardly reacts to the very steep incident waves.

The following list highlights the most conclusive results:

- Maximum Power Output:
 - Cylinder WEC = 4.61 kW
 - Sphere WEC = 4.86 kW
- Maximum Efficiency:
 - Cylinder WEC = 34%
 - Sphere WEC = 79%

- Maximum Capture Width:
 - Cylinder WEC = 8.96 m
 - Sphere WEC = 2.39 m
- Average Annual Energy Production:
 - Cylinder WEC = 14.87 MWh
 - Sphere WEC = 6.32 MWh
- Average Annual Power Output:
 - Cylinder WEC = 1.70 kW
 - Sphere WEC = 0.72 kW
- Average Full Load Hours per year:
 - Cylinder WEC = 3226 h
 - Sphere WEC = 1300 h
- Average Capacity Factor:
 - Cylinder WEC = 36.83%
 - Sphere WEC = 14.84%
- Average Efficiency:
 - Cylinder WEC = 1.88%
 - Sphere WEC = 5.37%
- Average Capture Width
 - Cylinder WEC = 0.4 m
 - Sphere WEC = 0.16 m

Observing the first two points of the list above it might seem that both devices have similar performances, even the spherical WEC's efficiency is higher, but taking a better look into the matrix efficiency figures for the sphere (5.13) and for the cylinder (5.14) a main difference comes to the surface, the red spots of showing high efficiencies are located in different places. Whereas high efficiencies for the cylinder are just at the same spot as the Wave Climate is more likely to happen; high efficiencies for the sphere are displaced to the bottom left corner of the figures. This is the main reason of the higher annual energy and power production of the cylinder, because it is efficient for the wave climates of the area where is thought to be working in. There is though, one major improvement that could be done in this field, it's about making the high efficiency regions, that currently are small and concentrated, bigger and wider embracing a major number of sea states and if it were possible, towards more energetic regimes.

Another very concluding result is the capture width, which in its maximum values is good enough for the spherical device but astonishingly good when talking about the cylindrical device. A 9 meter capture width means that the device, in specific conditions, is able to

capture the energy contained in 9 meters of wave crest. This in practical terms means that, taking into account that cylinder diameter is 2 meters; the device captures 4.5 times the energy contained within its physical dimensions. In the hypothetical case of a wave energy plant made of these devices the separation in between the buoys in each array should be at least 9 meters to avoid interferences between devices when capturing the energy and guarantee the optimal energy output of the wave power plant. However, the mean values of the capture width need to be raised through an optimization process that improves the general performance of the device.

Once again when comparing the average energy absorption of the two devices, the cylinder's performance is much better than the sphere's one, this result is strictly related with the capture width performance commented previously. Achieving the changes proposed above, for efficiencies and capture widths, would raise the annual energy outputs drastically. If the typical average annual electricity consumption in typical family house (working couple and two children) is about 2200 kWh per year a single cylinder device would reach to feed approximately 7 houses, in the hypothetical case of a wave energy plant of 10 arrays of 15 devices per array, the plant would feed around 1050 houses. Examples apart, this might be the main issue in the prospective stages, with this energy outputs this technology is not yet economically viable in the Mediterranean Sea.

To increase energy outputs a major increase of the average annual power outputs has to be achieved since the energetic regime of the Mediterranean Sea is as it. This is also achieved by spreading the high capture width and efficiency values of the devices over the wave climate regime of the Mediterranean Sea towards more energetic regimes.

The average full load hours and the capacity factor are strictly related, the latter is much more interesting than the former when drawing conclusions, so let's focus on it. Although its value, 36,83% for the cylinder, can still be increased this is also a magnificent result, in comparison with the capacity factor of other devices, which prototypes are currently being tested throughout the oceans, the performance of the cylindrical devices is a complete success. Devices like the Aquabuoy, the AWS and the Pelamis have capacity factors of around 5% in the same wave climate conditions.

Once the main conclusions have been drawn, they need to be applied in the next stages in the developing process of the design of a Wave Energy Converter. The next logical step will consist in the design of a three dimensional model of the floating body, to achieve more realistic results and optimization, a very common way to improve the performance of a floating body is to attach to it a deeply submerged body, by doing that the added mass is increased but the radiation damping coefficient remains barely untouched and as a consequence, the resonance frequency increases improving the power absorption. An example of that is illustrated in figure 6.1:

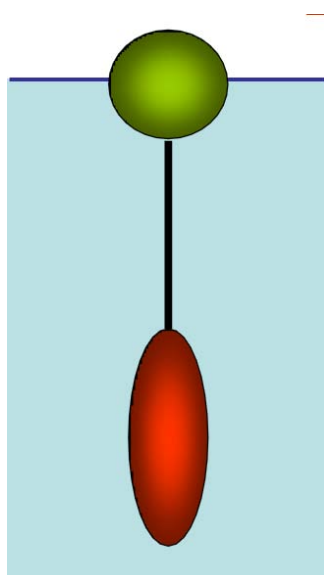


Figure 6.1: Deeply submerged body attached to the floating body to increase the resonance frequency.

Once the performance of the three dimensional device has been fully optimized the next step is to optimize the performance of the electric linear generator. In this work the linear generator used has not been designed for the wave climate regimes given in the Mediterranean Sea and, although its performance is acceptable enough, for sure that can also be optimized and thus, increasing the energy output. When all devices that compose a Wave Energy Converters have already been optimized the subsequent step is to introduce phase-control to increase even more the resonance frequency and improve the energy extraction. The phase-control commonly used in point absorber devices is called latching. Latching consist in holding the device in both extremes, top and bottom, and maintaining the devices blocked at these position for a certain period of time and then letting them off suddenly, once the device is free is forced to occupy its natural position as fast as possible resulting in high motion amplitudes and velocities and thus, increasing the energy output.

When all these stages will be accomplished, the next step will be leaving the office work to start the field work and develop a reduced scale prototype and figure out if the simulated behavior of the Wave Energy Converter corresponds with the behavior of the scaled prototype. When the desired results will be achieved will be time to build the full scale prototype and deploy it into open seas. The full scale prototype will have to be working for several years in order to verify that its behavior in all the possible situations is the desired one. After the testing stage, the only remaining stage is what is usually called the commercial stage when the device will produce energy and deliver it to the national grid during its lifespan.

References

- [1] Renata Archetti, Silvia Bozzi, Giuseppe Passoni. Feasibility study of a wave energy farm in the western Mediterranean sea: comparison among different technologies. OMAE, Rotterdam, The Netherlands, 2011
- [2] S. Bozzi, R. Archetti, G. Passoni. Wave energy exploitation in Italian seas: a feasibility study. OWEMES, Rome, Italy, July 2012.
- [3] R. Archetti, S. Bozzi, G. Passoni. Electricity from wave power in the Tyrrhenian sea. IDRA, Brescia, Italy, September 2012
- [4] João Cruz. Ocean Wave Energy. Current Status and Future Perspectives. Springer, Berlin, Germany, 2008.
- [5] António F. de O. Falcão. Wave energy utilization: A review of the technologies. Elsevier, Lisbon, Portugal, 2009.
- [6] J. Brooke. Wave energy conversion, volume 6. Elsevier ocean engineering book series. Elsevier, Oxford, UK, 2003.
- [7] Johannes Falnes. Ocean Waves and Oscillating Systems, linear interactions including wave energy extraction. Cambridge University Press, Cambridge, UK, 2004.
- [8] Roger H: Charlier, John R. Justus. Ocean Energies: Environmental, Economic and Technological Aspects of Alternative Power Sources. Elsevier Oceanographic series, 56, London, UK, 1993.
- [9] Johannes Falnes. Principles for capture of energy from ocean waves. Phase control and optimum oscillation. Department of Physics, NTNU, Trondheim, Norway.
- [10]www.ewtec.org, July 2012.

- [11] Maurice L. Schwarz. Encyclopedia of coastal science. Springer, Dordrecht, The Netherlands, 2005.
- [12] Robert M. Sorensen. Basic Coastal Engineering. Springer, New York, NY, USA, 2006.
- [13] Robert G. Dean, Robert A. Dalrymple. Water Wave Mechanics for Engineers and Scientists, volume 2. World Scientific, Singapore, 2000.
- [14] De Girolamo, Franco, Noli. Fondamenti oceanografi e idraulica marittima per ingegneri. 2003.
- [15] Marco Alves, Huw Traylor, António Sarmento. Hydrodynamic Optimization of a Wave Energy Converter Using a Heave Motion Buoy. IT Power Limited, Bristol, UK.
- [16] William Finnegan, Martin Mere, Jamie Goggins. The Wave Excitation Force on a Floating Vertical Cylinder in Water of Infinite Depth. World Renewable Energy Congress 2011, Linköping, Sweden, may 2011.
- [17] M. Folley, T.W.T. Whittaker, J. van't Hoff. The design of small seabed-mounted bottom-hinged wave energy converters. Queen's University, Belfast, UK.
- [18] Griet De Backer. Hydrodynamic Design Optimization of Wave Energy Converters Consisting of Heaving Point Absorbers. Universiteit Gent, Gent, Belgium.
- [19] M. Vantorre, R. Banasiak, R. Verhoeven. Modelling of hydraulic performance and wave energy extraction by a point absorber in heave. Elsevier, Gent, Belgium, 2004.
- [20] L. L. Huang, H. R. Riggs. The hydrostatic stiffness of flexible floating structures for linear hydroelasticity. Elsevier, Honolulu, HI, USA, 2000.
- [21] Alain Clément, Pat McCullen, António Falcao, Antonio Fiorentino, Fred Gardner, Karin Hammarlund, George Lomonis, Tony Lewis, Kim Nielsen, Simona Petroncini, M.-Teresa Pontes, Phillippe Schild, Bengt-Olov Sjöström, Hans Christian Sørensen, Tom Thorpe. Wave Energy in Europe: Current Status and Perspectives. Pergamon, 2002.

-
- [22] Mirko Previsic. E2I EPRI Assessment, Offshore Wave Energy Conversion Devices. EPRI, 2004.
- [23] Z. Yu, J. Falnes. State Space modeling of a vertical cylinder in heave. Elsevier, 1995.
- [24] Grégory S. Payne, Jamie R. M. Taylor, Tom Bruce, Penny Parkin. Assessment of boundary element method for modeling a free floating sloped wave energy device Part 1: Numerical Modeling. Elsevier, Edinburgh, UK, 2007.
- [25] Grégory S. Payne, Jamie R. M. Taylor, Tom Bruce, Penny Parkin. Assessment of boundary element method for modeling a free floating sloped wave energy device Part 2: Experimental Validation. Elsevier, Edinburgh, UK, 2007.
- [26] Marie-Aurélie Kerbiriou, Marc Prevosto, Christophe Maisondieu, Aurélien Babarit, Alain Clément. Influence of an improved sea-state description on a wave energy converter production. OMAE, San Diego, CA, USA, 2007.
- [27] J. R. Morison. The Force Distribution Exerted by Surface Waves on Piles. University of California, Berkeley, CA, USA, 1963.
- [28] Aurélien Babarit, Jorgen Hals, Adi Kurniawan, Torgeir Moan, Jorgen Krokstad. Power Absorption Measurements and Comparisons of Selected Wave Energy Converters. OMAE, Rotterdam, The Netherlands, 2011.
- [29] O. Danielsson. Design of a Linear Generator for Wave Energy Plant. Uppsala University, Uppsala, Sweden.
- [30] Assessment of Performance of Wave Energy Conversion Systems. European Marine Energy Center, 2009.
- [31] Feng Wu, Xiao-Ping Zhang, Ping Ju, Michael J. H. Sterling. Modeling and Control of AWS-Base Wave Energy Conversion System Integrated into Power Grid. IEEE, 2008.
- [32] João Cruz, António Sarmento, Fred Gardner. AWS Pilot Plant Test: Wave Characteristics. 6th European Wave and Tidal Energy Conference, Glasgow, UK, 2005.

- [33] Henk Polinder, Michael E. C. Damen, Fred Gardner. Linear PM Generator System for Wave Energy Conversion in the AWS. IEEE, 2004.
- [34] Karin Thorburn. Electric Energy Conversion Systems: Wave Energy and Hydropower. Uppsala Universitet, Uppsala, Sweden, 2006.
- [35] Karin Thorburn, Mats Leijon. Farm Size Comparison with Analytical Model of Linear Generator Wave Energy Converters. Elsevier, Uppsala, Sweden, 2006.
- [36] António F. O. Falcão. Wave Energy Utilization. Università degli Studi di Firenze, Florence, Italy, 2012.
- [37] D.J. Ewins, "Modal Testing - Theory, Practice and Application", Second Edition, Research Studies Press LTD.
- [38] G. Genta, "Vibration of Structures and Machines - Practical Aspects", Second Edition, Springer-Verlag
- [39] Cyril M. Harris, "Shock and Vibration Handbook", Fourth Edition, Mc.GRAW-HILL
- [40] Hoshin V. Gupta. Thorsten Wagener, Yiuquiong Liu. Reconciling Theory with observations: elements to diagnostic approach to model evaluation. InterScience, 2008.
- [41] Wachter A., Neilsen K. Mathematical and Numerical Model of the AquaBuoy Wave Energy Converter. MICS Journal, 2010.
- [42] M. G. de Sousa Prado, F. Gardner, M. Damen, H. Polinder. Modeling and Test Results of the Archimedes Wave Swing. SAGE, 2006.
- [43] Jorgen Hals. Modeling and phase control of wave energy converters. Doctoral Thesis, NTNU, Trondheim, Norway, 2003.
- [44] David Pizer. Numerical Modeling of Wave Energy Converters. University of Edinburgh, Edinburgh, UK, 1994.
- [45] João Cruz. Numerical and Experimental Modeling of WECs. Garrad Hassan and Partners LTD, Bristol, UK.

-
- [46] Ross Henderson. Design, simulation and testing of a novel hydraulic power take-off system for the Pelamis wave energy converter. Elsevier, Edinburgh, UK, 2005.
- [47] H. L. Bailey, I. G. Bryden. Optimizing power take-off using a non-linear model. Institute of Energy Systems, Edinburgh, UK.
- [48] Jakob Stroustrup. State Space Methods. Aalborg University, Aalborg, Denmark.
- [49] Valeria Castellucci. Tidal Effect Compensation System for Wave Energy Converters. Uppsala Universitet, Uppsala, Sweden.
- [50] K.K. Ahn, D.Q. Truong, Hoang Huu Tien, Jong Il Yoon. An innovative design of wave energy converter. Elsevier, Ulsan, Republic of Korea, 2011.
- [51] Mikael Eriksson. Modeling and Experimental Verification of Direct Wave Energy Conversion: Buoy Generator Dynamics. Uppsala Universitet, Uppsala, Sweden, 2007.
- [52] J. H. Lee, N. Xiros, M. M. Bernitsas. Virtual damper-spring systems for VIV experiments and hydrokinetic energy conversion. Elsevier, USA, 2011.
- [53] Iulian Munteanu, Antoneta Iuliana Bractu, Maria Andreica, Seddik Bacha, Daniel Roye, Joel Giraud. A new method of real-time physical simulation of prime movers used in energy conversion chains. Elsevier, Grenoble, France, 2010.
- [54] K. Rhinefranka, E.B. Agamloha, A. von Jouannea, A.K. Wallacea, J. Prudella, K. Kimblea, J. Aillsa, E. Schmidta, P. Chanb, B. Sweenyb, A. Schacher . Novel ocean energy permanent magnet linear generator buoy. Elsevier, Oregon, USA, 2005.
- [55] E. Sardini, M. Sarpelloni. Nonlinear Electromagnetic Generators with Polymeric Matherials for Power Harversting from Vibrations. Elsevier, Berscia, Italy, 2010.
- [56] USFOS Hydrodynamics: Theory Description of Use Verification.
- [57] Mats Leijon, Hans Bernhoff, Olov Agren, Jan Isberg, Jan Sundberg, Markus Berg, Karl Erik Karlsson, Arne Wolfbrandt. Multiphysics simulation of wave

- energy to electric energy conversion by permanent magnet linear generator. IEEE.
- [58] H. Yavuz, S. Mistikoglu, T. Stallard. Processing irregular wave measurements to enhance point absorber power capture performance. Elsevier, 2010.
- [59] Aurélien Babarit, Jorgen Hals, Adi Kurniawan, Torgeir Moan, Jorgen Krokstad, M. J. Muliawan. Numerical Benchmarking study of a selection of wave energy converters. Elsevier, 2011.
- [60] Aurélien Babarit, Jorgen Hals, Adi Kurniawan, Torgeir Moan, Jorgen Krokstad, M. J. Muliawan. Numerical estimation of energy delivery from a selection of wave energy converters. Starkraft, Centrale Nantes, NTNU, 2011.
- [61] B Drew, A R Plummer, M N Sahinkaya. A review of wave energy converter technology. University of Bath, Bath, UK, 2009.
- [62] David Dunnett, James S. Wallace. Electricity from wave power in Canada. ELSEVIER, Toronto, Canada, 2008.
- [63] Jeffrey A. Oskamp, H. Tuba Özkan-Haller. Power calculations for a passively tuned point absorber wave energy converter on the Oregon Coast. ELSEVIER, Corvallis, OR, USA, 2012.

APPENDIX A:

MATLAB CODES

A.1. MAIN SCRIPTS

A.1.1 Sim_WEC.m

This code calculates:

- The Spring Coefficients
- The Power Matrixes of the devices.

```
clear all
close all
clc

load KS.txt
load KC.txt

%%%% The buoys displacement is referred at the top part of the buoys
surface,
%%%% so if the displacement=0 the whole buoy is submerged, if
%%%% displacement=D the whole buoy is emerged.
P_rms_S=zeros;
P_rms_C=zeros;
P_avg_S=zeros;
P_avg_C=zeros;

Ti=[2 3 4 5 6 7 8 9 10];% Wave Period's array
Hi=[0.5 1 1.5 2 2.5 3 3.5 4 4.5 5 5.5 6]; %Wave Height's array

Cdc=1.55; %Drag Coefficient
Cds= [0.24 0.34 0.33 0.27 0.18 0.095 0.05 0.04 0.03];
Cac= [1.99 1.96 1.93 1.89 1.85 1.81 1.77 1.74 1.7 1.67 1.62 1.58];
%%Added Mass Coefficient
Cas= [0.425 0.64 0.72 0.78 0.82 0.825 0.81 0.79 0.79];
```

```
% Parametri del modello
Re=[1.5 1] ; %External Radius m
Ri=[1.485 0.85]; %Internal Radius m
rho=1025;%ocean water density kg/m3
Ve(1)=4/3*pi*(Re(1)^3);
Ve(2)=pi*Re(2)^2*4; % External Volume m3
Vi(1)=4/3*pi*(Ri(1)^3);
Vi(2)=3.70*pi*(Ri(2)^2); % Internal Volume m3
V(1)=Ve(1)-Vi(1);
V(2)=Ve(2)-Vi(2); % PVC Volume m3
PPVC= 14000; %Bouy Material Specific Weight (PVC) N/m3
Pg(1)=V(1)*PPVC;
Pg(2)=V(2)*PPVC;% Spheres Weigth
Paggiu=0; % External Elements Weight N
Area(1)=((Re(1)^2)*pi);
Area(2)=((Re(2)^2)*pi);% Maximums buoy surface section

rho_trans= 4700; %Ferrite Density [kg/m^3] Material of
Translator.
trans_length= 5.425; % Length of the translator [m]
trans_width= 0.3-0.002; %Width of the translator [m]
trans_area=trans_width^2;
trans_volume= trans_area*trans_length;
M= trans_volume*rho_trans; %Total Translators Mass kg
m_trans=M;

g=9.80665; % gravity m/s2

%%%%%MASS%%%%%
mg_n(1) = (Pg(1)/g); % Mass of the sphere kg
mg_n(2) = (Pg(2)/g);

%%%%%LINEAR GENERATOR PARAMETERS%%%%%

Bt=1.55; %Magnetic Field in tooth [T]
wt=8*10^-3; %Tooth width [m]
d=0.4; %Width of Stator Side [m]
p=100; %Numero di Poli
q=6/5; %Winding ratio [slots/(pole, phase)]
ci=6; %Number of cables per slot
wp=0.1; %Pole pair width [m]
L=11.5*10^-3; %generator inductance [H]
Rc=0.3735; %Generator resistance [ohm]
Rload=3.1; %Load resistance [ohm]
eff=0.791; %efficiency
cont=1;

%%%%%ODES SIMULATION PARAMETERS%%%%%

Fs=0.0005; %Sampling Period [s]
```

```

tspan = [0 30];% Simulation Timespan [s]
y0s = [2.49 0.001];
y0c = [1.69 0.001];    % Initial Conditions

[Farcs, Farcc, Pss, Psc]=archimede(Pg,Vi,Re);
for ii=1:length(Hi)
    for jj=1:length(Ti)
        Ks=KS(jj,ii);
        Kc=KC(jj,ii);

%%%SIMULATION LOOPS FOR DIFFERENT WAVE HEIGHTS AND PERIODS%%%
for he=1:length(Hi);

A=Hi(he)/2;
pe=1;
H=2*A;

m_ad_g(2)=Cac(pe)*mg_n(2); %Added Mass kg
mg_Tot(2)=m_ad_g(2)+mg_n(2)+m_trans; %Total WEC Mass kg

for pe=1:length(Ti);

T=Ti(pe);
omega = 2*pi/T; %Forcing Wave Frequency

c(1)=0.5*rho*Cds(pe)*Area(1); %Drag Force
c(2)=0.5*rho*Cdc*Area(2); %Drag Force
m_ad_g(1)=Cas(pe)*mg_n(1); %Added Mass kg

mg_Tot(1)=m_ad_g(1)+mg_n(1)+m_trans; %Total WEC Mass kg

m=mg_Tot; %Total Mass
time=(0:Fs:30)';

%%%IMPLEMENTATION OF THE WEC MODEL VIA ODE%%%

options = odeset('RelTol',1e-10,'AbsTol',1e-10);
[ts,sols]=ode15s('ciambS',tspan,y0s,options,m(1),c(1),A,omega,Bt,wt,
d,p,q,ci,wp,L,Rc,Rload,eff,Farcs,Pss,Ks);
[tc,solc]=ode15s('ciambC',tspan,y0c,options,m(2),c(2),A,omega,Bt,wt,
d,p,q,ci,wp,L,Rc,Rload,eff,Farcc,Psc,Kc);

sol_inters=zeros(length(time),2);
sol_inters(:,1)=interp1(ts,sols(:,1),time);
sol_inters(:,2)=interp1(ts,sols(:,2),time);

sol_interc=zeros(length(time),2);
sol_interc(:,1)=interp1(tc,solc(:,1),time);
sol_interc(:,2)=interp1(tc,solc(:,2),time);

```

```
eta=A*sin(omega*time);

%%%%RESULTS SAVING FOR SPHERE%%%%
risultati=[time((30/Fs-Ti(pe)/Fs):30/Fs) sol_inters((30/Fs-
Ti(pe)/Fs):30/Fs,1) sol_inters((30/Fs-Ti(pe)/Fs):30/Fs,2)
eta((30/Fs-Ti(pe)/Fs):30/Fs)];

[p_elrmsS,avg_powerS,P_elS,~,~, f_mag_S, ~, force_S, ~, Fs] = PTO
(H,T,Fs,risultati(:,2), risultati(:,3),tspan);

P_avg_S(pe,he)=avg_powerS;

%%%%RESULTS SAVING FOR CYLINDER%%%%
time=(0:Fs:30)';
risultati=[time((30/Fs-Ti(pe)/Fs):30/Fs) sol_interc((30/Fs-
Ti(pe)/Fs):30/Fs,1) sol_interc((30/Fs-Ti(pe)/Fs):30/Fs,2)
eta((30/Fs-Ti(pe)/Fs):30/Fs)];

[p_elrmsC,avg_powerC,P_elC,Y,harm, f_mag_C, pos, force_C, time, Fs]
= PTO (H,T,Fs,risultati(:,2), risultati(:,3),tspan);

P_avg_C(pe,he)=avg_powerC;

clear ts
clear tc
clear sols
clear solc
clear eta
percent=(cont/11664)*100
cont=cont+1;
end
end

filename= ['P_avg_S_ks_H=' num2str(Hi(ii)) '_T=' num2str(Ti(jj))
'.txt'];

save (filename, 'P_avg_S', '-ascii')

filename= ['P_avg_C_kc_H=' num2str(Hi(ii)) '_T=' num2str(Ti(jj))
'.txt'];

save (filename, 'P_avg_C', '-ascii')
end
end
```

A.1.2 Energy_Production.m

Calculates the energy output, power output, full load hours and capacity factor of the devices with real sea state's data.

```
clc
clear all

%Inputs
station = questdlg('Select the
station','Station','Alghero','Mazara','Alghero');
filename = [station '_all_years_y_Hs_Tp_dt.txt']; %column1 = year;
column2 = Hs; column3 = Tp; column4 = dt
input = load(filename);

if station(1:3) == 'Alg'
    years = [1990; 1991; 1992; 1993; 1994; 1995; 1996; 1997; 1998;
1999; 2000; 2001; 2002; 2003; 2007; 2010; 2011];
else
    years = [1990; 1991; 1992; 1993; 1994; 1995; 1996; 1997; 1998;
1999; 2000; 2001; 2002; 2003; 2011];
end

device = questdlg('Select the
device','Device','PM_S_A','PM_S_M','PM_C_M','PM_C_M');
filename = [device '.txt'];
matrix = load(filename); % Power matrix
Ts = matrix(1,2:size(matrix,2)); % Ts [s]
Hs = matrix(2:size(matrix,1),1); % Hs [m]
Pe = matrix(2:size(matrix,1),2:size(matrix,2)); %Electric power
[kW/m]

fprintf('\nStation = %s\n', station);
fprintf('Device = %s\n', device);

%Calculations (Device power and Energy production)
P = zeros(length(input),1); E=P;
for i = 1:length(input) % for each registraton
if input(i,3)>0 % if Tp>0
if ( (input(i,3)*0.95)>=Ts(1) && (input(i,3)*0.95)<=Ts(length(Ts))
&& input(i,2)>=Hs(1) && input(i,2)<=Hs(length(Hs)) )
    P(i) = interp2(Ts,Hs,Pe,(input(i,3)*0.95),input(i,2));
% power [kW] (bilinear interpolation)
    E(i) = P(i)*input(i,4); %Energy production [kWh]
end
end
end
Flh = P * 365*24 /max(max(Pe)); %Full load hours
Cf = P / max(max(Pe)); % Capacity factor [%]
output1 = [P E Flh Cf];
filename = [station '_' device '_P_E_Flh_Cf.txt'];
save(filename, 'output1', '-ascii');
fprintf('\nEnd\n');
```

```
%Calculations (Annual values)
annual_EP = zeros(length(years),1);
for k = 1:length(years) %for each year
    [a,b] = find(input(:,1) == years(k));
    annual_EP(k) = sum(E(a,1))/sum(input(a,4))*365*24/1000; %
Annual energy production [MWh]
end
annual_MP = annual_EP/365/24 * 1000; %Annual mean device power [kW]
annual_Flh = annual_MP * 365*24 /max(max(Pe)); %Full load hours
annual_Cf = annual_MP / max(max(Pe)); % Capacity factor [%]
output = [years annual_EP annual_MP annual_Flh annual_Cf];
filename = [station '_' device '_year_AEO_P_Flh_Cf.txt'];
save(filename, 'output', '-ascii');
```

A.1.3 optimization.m

```
clear all
close all
clc

dati_al= load( 'Alghero_all_years_y_Hs_Tp_dt.txt');
dati_ma= load ( 'Mazara_all_years_y_Hs_Tp_dt.txt');
Alghero_wave_clim= load ('Alghero_wave_clim.txt');
Mazara_wave_clim= load('Mazara_wave_clim.txt');
KC= load ('KC.txt');
KS=load ('KS.txt');
max1=0;
max2=0;
max3=0;
max4=0;
K_Cf_C=zeros;
K_Cf_S=zeros;
cont=1;

Ti=[2 3 4 5 6 7 8 9 10];% Wave Period's array
Hi=[0.5 1 1.5 2 2.5 3 3.5 4 4.5 5 5.5 6]; %Wave Height's array

for ii=1:length(Hi)
    for jj=1:length(Ti)

        filename= ['P_avg_C_kc_H=' num2str(Hi(ii)) '_T=' num2str(Ti(jj))
'.txt'];
        P_mat_Ca= load(filename);

        filename= ['P_avg_S_ks_H=' num2str(Hi(ii)) '_T=' num2str(Ti(jj))
'.txt'];
        P_mat_Sa= load (filename);

        [P_mat_C, P_mat_S]= formats(P_mat_Ca,P_mat_Sa);
```

```

[perf_C_al,perf_C_al_y]=Energy_Production_Alghero(P_mat_C,dati_al);
[perf_C_ma,perf_C_ma_y]=Energy_Production_Mazara(P_mat_C,dati_ma);
[perf_S_al,perf_S_al_y]=Energy_Production_Alghero(P_mat_S,dati_al);
[perf_S_ma,perf_S_ma_y]=Energy_Production_Mazara(P_mat_S,dati_ma);

Cf_C_al=mean(perf_C_al_y(:,5));
Cf_C_ma=mean(perf_C_ma_y(:,5));
Cf_S_al=mean(perf_S_al_y(:,5));
Cf_S_ma=mean(perf_S_ma_y(:,5));

if Cf_C_al > max1
    max1=Cf_C_al;
    opt_cond_C_al=[Hi Ti];
    def_perf_C_al=perf_C_al;
    def_perf_C_al_y=perf_C_al_y;
    P_mat_C_al=P_mat_Ca;
else
end

if Cf_C_ma > max2
    max2=Cf_C_ma;
    opt_cond_C_ma=[Hi Ti];
    def_perf_C_ma=perf_C_ma;
    def_perf_C_ma_y=perf_C_ma_y;
    P_mat_C_ma=P_mat_Ca;
else
end

if Cf_S_al > max3
    max3=Cf_S_al;
    opt_cond_S_al = [Hi Ti];
    def_perf_S_al=perf_S_al;
    def_perf_S_al_y=perf_S_al_y;
    P_mat_S_al=P_mat_Sa;

else
end

if Cf_S_ma > max4
    max4=Cf_S_ma;
    opt_cond_S_ma= [Hi Ti];
    def_perf_S_ma=perf_S_ma;
    def_perf_S_ma_y=perf_S_ma_y;
    P_mat_S_ma=P_mat_Sa;
else
end

K_Cf_C(cont,1)=KC(jj,ii); K_Cf_C(cont,2)=Cf_C_al;
K_Cf_C(cont,3)=Cf_C_ma;
K_Cf_S(cont,1)=KS(jj,ii); K_Cf_S(cont,2)=Cf_S_al;
K_Cf_S(cont,3)=Cf_S_ma;

```

```
percent= (cont/108)*100
cont=cont+1;

end

end

[Eff_C_A, Eff_C_M, Eff_S_A, Eff_S_M, CW_C_A, CW_C_M, CW_S_A, CW_S_M] =
efficiencias(P_mat_C_al, P_mat_C_ma, P_mat_S_al, P_mat_S_ma);
%results(P_mat_C_al, P_mat_C_ma, P_mat_S_al, P_mat_S_ma, def_perf_C_al_y
, def_perf_C_ma_y, def_perf_S_al_y, def_perf_S_ma_y, K_Cf_C, K_Cf_S);

filename= 'K_Cf_C.txt'; save(filename, 'K_Cf_C', '-ascii');
filename= 'K_Cf_S.txt'; save(filename, 'K_Cf_S', '-ascii');

filename= 'PM_C_A_opt.txt'; save (filename, 'P_mat_C_al', '-ascii')
filename= 'PM_C_M_opt.txt'; save (filename, 'P_mat_C_ma', '-ascii')
filename= 'PM_S_A_opt.txt'; save (filename, 'P_mat_S_al', '-ascii')
filename= 'PM_S_M_opt.txt'; save (filename, 'P_mat_S_ma', '-ascii')

filename= 'Eff_C_A.txt'; save (filename, 'Eff_C_A', '-ascii')
filename= 'Eff_C_M.txt'; save (filename, 'Eff_C_M', '-ascii')
filename= 'Eff_S_A.txt'; save (filename, 'Eff_S_A', '-ascii')
filename= 'Eff_S_M.txt'; save (filename, 'Eff_S_M', '-ascii')

filename= 'CW_C_A.txt'; save (filename, 'CW_C_A', '-ascii')
filename= 'CW_C_M.txt'; save (filename, 'CW_C_M', '-ascii')
filename= 'CW_S_A.txt'; save (filename, 'CW_S_A', '-ascii')
filename= 'CW_S_M.txt'; save (filename, 'CW_S_M', '-ascii')

filename= 'Perf_C_A_P_E_Flh_Cf.txt'; save (filename,
'def_perf_C_al', '-ascii')
filename= 'Perf_C_M_P_E_Flh_Cf.txt'; save (filename,
'def_perf_C_ma', '-ascii')
filename= 'Perf_S_A_P_E_Flh_Cf.txt'; save (filename,
'def_perf_S_al', '-ascii')
filename= 'Perf_S_M_P_E_Flh_Cf.txt'; save (filename,
'def_perf_S_ma', '-ascii')

filename= 'Mean_annual_Perf_C_A_year_AEO_P_Flh_Cf.txt'; save
(filename, 'def_perf_C_al_y', '-ascii')
filename= 'Mean_annual_Perf_C_A_year_AEO_P_Flh_Cf.txt'; save
(filename, 'def_perf_C_al_y', '-ascii')
filename= 'Mean_annual_Perf_S_A_year_AEO_P_Flh_Cf.txt'; save
(filename, 'def_perf_S_al_y', '-ascii')
filename= 'Mean_annual_Perf_S_M_year_AEO_P_Flh_Cf.txt'; save
(filename, 'def_perf_S_ma_y', '-ascii')
```

A.2. FUNCTIONS

A.2.1 Archimede.m

Computes the Buoyancy Forces.

```
function [Farcs, Farcc, Pss, Psc]=archimede(Pg, Vi, Re)

Vols=zeros;
Fgals=zeros;
Farcs=zeros;
Volc=zeros;
Fgalc=zeros;
Farcc=zeros;
i=1;

for h=0:0.1:2*Re(1)

    Vols(i)=(4/3*pi*Re(1)^3)-(pi/6*h^2)*(3*(2*Re(1)-h)+h); %Sphere

    Fgals(i)=Vols(i)*9.80665*1025;

    Pss= Pg(1)+ Vi(1)*1.2041*9.8066558380; %Sphere

    Farcs(i)=Fgals(i)-Pss;

    i=i+1;
end

i=1;

for h=0:0.1:4

    Volc(i)= pi*Re(2)^2*4-pi*Re(2)^2*h; %Cilinder

    Fgalc(i)=Volc(i)*9.80665*1025;

    Psc= Pg(2)+ Vi(2)*1.2041*9.8066558380; %Cylinder

    Farcc(i)=Fgalc(i)-Psc;

    i=i+1;
end
```

A.2.2 CiambC.m

ODE solver for the cylindrical device.

```
function dydt = ciambC(t,y,varargin)
m = varargin{2}; c = varargin{3};
A = varargin{4}; omega = varargin{5};
Bt=varargin{6}; wt=varargin{7};
d=varargin{8}; p=varargin{9};
q=varargin{10}; ci=varargin{11};
wp=varargin{12}; L=varargin{13};
Rc= varargin{14}; Rload=varargin{15};
eff= varargin{16}; Farcc=varargin{17};
Psc=varargin{18}; Kc=varargin{19};

ssp=A*omega*cos(omega*t);
ss=A*sin(omega*t);
%%ODE model equation%%
dydt=[y(2);(((c*((ssp)-(y(2))))*abs(((ssp)-
(y(2)))))+interpolazione_cilindro((max(0,(y(1))-(ss))),Farcc,Psc)-
LIN_GEN(y,Bt,wt,d,p,q,ci,wp,L,Rc,Rload,eff)-Kc*y(1))/m)];
```

A.2.3 CiambS.m

ODE solver for the spherical device.

```
function dydt = ciambS(t,y,varargin)
m = varargin{2}; c = varargin{3};
A = varargin{4}; omega = varargin{5};
Bt=varargin{6}; wt=varargin{7};
d=varargin{8}; p=varargin{9};
q=varargin{10}; ci=varargin{11};
wp=varargin{12}; L=varargin{13};
Rc= varargin{14}; Rload=varargin{15};
eff= varargin{16}; Farcs=varargin{17};
Pss=varargin{18}; Ks=varargin{19};

ssp=A*omega*cos(omega*t);
ss=A*sin(omega*t);
%%ODE model equation%%
dydt=[y(2);(((c*((ssp)-(y(2))))*abs(((ssp)-
(y(2)))))+interpolazione1((max(0,(y(1))-(ss))),Farcs,Pss)-
LIN_GEN(y,Bt,wt,d,p,q,ci,wp,L,Rc,Rload,eff)-Ks*y(1))/m)];
```

A.2.4 interpolazione1.m

Function that interpolates to obtain the exact buoyancy force for the spherical device.

```
function [A]= interpolazione1(xi,Farc,Ps)

%%%INTERPOLATION OF THE EXCITING FORCE DEPENDING ON THE FLOATING
LEVEL OF
%%%THE BUOY%%%%%%%%%%
if xi<=3
x=[0
0.100
0.2
0.300
0.4
0.500
0.6
0.700
0.8
0.900
1
1.100
1.2
1.300
1.4
1.500
1.6
1.700
1.8
1.900
2
2.100
2.2
2.300
2.4
2.500
2.6
2.700
2.8
2.900
3];

A=interp1(x,Farc,xi,'linear','extrap');

else
A=-Ps;
end
```

A.2.5 interpolazione_cilindro.m

Function that interpolates to obtain the exact buoyancy force for the spherical device.

```
function [A]= interpolazione_cilindro(xi,Farc,Ps)
```

```
%%%INTERPOLATION OF THE EXCITING FORCE DEPENDING ON THE FLOATING  
LEVEL OF
```

```
%%%THE BUOY%%%%%%%%%
```

```
if xi<=4
```

```
x=[0
```

```
0.100
```

```
0.2
```

```
0.300
```

```
0.4
```

```
0.500
```

```
0.6
```

```
0.700
```

```
0.8
```

```
0.900
```

```
1
```

```
1.100
```

```
1.2
```

```
1.300
```

```
1.4
```

```
1.500
```

```
1.6
```

```
1.700
```

```
1.8
```

```
1.900
```

```
2
```

```
2.100
```

```
2.2
```

```
2.300
```

```
2.4
```

```
2.500
```

```
2.6
```

```
2.700
```

```
2.8
```

```
2.900
```

```
3
```

```
3.1
```

```
3.2
```

```
3.3
```

```
3.4
```

```
3.5
```

```
3.6
```

```
3.7
```

```
3.8
```

```
3.9
```

```
4];
```

```
A=interp1(x,Farc,xi,'linear','extrap');
else
    A=-Ps;
end
```

A.2.6 LIN_GEN.m

Computes the magnetic force generated by the linear generator.

```
%%%%%LINEAR GENERATOR EQUATIONS USED IN THE ODE WEC MODEL%%%%%%%%%
function [f_pto] = LIN_GEN (y,Bt,wt,d,p,q,ci,wp,L,Rc,Rload,eff)

freq= 2*pi*y(2)/wp; %Electric Angular Frequency
Xs=freq*L; %Equivalent circuit impedance
delta = atan(Xs/Rc); %Electric phase angle
%Computing of the Generated Electric Field (Triphasic system)%%%
ea=(2*pi*Bt*wt*d*p*q*ci/wp)*y(2)*sin((2*pi*y(1)/wp)-delta);
eb=(2*pi*Bt*wt*d*p*q*ci/wp)*y(2)*sin((2*pi*y(1)/wp)-delta + degtorad
(120));
ec=(2*pi*Bt*wt*d*p*q*ci/wp)*y(2)*sin((2*pi*y(1)/wp)-delta +
degtorad(-120));
%Computing of the equivalent circuit currents%
cua=ea*cos(delta)/(Rc + Rload); cub= eb*cos(delta)/ (Rc + Rload);
cuc=ec*cos(delta)/(Rc + Rload);
%Computing of the equivalent circuit tension%
ua= ea*cos(delta) - (Rc*cua); ub= eb*cos(delta) - (Rc*cub); uc=
ec*cos(delta) - (Rc*cuc);
%Computing of the generated power
p_ela= ua*cua; p_elb= ub*cub; p_elc=uc*cuc;
p_el=p_ela + p_elb + p_elc;
p_mag=p_el/eff;
%computing of the PTO force%
f_pto= p_mag/y(2);

if f_pto==0
    f_pto=4e-12;
else
end

if f_pto>1e10
    f_pto=4e-12;
else
end

end
```

A.2.7 fou.m

Calculates the magnetic force with only three harmonic components.

```
function [Y,force,harm]= fou (f_mag, time, Fs)

[Y, freq] = positiveFFT(f_mag,Fs);

spettro_polare= [abs(Y); radtodeg(angle(Y));freq]';
spett_ord=sortrows(spettro_polare);

harm.one.freq=spett_ord(length(spett_ord),3);
harm.one.amp=2*spett_ord(length(spett_ord),1);
harm.one.phase =spett_ord(length(spett_ord),2);

harm.two.freq=spett_ord(length(spett_ord)-1,3);
harm.two.amp=2*spett_ord(length(spett_ord)-1,1);
harm.two.phase =spett_ord(length(spett_ord)-1,2);

harm.three.freq=spett_ord(length(spett_ord)-2,3);
harm.three.amp=2*spett_ord(length(spett_ord)-2,1);
harm.three.phase =spett_ord(length(spett_ord)-2,2);

[force] = positiveiFFT(Y,harm,f_mag);
```

A.2.8 linear generator.m

Computes the instantaneous electric power absorbed by the device.

```
function
[p_elrms,curms,erms,avg_force,avg_power,eab,ea,eb,ec,cua,cub,cuc,p_e
l,p_mag,f_mag,v,time,x] = linear_generator( Bt,
wt,d,p,q,ci,h,w,wp,L,eff,Rc,Rload,T,Fs,pos,vel,time)
% x = load; %load position from results
% v = load; %load velocity from results

ea=zeros;
eab=zeros;
eb=zeros;
ec=zeros;
cua=zeros;
cub=zeros;
cuc=zeros;
ua=zeros;
ub=zeros;
uc=zeros;
p_el=zeros;
```

```
p_ela=zeros;
p_elb=zeros;
p_elc=zeros;
p_mag=zeros;
f_mag=zeros;
v=zeros;
i=1;
x=zeros;

for i=1:length(vel)

    freq= 2*pi*vel(i)/wp; %Electric Angular Frequency
    Xs=freq*L; %Equivalent circuit impedance
    delta = atan(Xs/Rc); %Electric phase angle

    %Computing of the Generated Electric Field (Triphasic system)%%
    ea(i)=(2*pi*Bt*wt*d*p*q*ci/wp)*vel(i)*sin((2*pi*pos(i)/wp)-delta);
    eb(i)=(2*pi*Bt*wt*d*p*q*ci/wp)*vel(i)*sin((2*pi*pos(i)/wp)-
    delta+ degtorad(120));
    ec(i)=(2*pi*Bt*wt*d*p*q*ci/wp)*vel(i)*sin((2*pi*pos(i)/wp)-
    delta+ degtorad(-120));

    eab(i)=ea(i)*sqrt(3);

    %Computing of the equivalent circuit currents%
    cua(i)=ea(i)*cos(delta)/(Rc+Rload);
    cub(i)=eb(i)*cos(delta)/(Rc+Rload);
    cuc(i)=ec(i)*cos(delta)/(Rc+Rload);

    %Computing of the equivalent circuit tension%
    ua(i)= ea(i)*cos(delta)-Rc*(cua(i));
    ub(i)= eb(i)*cos(delta)-Rc*(cub(i));
    uc(i)= ec(i)*cos(delta)-Rc*(cuc(i));

    %Computing of the generated power
    p_ela(i) = ua(i)*cua(i);
    p_elb(i) = ub(i)*cub(i);
    p_elc(i) = uc(i)*cuc(i);

    p_el(i) = p_ela(i) + p_elb(i) + p_elc(i);
    p_mag(i)=p_el(i)/eff;

    %computing of the PTO magnetic force%
    f_mag(i)=p_mag(i)/(vel(i));

    if f_mag(i)==0
        f_mag(i)=4e-12;
    else
```

```
end

if f_mag(i)>1e10
    f_mag(i)=4e-12;
else
end

    cont=i
end

%f_mag(1)=0;
avg_power=mean(p_e1);
avg_force=mean(f_mag);
erms= max(ea)/sqrt(2);
urms=max(ua)/sqrt(2);
curms=max(cua)/sqrt(2);
p_elrms=urms*curms;
end
```

A.2.9 positiveFFT.m

Computes the Fourier transform.

```
function [X, freq ]= positiveFFT(x,Fs)

N=length(x);
k=0:N-1;
T=N/(1/Fs);
freq= k/T;
X=fft(x)/N;

cutOff = ceil (N/2);
X=X(1:cutOff);
freq=freq(1:cutOff);
```

A.2.10 positiveiFFT.m

Computes the inverse transfor of Fourier.

```
function [X]= positiveiFFT(x,harm,f_mag)
YY=zeros;
for i=1:length(x)
if 2*abs(x(i))>= harm.three.amp
    YY(i)=x(i);
else
end
end
```

```
XR=ifft(YY,length(f_mag));
X=real(XR)*2*length(f_mag);
```

A.2.11 PTO.m

Simulates the power take-off system behavior.

```
%%PTO MODEL%%
function [p_elrms,avg_power,p_el,Y,harm,f_mag,pos, force,time, Fs ]
= PTO (Height, Period, Fs,pos,vel,time)

Bt=1.55;      %Magnetic Field in tooth [T]
wt=8*10^-3;  %Tooth width [m]
d=0.4;       %Width of Stator Side [m]
p=100;       %Numero di Poli
q=6/5;       %Winding ratio [slots/(pole, phase)]
ci=6;        %Number of cables per slot
h=Height/2;  %wave amplitude [m]
T=Period;    %Wave period [s]
w=2*pi/T;    %wave frequency [rad/s]
wp=0.1;      %Pole pair width [m]
L=11.5*10^-3; %generator inductance [H]
Rc=0.3735;   %Generator resistance [ohm]
Rload=3.1;   %Load resistance [ohm]
eff=0.791;   %efficiency

%%LINEAR GENERATOR MODEL%%
[p_elrms,~,~,avg_power,~,~,~,~,~,~,p_el,~,f_mag,~,~,~] =
linear_generator ( Bt,
wt,d,p,q,ci,h,w,wp,L,eff,Rc,Rload,T,Fs,pos,vel,time);

%%FOURIER ANALYSIS%%
[Y,force,harm]= fou (f_mag,time, Fs);
```

A.2.12 efficiencies.m

Performs the post processing of the simulation data, extracting its efficiency and capture width values.

```
function
[Eff_C_alg, Eff_C_ma, Eff_S_alg, Eff_S_ma, CW_C_alg, CW_C_ma, CW_S_alg, CW_
S_ma]=efficiencies ( P_avg_C_alg, P_avg_C_ma, P_avg_S_alg,
P_avg_S_ma)

load Alghero_wave_clim.txt
load Mazara_wave_clim.txt

rho=1025;
g=9.81;
Ti=[2 3 4 5 6 7 8 9 10];% Wave Period's array
Hi=[0.5 1 1.5 2 2.5 3 3.5 4 4.5 5 5.5 6]; %Wave Height'sarray
Wave_Power=zeros;
Eff_C_alg=zeros;
Eff_C_ma=zeros;
Eff_S_alg=zeros;
Eff_S_ma=zeros;
Clim_pow_al=zeros;
Clim_pow_ma=zeros;
L=zeros;
k=zeros;
omega=zeros;
Wave_Energy_Flux=zeros;
CW_C_alg=zeros;
CW_C_ma=zeros;
CW_S_alg=zeros;
CW_S_ma=zeros;

for i=1:length(Ti)
    L(i)=g*Ti(i)/(2*pi);
    k(i)=2*pi/L(i);
    omega(i)=2*pi/Ti(i);
    for j=1:length(Hi)
        Wave_Energy_Flux(i,j)=(rho*g*omega(i)*((Hi(j)/2)^2)/4*k(i))*((2*k(i)
*50+sinh(2*k(i)*50))/sinh(2*k(i)*50));
        Wave_Power(i,j)=(rho*(g^2)*(Hi(j)^2)*(Ti(i)/0.95)/64);
        Eff_C_alg(i,j)=P_avg_C_alg(i,j)/(Wave_Power(i,j)*2);
        Eff_C_ma(i,j)=P_avg_C_ma(i,j)/(Wave_Power(i,j)*2);
        Eff_S_alg(i,j)=P_avg_S_alg(i,j)/(Wave_Power(i,j)*3);
        Eff_S_ma(i,j)=P_avg_S_ma(i,j)/(Wave_Power(i,j)*3);
        Clim_pow_al(i,j)=Wave_Power(i,j)*Alghero_wave_clim(i,j);
        Clim_pow_ma(i,j)=Wave_Power(i,j)*Mazara_wave_clim(i,j);
        CF_C_alg(i,j)=P_avg_C_alg(i,j)/Wave_Energy_Flux(i,j);
        CF_C_ma(i,j)=P_avg_C_ma(i,j)/Wave_Energy_Flux(i,j);
        CF_S_alg(i,j)=P_avg_S_alg(i,j)/Wave_Energy_Flux(i,j);
        CF_S_ma(i,j)=P_avg_S_ma(i,j)/Wave_Energy_Flux(i,j);
    end
end
```

